University of Strathclyde

Design, Manufacture and Engineering Management

Laser Processing of Carbon Fibre Reinforced Plastic
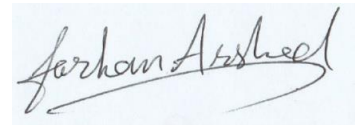
Farhan Arshed

A thesis presented in fulfilment of the requirements for the degree of Doctor of Philosophy.

June 2021

Declaration of author's rights

The copyright of this thesis belongs to the author under the terms of the United Kingdom Copyright Acts as qualified by University of Strathclyde Regulations 3.50. Due acknowledgement must always be made of the use of any material contained in, or derived from, this thesis.

Farhan Arshed

June 2021

i

Abstract

Carbon fibre reinforced plastic (CFRP) is extensively used in automotive and aerospace industries with the aim to achieve reduction on emission by reducing weight and consequently fuel usage. Due to high demand and governmental regulations to reduce the environmental impact, the need for re-using CFRP is becoming an interesting area of application with economic benefits to industry. Cutting CFRP to meet large manufacturing demands with fast cutting speeds and high-quality cuts can impose significant problems for conventional cutting methods. High power lasers can provide fast and efficient cutting speed, but if not controlled effectively can cause excessive fibre damage that has significant impact on the mechanical strength.

Secondly, the joining technology is one of the major obstacles in composite parts application. Traditional joining techniques such as screwing and riveting damage the fibres, leading to major stresses due to drilled holes. One way to achieve higher degree of material application is to use adhesive bonding between two surfaces. However, a good adhesion between two surfaces is necessary to achieve strong and high resistance bonds. A surface pre-treatment is essential before the adhesive bonding to bring reproducibility a clean, slightly rough, and preferably active surface. One of the approaches is to use laser as a method of cleaning. Currently lasers are only used to clean the surface of virgin material for surface contamination.

This thesis presents a research work using a 1.5 kW single mode fibre laser to investigate the effects of process parameters such as cutting speed, multi-pass, stand-off, large diameter aperture, double aperture and trenching on the reduction of fibre damage to under 100 μm. The fibre damage was observed using scanning electron microscope. Thermal cameras were used to observe the temperature throughout the cutting process. Regression analysis was carried out to develop five models for CAD/CAM interface for quick adaptation of the laser cutting process – in

addition, contour plots have been developed for analysis of process parameters on the fibre damage.

For laser cleaning a novel approach was used that employs a flash pumped Nd:YAG laser to clean the glue remained on separated CFRP parts, previously joined with PU and EP adhesive with the aim to reduce the CFRP waste by limiting the damage fibre and composite material substrate as a whole and for re-joining purposes. A feasibility study was conducted to assess the developed laser cleaning process in removing adhesive residue from internal curvatures of 3D CFRP components.

Acknowledgements

Contents

List of Figures

List of Tables

Nomenclature

v'	Frequency of light
λ	Wavelength of light
c	Speed of light
h	Plank's constant
E'	Photon energy
N_1	Electron at energy level 1
N_2	Electron at energy level 2
E_1	Energy value of state 1
E_2	Energy value of state 2
T	Absolute temperature of medium
k_B	Boltzmann's constant
d_w	Beam waist diameter
θ	Beam divergence angle
M^2	Beam quality
z	Depth
I_z	Intensity of the beam at depth z
I_0	Incident laser beam intensity
η	Absorption coefficient
R_a	Reynolds number
U	Gas flow velocity
D	Work piece thickness
ρ_g	Gas density
ϕ	Viscosity of the gas
V_{Bmax}	Maximum cutting speed
ρ	Density of material
P_0	Beam power
d_B	Focal spot diameter

L_v	Latent heat of vaporisation
C_p	Specific heat capacity
T_v	Vaporisation temperature
T_0	Initial temperature
δ	Constant for a giver material of given laser
P_p	Peak power
τ	Pulse width
t_d	Cutting time
n	Number of pulses
$\dfrac{1}{f}$	Period between pulses
E_p	Pulse energy

Acronyms

FRP	Fibre Reinforced Plastic
CFRP	Carbon Fibre Reinforced Plastic
AWJ	Abrasive Water Jet
HAZ	Heat Affected Zone
CW	Continuous Wave
Yb	Ytterbium
SEM	Scanning Electron Microscope
OM	Optical Microscope
CAD	Computer Aided Design
CAM	Computer Aided Manufacturing
Nd:YAG	Neodymium doped Yttrium Aluminium Garnet
EP	Epoxy
PU	Polyurethane
EM	Electromagnetic
UV	Ultraviolet
IR	Infrared
LASER	Light Amplification by Stimulated Emission of Radiation
MASER	Microwave Amplification by Stimulated Emission of Radiation
TEM	Transverse Electromagnetic
BPP	Beam Parameter Product
DPSS	Diode Pumped Solid State
RGH	Rare Gas Halide
XeF	Xenon Fluoride
XeCl	Xenon Chloride
KrF	Krypton Fluoride

ArF	Argon Fluoride
MSD	Mach Shock Disc
PAN	Poly Acrylo Nitrile
HS	High Strength
IM	Intermediate Modulus
HM	High Modulus
UHM	Ultra High Modulus
GFRP	Glass Fibre Reinforced Plastic
WJ	Water Jet
EDM	Electro discharge Machining
WEDM	Wire Electro Discharge Machining
MMR	Material Removal Rate
APD	Ablative Photo Decomposition
RSM	Response Surface Methodology
MPA	Multi-Purpose Analyser
NIR	Near Infra-Red
LIBS	Laser Induced Breakdown Spectroscopy
AES	Atomic Emission Spectroscopy

CHAPTER 1

1. Introduction

In an area of manufacturing technology, machining of composites gains a greater attention due to its extensive use in aerospace and automotive industry. Reduction in machining requirements by net shape manufacturing for complex components is one of the main advantages. However, post-processing such as edging, cutting and drilling is still required for these components [1][2]. Generally, the machining of composites, especially fibre-reinforced plastic composites (FRPs) in very complicated and different from that of metals, due to its heterogeneous and anisotropic properties. As the matrix and fibres are joined physically, not chemically, they do not retain their thermal and mechanical properties [3].

In automotive and aerospace industry, carbon fibre reinforced plastics (CFRP) have slowly replaced existing materials due to its exceptional mechanical properties with corrosive resistance and low thermal expansion. CFRP has a heterogeneous structure but lacks a standardised machining technique. One of the most common machining technique is drilling, but 60% of all parts are rejected due to low finishing quality [2]. Other techniques, such as milling causes delamination, fibre pulling, interior cracks and tool wear [4]. Abrasive water jet (AWJ) is an alternative to milling and drilling. AWJ uses sand, and high pressure accelerated water to cut CFRP. This process does not cause tool damage and heat generation. However, the delamination and moisture penetration cause softness of polymers and reduces fibre matrix adhesion [5].

In material processing, lasers display a unique advantage as a non-contact and non-abrasive cutting tool. This process eliminates tool wear, cutting forces and vibrations. Over the years, lasers are used as a promising tool for cutting composites. In laser cutting, the heat generated by laser beam evaporates carbon fibres and binder material. The dominant obstruction for lasers cutting as an industrial application is quality defects such as heat-affected zone (HAZ), burning and delamination due to

intense heat [6]. The continuous development in laser material processing have opened new avenues such as high-power laser with high beam quality. The development of galvanometer scanner systems with quick laser-material interaction enhances productivity and accuracy.

For laser cutting, continuous-wave (CW) or pulsed laser are generally used. In pulsed mode, short or ultrashort lasers can be used, with minimal small spot size and adequate cooling between pulses causing small thermal damage. However, with low average power, the cutting speed is slower than CW laser, this also leads to low output [7]. A higher processing speed could be achieved with high-power CW laser. The HAZ generated by CW laser is more significant than pulsed laser; this could be minimised with the use of multi-pass techniques and increased laser scanning speed.

Processing of carbon fibre with ytterbium (Yb) – doped laser indicated that the width of HAZ decreased with the increase in scanning speed investigated by Geoke and Emmelmann [8]. Klotzbach et al., [9] also confirmed that HAZ reduces when scanning speed and number of passes increased. The effect of cutting speed on the width of fibre damage is investigated by Bluemel et al. [10] who concluded that the width of fibre damage decreases as processing speed increases for given power of laser.

One of the major obstacles of CFRP part application is the CFRP joining technique. Traditional joining techniques such as riveting and screwing causes fibre damage, leading to stress concentrations dur to drilled holes. The weight of these reinforcements reduces the lightweight potential of the CFRP. Adhesive bonding between surfaces is one of the methods to achieve a higher degree of material application. However, to achieve strong and resistive bonds, good adhesion between two surfaces is necessary. A surface pre-treatment is essential before the adhesive bonding. This is required to bring a reproducible clean, slightly rough, and preferably active surface. One of the approaches is to use lasers as cleaning method.

This PhD Thesis studies laser cutting and laser cleaning aspects of CFRP processing using lasers. For laser cutting, a single-mode fibre laser was used, and in results the process window was studied which is defined in terms of cutting speed, no of passes,

nozzle distance from the surface and nozzle diameter to reduce fibre damage extent (µm) by varying those parameters. Thermal effects were analysed using a scanning electron microscope (SEM) and optical microscope (OM). Further optimisation of fibre damage extent was performed using double an aperture and trenching technique. Regression analysis was also carried out and five mathematical models were developed for quick adaptation of the process parameters. These models could be used as CAD/CAM interface for future process automation.

For laser cleaning, a novel approach is used to clean the glue remained on separate CFRP parts previously joined with adhesives using a flash pump Nd: YAG (neodymium-doped yttrium aluminium garnet) laser with aim to reduce CFRP waste with limiting damage to the fibres and the composite material substrate as a whole and for re-joining purposes.

1.1. Objectives

The objective of this PhD Thesis are the following (with focus on laser cutting and cleaning of CFRP composites:

- Removal of worn area on CFRP flat plate samples using laser cutting.
- Development of correlation between process time, process parameters and machining quality.
- Offline process optimisation for maximising the efficiency of the removal process.
- Laser cleaning of Epoxy-based (EP) and Polyurethane (PU) from separated CFRP flat plates.
- Post laser cleaning tensile testing for re-joining purposes.

1.2. Thesis Structure

This thesis addresses several scientific and experimental aspects associated with laser cutting and laser cleaning of CFRP. It consists of seven chapters. After the introduction chapter, Chapter 2 discuss the introduction to lasers, laser processing and carbon-fibre reinforced plastic. Configuration principles, history of lasers, laser types, laser-material interaction and laser cutting are discussed in Chapter 2. In laser

cutting section of Chapter 2, the use of assist gas and improvement in laser cutting was discussed. The last section of Chapter 2 has two parts, in first part definition and properties of fibre-reinforced plastic composites are discussed, in the second part the constituent and applications of CFRP was discussed. Chapter 3 discussed literature review for both laser cutting and laser cleaning.

Chapter 4 consists of four parts. The first part introduces the laser cutting methodology and equipment used. The major quality factors are identified and characterised. The second section discuss the results, the third section contain discussion to analyse the results in second section and the last section consist of regression analysis for CAD/CAM interface.

Chapter 5 investigate the laser cleaning aspect of the thesis. This chapter has six sections. The first section discusses the spectroscopic analysis to determine the best approach in laser cleaning of adhesives from CFRP and experimental setup for spectroscopic analysis. The second section consist of material description and experimental setup of laser cleaning trials. The third section consist of results and discussion for both spectroscopic analysis and laser cleaning trials. The last two sections discuss the thermographic analysis and re-joining, and testing of laser cleaned samples.

Chapter 6 discuss the case study of laser cleaning of internal structures from reused CFRP. Finally, Chapter 7 and 8 consists of the conclusions of the work and recommendations for future work.

1.3. List of publications from this work.

Journal papers:

Arshed, F., Ahmad, A., Xirouchakis, P. and Metsios, I., 2021. "Laser cutting of carbon fibre reinforced plastic components for remanufacturing". *Journal of Remanufacturing*. (**Under review**)

Arshed, F., Ahmad, A., Xirouchakis, P., Metsios, I., de Wit, J. and Huxdorf, O., 2021. "Removal of glue on carbon fibre reinforced plastic using diode pumped Nd:YAG laser for remanufacturing". *Journal of Remanufacturing*. (**Under review**)

Book chapter:

Justus Von Freeden, Jesper de Wit, Stefan Caba, Susanne Kroll, Huan Zhao, Jinchang Ren, Yijun Yan, **Farhan Arshed**, Abdul Ahmad, Paul Xirouchakis. 2021. "Composite repair and remanufacturing." In *Generalisation of future industrial scenarios* . Springer. (**Under review**)

CHAPTER 2

2. Lasers, Laser Processing and CFRP

As an energy source, light consist of electromagnetic (EM) waves. These EM waves consist of gamma-rays, X-rays, ultraviolet (UV), optical, infrared (IR) and radio waves. A wide range of applications has opened after the discovery of materials that can absorb EM radiation.

The modern application of light according to its characteristics is shown in Figure 1 [11]. Light waves travelled in a straight line and in all directions once originated from a source such as the sun or a light bulb. A directed monochromatic light of single wavelength and frequency is an effective use of its power source, by exciting the atoms of materials which in reacting with absorbing energy release light. This phenomenon is the basis of the emergence of Light Amplification by Stimulated Emission of Radiation (LASER) emerged. The early applications of the laser light as communication and measurement systems started in 1960's and in later years used is industry as material processing [12].

Alongside laser evolution, engineering materials evolution started a dramatic turning point in 1960' [13]. Since then, a rapid growth has been made in polymer, composites, and ceramic based materials (Figure 2) [13]. One of the challenges for fast and cheaper laser cutting system for composites are the high processing cost and time for composites.
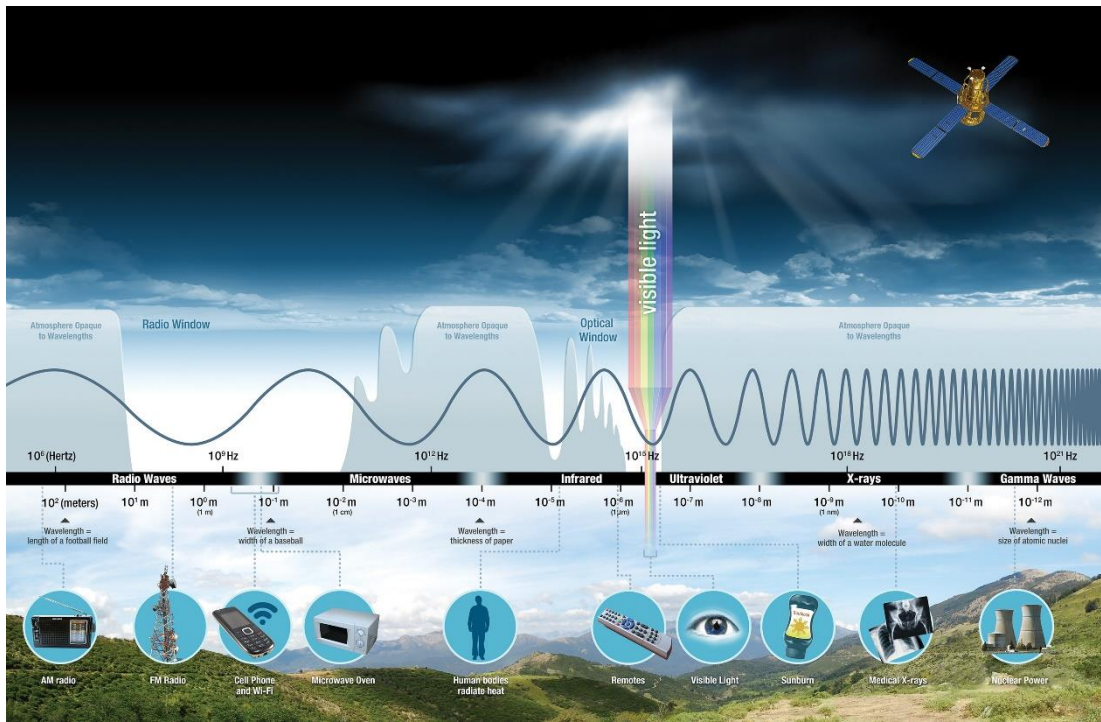
Figure 1: Electromagnetic spectrum and applications [11]
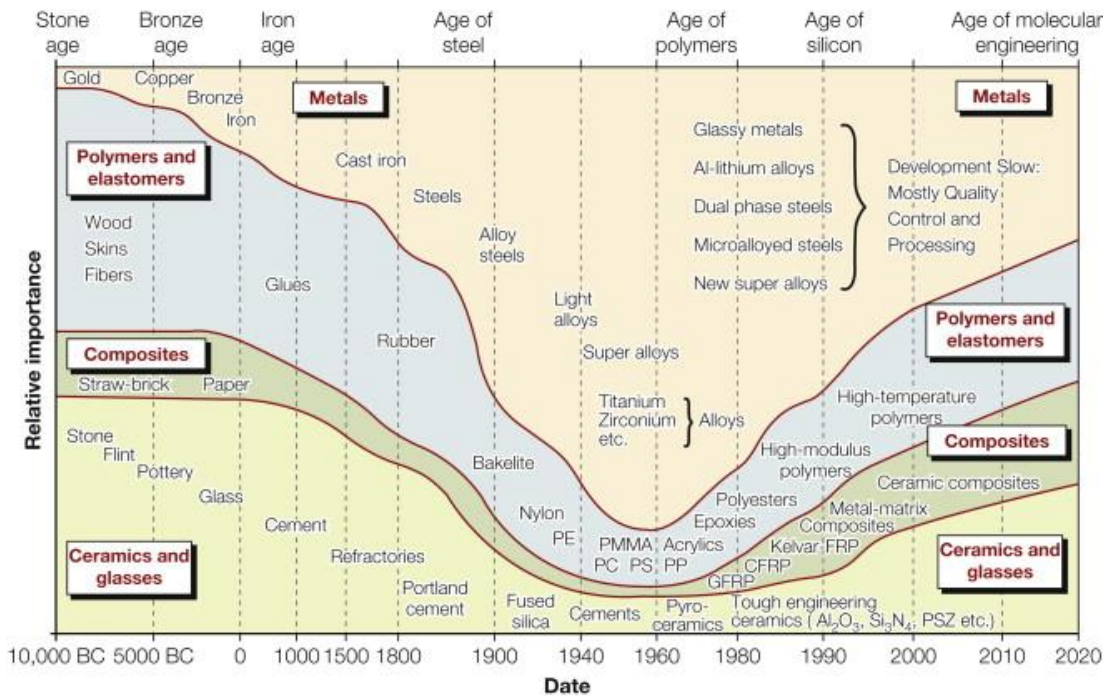
Figure 2: Engineering material revolution with time and relative importance [13]

This chapter covers two topics, firstly introduction to lasers, its application, types, and principles and secondly, introduction to composite material with importance given to fibre-reinforced composites.

2.1. Lasers

2.1.1. History

In 1905 Albert Einstein introduced a revolutionary insight of the light by proposing that light consist of bundles of energy which he called photons. In 1913, an introduction of Bohr's quantum theory, the interaction between photons and atoms gains significance. At the start the understanding was that once the photon is interacts with an atom it might be absorbed or emitted as a spontaneous emission of a photon by an atom in a higher energy state. However, Einstein studied the thermodynamics of photon emission and concluded a prospect of stimulated photon emission by interaction with another photon. These emissions can be coherent and such observations were first made in 1982 [12], [14], [15].

An unpublish idea of microwave amplification by stimulated emission of radiation (MASER) by high resolution microwave spectroscopy was developed by Charles Townes in 1951 [14]. Similar ideas were published by Weber [16] and Basov and Prokhorov [17]. In 1958, Schawlow and Townes extended the idea of Maser into optical and infrared radiation [18]. The first pulsed flash pumped ruby crystal laser was developed by Maiman [19] by using fundamentals of Masers. The first continuous wave He:Ne gas laser was developed by Javan et al. [20] in 1961. After that, various materials in different phases were illustrated as laser and optical amplifiers based on Schawlow's law [17], which propose that any material under certain circumstances can result in stimulated emission.

Between 1962 and 1968 the development of different types of lasers were basic and usually suffers with poor reliability and durability. Also, those were limited for demonstrations in the laboratory [21]. From 1968, the lasers dramatically improved in engineering terms that lasers were used in industry for cutting, welding and distance measurement tool by mid-1970's [14]. From 1980's to mid 1990's, lasers

were used in consumer goods such as CD players, laser printer and barcode scanner to advanced application as uranium isotope separation [14]. By 2020, the annual worldwide commercial sales of lasers forecasts are at $16.63 billion [22].

Laser industry improved significantly by the replacement of the energy source from flash-law pumping to diode-pumping and advancement of fibre optic as the gain medium. These advancements have led to systems with negligible energy coupling loss, high beam quality and systems with minimal maintenance requirements. CO_2 and Nd:YAG lasers are two competing technologies for disk and fibre lasers to change the operational performance of industrial lasers [23].

2.1.2. Configuration Principals

2.1.2.1. Fundamentals of Operation

Laser light is monochromatic that consist of photons that has the same frequency and phase with temporal coherence and low divergence. This allows a laser beam to be focused to a small spot and with extremely high-power density. This allows lasers to be used in a wide range of material processing applications alongside in surgery, communications, and measurements.

Quantum levels are known as the energy levels of atoms. Once energy is received, in the form of in-elastic or elastic collision with other atoms or in the form of electromagnetic radiation, by an electron, it jumps from a lower quantum level to a higher level. This energy is released once the electron returns to its lower state. This released energy can be in form of kinetic (non-irradiative) or electromagnetic (irradiative). The lasers are based on irradiative transition. The relation corresponding to the propagation of light energy are [24]:

$$v' = \frac{c}{\lambda} \tag{1}$$

$$E' = hv' = \frac{hc}{\lambda} \tag{2}$$

Where, v' is the frequency of light (Hz), λ is the wavelength of light (μm), c is speed of light in vacuum (m/s), h is Plank's constant (4.135×10^{-15} eV.s) and E' is the photon energy (eV).

The electron jumps from a lower energy state to a higher energy state known as excitation or pumping if the energy of the photon equals the difference of energy between the two states. As an electron decays from an excited state to a lower state, a photon is released with energy magnitude equal to the difference of the two states. This photon is released in a random direction and phase known as "spontaneous emission". Before this emission occurs if, a photon with significant energy passes by, it can cause the releasing of a photon of the same phase, wavelength, and direction, known as "stimulated emission". Laser "amplification" occurs if the laser cavity consists of a lasing medium between pairs of aligned mirrors. The light reflects back and forth between mirrors, passing through the lasing medium, stimulating more emissions, and amplifying the light. One of the mirrors in the laser cavity is totally reflective and the other is partially transmissive (~5 %), this allows the generated beam to leave the cavity [25]. A schematic of laser light evolution is shown in Figure 3.
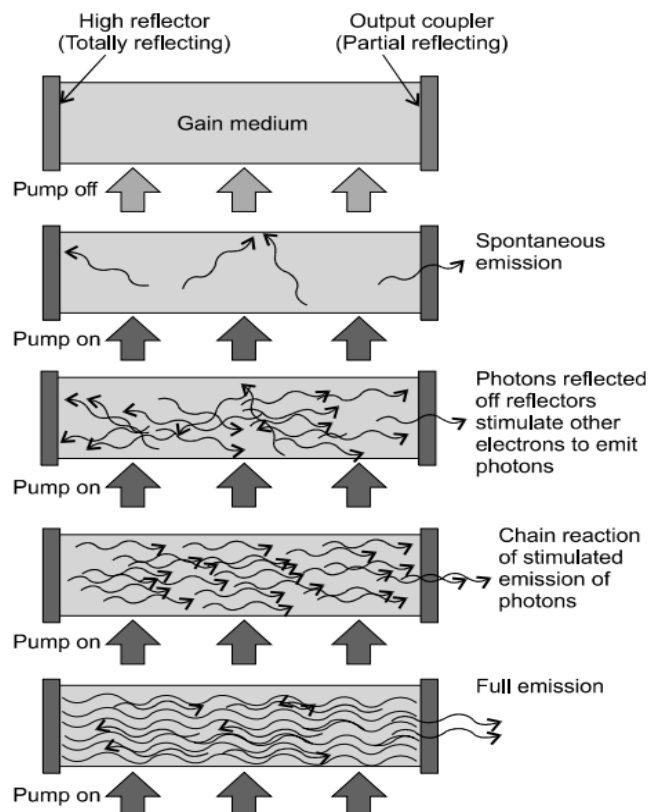
Figure 3: Light Amplification of Stimulated Emission of Radiation (LASER) [26]

The Boltzmann equation can be used to describe the population of electrons at any energy state [24].

$$\frac{N_1}{N_2} = \exp - \left(\frac{E_2' - E_1'}{k_B T}\right) \tag{3}$$

where N_1 and N_2 represents the number of electrons at energy state 1 and 2. E_1 and E_2 are the energy values of state 1 and 2, T is the absolute temperature of medium (K), and k_B is Boltzmann's constant (1.38 x 10^{-23} J/K).

The upper energy level is always less densely populated than the lower energy level under equilibrium. For stimulated emission, the number of electrons in the upper energy level must be greater that number of electrons in the lower energy level. This process is known as "population inversion". Therefore, through pumping, stimulation, population inversion and amplification, a laser beam is created that is temporal and spatial coherent.

The properties that separate the laser light from ordinary light is monochromaticity, coherence, directionality, and brightness.

2.1.2.2. Monochromaticity

A laser with high monochromaticity signifies that a small range of frequencies is emitted by the light source, generally assessed by measuring the width of the spectral lines. There are single or very few spectral lines of narrow width in laser light when compared with ordinary light source which has multiple wide lines (Figure 4) [27].
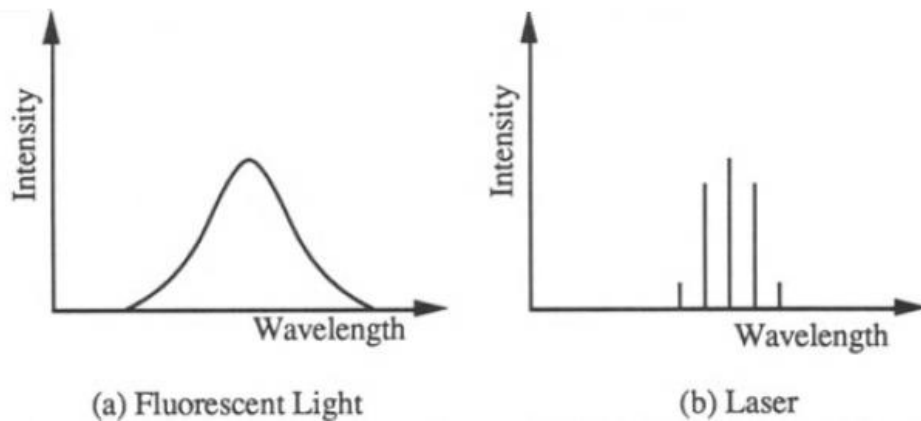
Figure 4: Monochromaticity of laser light [27]

2.1.2.3. Coherence

The relationship between the magnetic and electronic component of an electromagnetic wave indicates its spatial and temporal coherence (Figure 5). The laser beam is coherent when these components are all aligned. Spatial coherence indicates a relationship of phases at different points in space at single moment in time, whereas temporal coherence indicates a relationship of phases over a period of time at single point is space [27].

(a) Coherent Light

(b) Incoherent Light
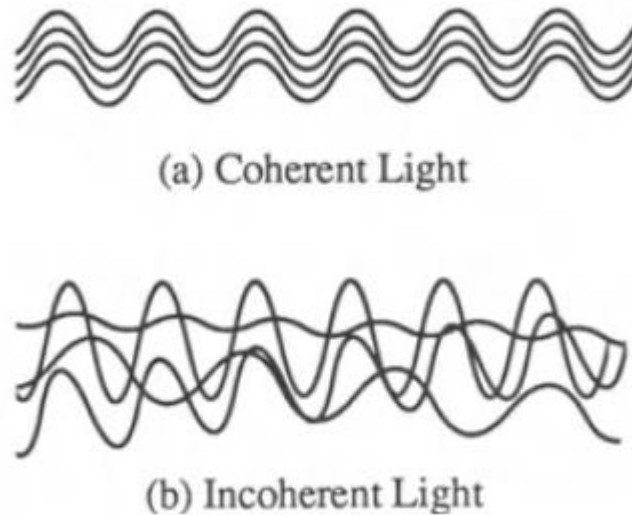
Figure 5: Coherence of laser light [27]

2.1.2.4. Directionality

The energy carried by a laser beam is focused on a small area by its highly collimated and directional nature [12]. Due to low diffraction, a laser beam has low divergence angles and can propagate to a long distance with little loss of beam intensity. The beam divergence angle is the angle at which the beam leaves the laser invariably and spreads out. For a beam with wavelength of λ and beam waist diameter of d_w, the lower limit of beam divergence is [12].

$$\theta = \frac{2\lambda}{\pi d_w} \qquad (4)$$

2.1.2.5. Radiance

High radiance of the laser is one of its significant features. The radiance is defined as the power emitted per unit area per unit solid angle. As an important quantity, it

cannot be increased by using lens or other optical systems. Furthermore, high radiance is required to deliver high irradiance (power per unit area) to a sample. Therefore, high radiance of laser is important in material processing applications [12].

2.1.2.6. Mode Structure

Due to the elongated nature of the laser resonator, the length between the mirrors are greater than the lateral dimension, the field configurations are separated into transverse and longitudinal modes that are nearly independent to each other. The longitudinal mode represents the specific wavelength at which a given laser can operate. The transverse mode represents the beam intensity variation along a path which is perpendicular to the direction of propagation. Transverse modes are important in laser material processing as beam divergence, beam diameter and energy distribution are driven by this mode [12]. Inside and optical resonator, electromagnetic (EM) field variations are described as transverse electromagnetic modes (TEM_{mnq}), where m, n and q represent the number of radial zero fields, angular zero fields and longitudinal fields, respectively. Only the first two indices are normally used to represent a TEM mode, with the first and second subscript representing the number of rings and bars respectively (Figure 6). The most desirable mode is Gaussian mode (TEM_{00}) as it can be focused to the smallest spot with maximum intensity on the beam axis [12].
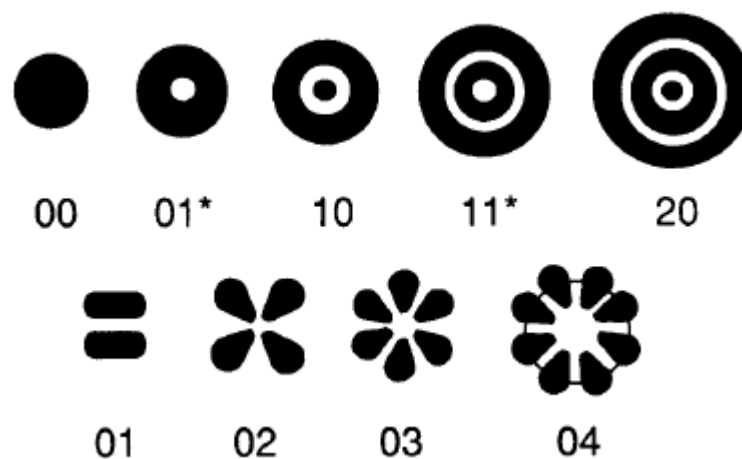
Figure 6: TEM modes [12]

2.1.2.7. Beam Quality and Polarisation

The quantitative measure of beam quality is normally called M^2. It compares the beam divergence with a pure Gaussian beam, which has a M^2 value of 1, with the same waist located at the same position. The lasers with M^2 greater than 1 is of poor quality. The M^2 is defined as:

$$M^2 = \frac{\pi \, d_w \theta}{4\lambda} \tag{5}$$

Where d_w is beam diameter, λ is wavelength of beam and ϑ is full divergence angle [12]. When a fibre optic is used for beam delivery, the beam parameter product (BPP) is used for quality measurement [28]:

$$BPP = \frac{d_w \theta}{4} = \frac{M^2 \lambda}{\pi} \tag{6}$$

An electromagnetic wave consists of orthogonally oscillating electric and magnetic fields. The electric field is more important in material processing because it affects the amount of beam absorption by the material and due to its reflectivity effects, polarisation has a directional effect [15]. A polarised laser beam has two forms, p-polarised and s-polarised. In p-polarised form, the oscillating electric field is parallel to the plane of incidence, whereas, in s-polarised, the oscillating electric field is perpendicular to the plane of incidence.

2.1.2.8. Temporal Configuration

Usually, a laser system consists of an energy source, resonator, gain medium, cavity and cooling system. A gain medium is used for the optical gain and can be in the form of solid, liquid, gas, or semi-conductor. The energy source provides energy to the gain medium atoms to undergo excitation. The energy could be in the form of highly charged electrons or electromagnetic radiation ions formed of neutron, protons, or other heavier atoms [25]. Gas or semi-conductor lasers mostly used electrons whereas, liquid and solid-state lasers used electromagnetic radiation. A resonator cavity consists of two mirrors, one totally reflective and the other is partially reflective used as feedback system to increase the stimulated emission. A cooling system in form of water or air is used to control the temperature of the gain medium.

Different crystal and pumping variations are used in lasers depending on the quality of beam and power. A cylindrical rod lasing medium is usually 10 cm in length and 1.2 cm in diameter. Rod length is directly proportional to laser power and inversely proportional to beam quality. An optical pump source in the form of flash lamps or laser diode, can influence laser characteristics. When compared with lamp-pumped lasers, diode-pumped-solid-state (DPSS) systems have much greater efficiency, smaller beam size and compactness [12]. The laser diodes have further improved the laser system configuration: Q-switching, harmonic generation and mode locking for efficiency, high energy, cost effectiveness and system compactness with short and ultra-short pulses. Mode locking can achieve lower pulse repetition rate, higher pulse energy and longer pulse duration. Q-switching produces high power burst by slowly accumulating energy in the gain medium. In q-switching, pulse duration is longer than nanoseconds due to pulse build up time, whereas, in mode locking pulse duration is very short typically in the picosecond range and very high peak power.

2.1.3. Laser Types

2.1.3.1. CO_2 (Carbon Dioxide)Laser

In industry 40% of lasers are used as CO_2 gas lasers [29]. These lasers are one of the most powerful lasers with a wavelength of 10.6 μm, operating mainly in mid infrared region. In smaller version and continuous wave mode they range from few milliwatts to a larger version producing over 10 kJ of energy in pulsed mode. With efficiency up to 30%, they can produce continuous output power of 100 kW. The smaller version of CO_2 laser is called waveguide lasers because the excitation region is of cylindrical shape which is small enough to guide a beam through wave guide and can produce continuous power of 100 W. The lasers operate with mixture of a CO_2, N_2 (nitrogen)and He (helium) gasses. The average electron energy is kept high in the gas discharge region by He gas. This laser used in a variety of application including but not limited to eye surgery, welding, cutting and beam weapons [25].

2.1.3.2.   Fibre Laser

Since the laser invention it was concluded that an optical waveguide can significantly improve laser technology. The first fibre laser was designed in 1960's but their

inclusion in practical applications was limited to lab demonstrations until 1990's. Commercialisation of these lasers were possible with the advancement of fibre grating technology that leads to narrow linewidth fibre lasers and the development of double clad fibre laser for material processing. High power, brightness and efficiency are some of the advantages of fibre lasers. Fibre lasers also have small beam spot, low maintenance and high flexibility [30], [31], [32], [33].

Figure 7 (a, b) shows the fibre laser fundamentals. Optical fibre structure consist of multilayer coaxial cylinder, divided into fibre core, cladding and coating layer [34]. Most of the light is confined to the fibre core by diode pump. To prevent signal attenuation, the cladding region has lower refractive index than the core region. The coating layer protects the cladding and core. The light (visible or near infra-red) travels along the fibre core by total internal reflection.

(a)

(b)
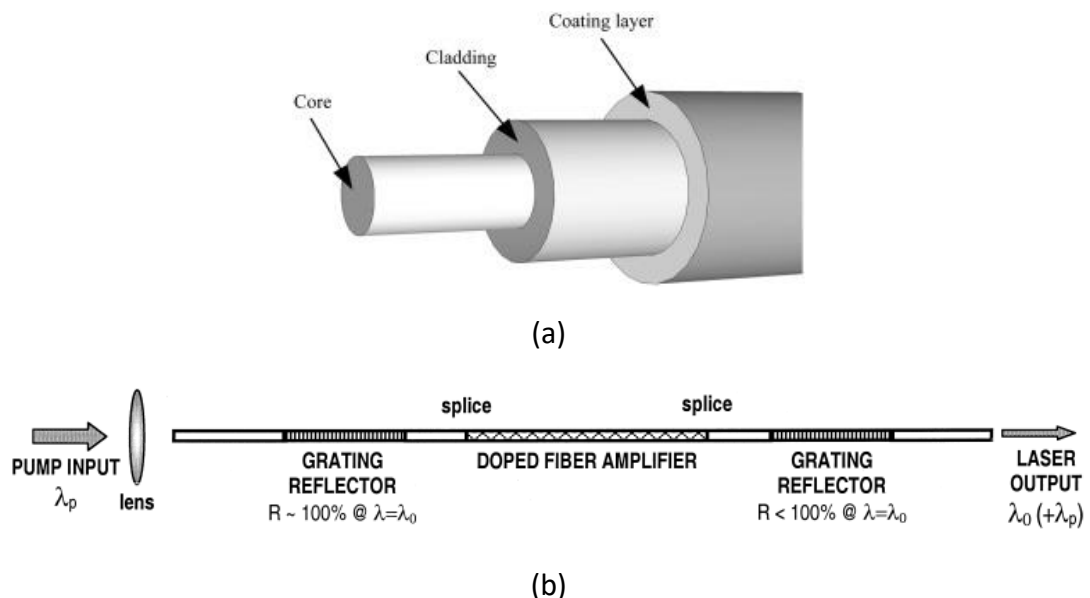
Figure 7: (a) Schematic of optical fibre structure, (b) Schematic of simple all-fibre laser oscillator [31], [34]

For communication purposes optical fibre normally used silica (SiO_2). Silica is always doped with high refractive index dopants such as neodymium (1.06 µm), ytterbium (1.07 µm), thulium (1.45 µm), erbium (1.55 µm) and praseodymium (1.07 µm). Fibre Bragg Gratings (FBG) are used as reflectors in a wave cavity. Waveguide characteristics of the core controls the transverse electromagnetic wave

distributions. Single mode is produced by narrow fibres whereas, higher modes produced by larger core diameter [31], [34].

2.1.3.3. Excimer Laser

The development of rare-gas halide (RGH) discharge pumped excimer laser formed the basis of commercial development of this type of laser [35]. In excimer laser, a complex molecule of two atoms can only be stable in electronically excited state. Excimer lasers are only available as pulsed laser with intense output in the UV or deep UV region. Schematic of an excimer laser workstation for micro machining is shown in Figure 8.
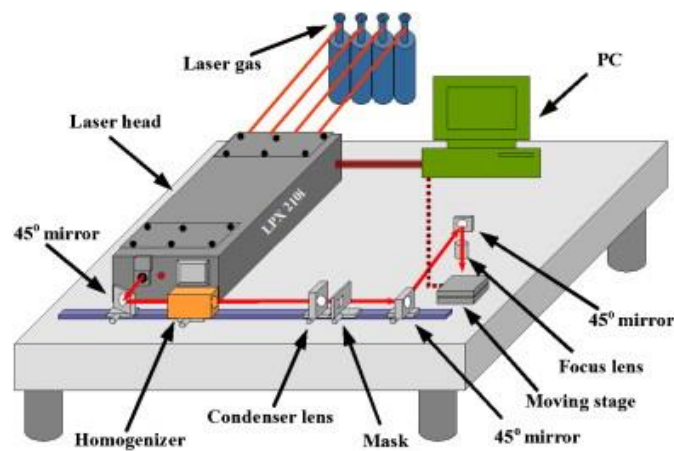
Figure 8: Excimer laser as micromachining unit [35]

Excimer laser has an active medium containing high pressure plasma of helium and /or neon and trace amounts of rare gas such as argon, krypton and xenon and halide such as fluorine, chlorine etc. The mixture of gas and halide has a characteristic wavelength, and by changing the gas mixture the wavelength of the excimer laser can be altered. Commonly used excimer lasers are Xenon fluoride (XeF) 351 nm, Xenon chloride (XeCl) 308 nm, Krypton fluoride (KrF) 248 nm, Argon fluoride (ArF) 193 nm and molecular fluoride (F_2) 157 nm [36]. Due to its short wavelength these lasers have good coupling energy to the work piece. Excimer lasers are very good for ablation of organic material and successfully used in photolithography, micromachining, and medical applications. Excimer lasers with all its precision and small spot size have a

major disadvantage in terms of limited laser power, low feed rate and limited flexibility in material processing [12], [28], [35], [36].

2.1.4. Laser Matter Interaction

During laser processing, the optical energy is absorbed by the interaction of electrons with the electric field of the electromagnetic radiation. This force is transferred to near surface region of the structure in solids and is known as skin depth optical penetration as explained by Beer's law:

$$I_z = I_0 e^{-\eta z} \tag{7}$$

Where z (mm) is the depth, I_z (W/mm^2) is the intensity of the beam at the depth z, I_0 (W/mm^2) is the incident laser beam intensity and η (mm^{-1}) is the absorption coefficient. This process depends on the photon energy, if it is low such as in CO_2 (~0.12 eV) and Nd:YAG (~1.2 eV) then only heat is generated by vibration of excited electrons of the solid, this process is known as "photo thermal" mechanism. Once the vibration is sufficient to break the solid structure and phase changes to first melt, and vaporisation and plasma formation. The photo thermal mechanism is shown in Figure 9.
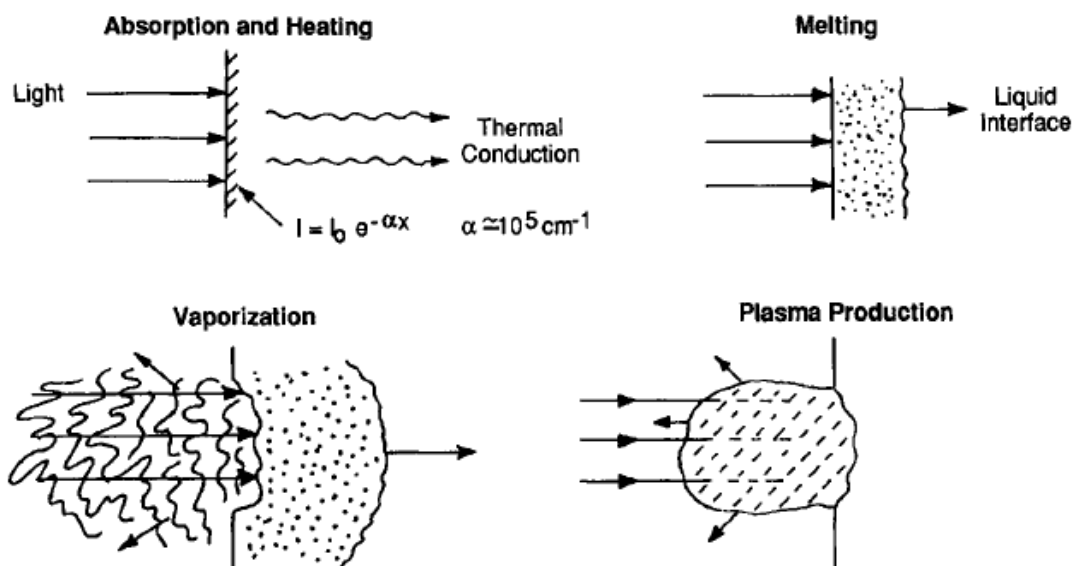
Figure 9: Photo-thermal phenomenon as laser beam strikes the material [12]

Molecular bonds in organic matter can be easily broken with a high photon energy such as UV lasers, this is known as "photo-chemical" mechanism. In photo-chemical process, there is a minimal thermal damage as energy stored in the material is dissipated as kinetic energy of particles removed. This mechanism is shown in Figure 10.
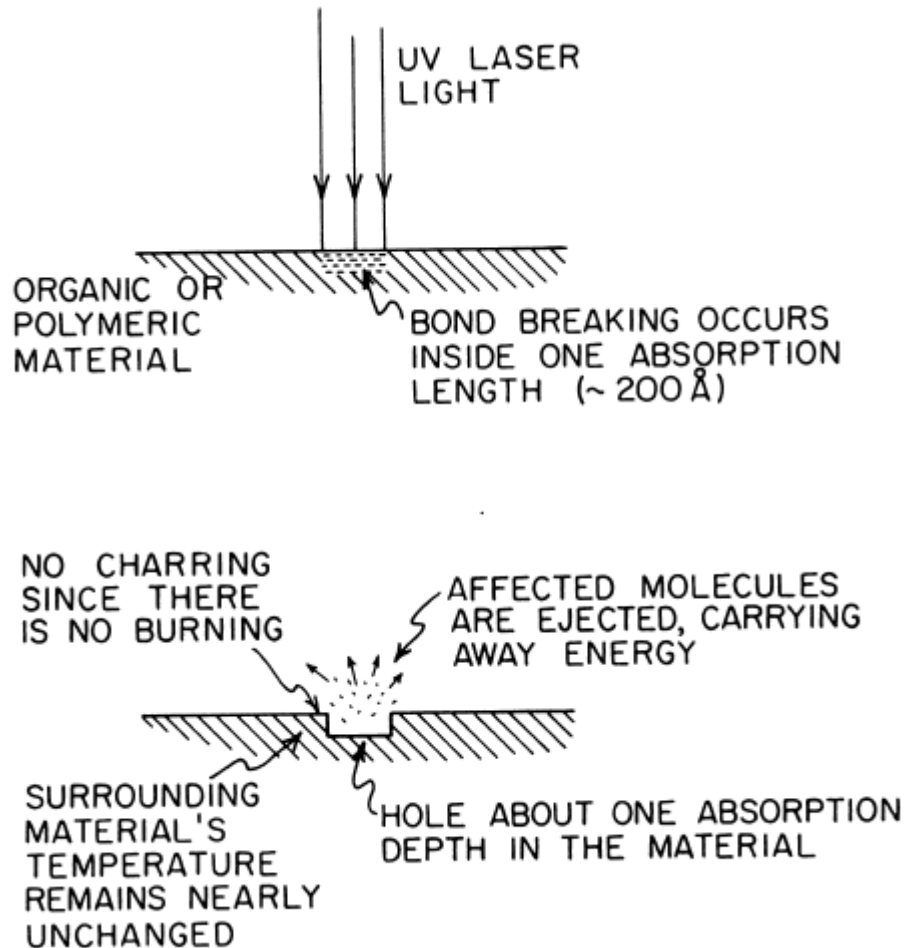
Figure 10: Photo-chemical mechanism in UV laser [37]

If the electromagnetic radiation has a photon energy higher than several eV or in case of ultra-short pulses, the excited electrons removed directly, this process is known as "photo-electric" mechanism [12], [29], [38], [39].

2.1.5. Laser Cutting

Laser cutting is known as a superior and cost effective method in manufacturing technology and a widely used application in material processing [29]. Fast cutting

speed with high quality and precision are one of the advantages of the process. This process is successfully used to cut 25 mm thick steel sheets [40]. Figure 11 shown laser cutting alongside its quality factors [41].
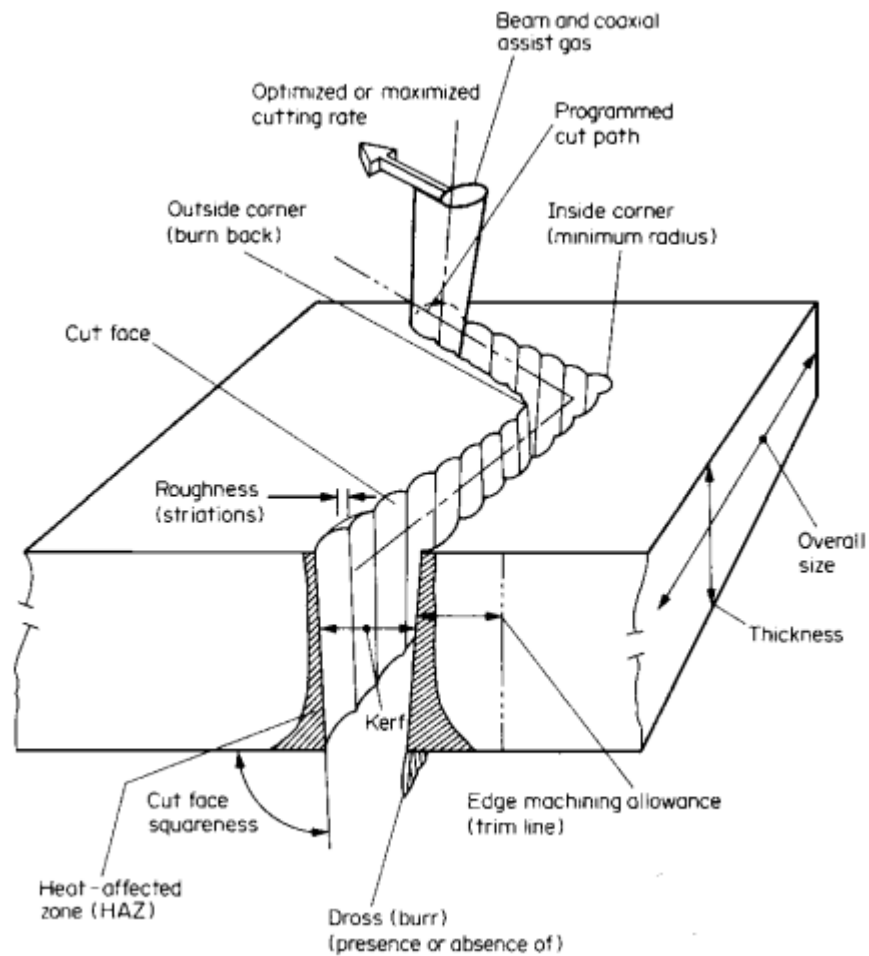
Figure 11: Laser cutting illustrating quality factors [42]

In laser cutting, a focused beam is used for localised material removal using a programmed cutting path. The process can be assisted by a coaxial jet gas to remove heated material from interface, prevent surrounding material heating and unwanted re-solidification. The laser type, its beam quality, power and cutting speed determines the quality factors such as kerf width, dross, and striations. Striations are the series of ridges seen on the cut surface and caused surface roughness mainly in laser cutting of steel. The main cause of striation formation is a cyclic variation in the driving force of the oxidation reaction, the viscosity and surface tension linked to molten metal [43]. The laser beam can move through the cutting path by either

movement of laser head or work piece of even both. The beam energy is balanced by heat conduction, energy for melting or vaporisation and environmental heat losses. Laser cutting is regarded as steady-state thermal process since the workpiece movement and beam is relatively fixed.

2.1.6. Assist Gas in Laser Cutting.

Additional to laser beam, assist gas is an integral part of the laser cutting process. The role of assist gas is to activate shear forces and pressure gradients to remove molten or gaseous by products from the kerf, protecting the focusing optic from vapour and spatter from the interaction zone and protecting the interaction zone from oxidisation. Assist gas also enhances the process performance by providing additional energy through exothermic reactions.

In laser cutting, the role of assist gas is governed by composition, pressure, and nozzle conditions. Pressure and nozzle conditions confirm the dynamic effects of assist gas on the kerf. There is a complex aerodynamic behaviour of high-pressure assist gas in laser cutting and divided into two categories, low pressure (~1-6 bar with oxygen) an high pressure (up to 20 bar with inert gas). The acceleration of the jet is achieved by supplying high pressure to the nozzle where the gas flow is expanded and injected to the cutting front. Gas flow is directly proportional to the pressure gradient and shear forces. When a converging nozzle is used, the gas flow goes through a transition from laminar to turbulent flow when the Reynold number (R_e) exceeds 3.2 x 10^5, known as critical Reynold number [44]. R_e is defined as:

$$R_e = \frac{UD\rho_g}{\varphi} \tag{8}$$

Where U (m/s) is the gas flow velocity, D (m) is the work piece thickness, ρ_g (kg/m^3) is the gas density and ϕ (kg/m.s) is the viscosity of the gas. The gas velocity is equal to the sound velocity at the separation point at the separation point and absolute critical pressure equals to the initial pressure [45], [46], [47]. Above ambient pressure, radial waves expand to adjust the exit pressure to ambient pressure. A pressure in reduced in the core of jet gas when the pressure point is exceeded. This

causes the gas to reverse in the direction of the movement and a shock wave is generated. Therefore, some strong asymmetrical and normal shock wave occurs which results in the loss of energy. The gas flow is decelerated as a normal shock called Mach shock disc (MSD) formed over the plate. Excessive burning is caused by the reactive gas with high gas flow, however, if inert gas is used, it increases the heat dissipation and drag force. Figure 12 shows the main aerodynamics interaction of the assist gas in the cutting process [47].
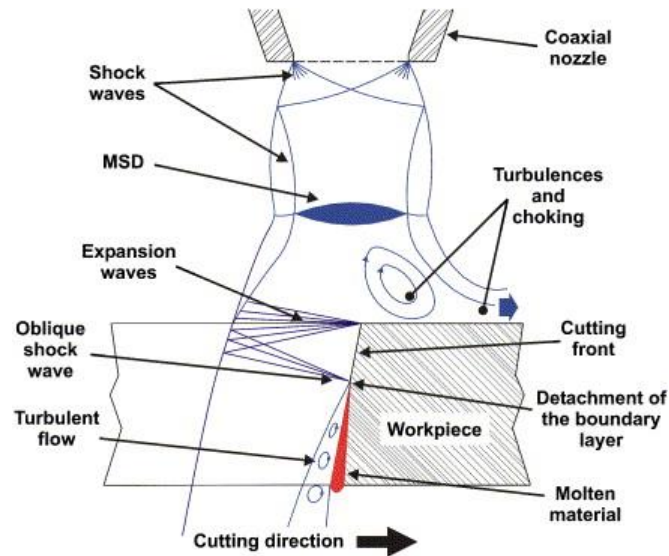
Figure 12: Assist gas interactions in laser cutting [46]

2.1.7. Improvement in Laser Cutting.

Laser cutting is a non-contact process generally accepted in industry and the process improvement in terms with cut quality, practicality, and precision is necessary. To improve the cutting process, various techniques have been developed, summarised in Figure 13 [15], [28], [48], [49].
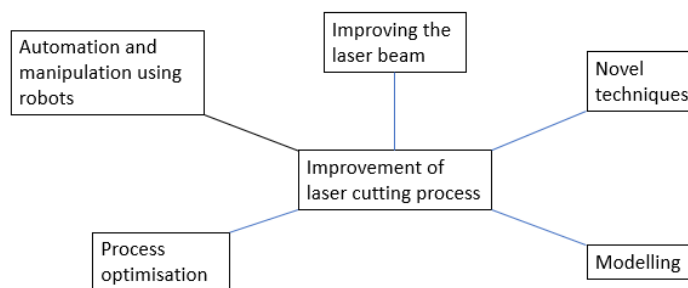
Figure 13: Approaches used to improve laser cutting process.

The laser cutting process can be affected by beam power, wavelength, mode, stability, and temporal configuration. A thick metal plate can be cut without dross with rectangular waveform and high peak power. Uniform cutting widths and smoother cutting surface is achieved by smaller beam power fluctuations. For quality and reliability of the laser cut, a consistent beam mode is important [50], [51]. An in direct approach to improve quality and performance is by improving laser beam and optics. In this process the material variation of work piece, formation of plasma and other phenomenon occurring in interaction zone are not considered. The beam material interaction is a complex phenomenon in laser cutting. Before significant heating occurs, the incident beam is reflected, scattered, and absorbed in proportion determined by the beam wavelength, state of polarisation, angle of incidence and optical properties of the material. Also, the fraction of beam coupling into the material varies. This partially reflects the material properties and their temperature dependency and partially reflects the effects of metallurgical nature [29], [52], [53]. Optimisation of process parameters remains important in achieving high quality cuts. Improvement in laser cutting process using modelling such as finite element were considerably investigated to understand various fields such as material beam interaction [54], quality conditions and processing [55], [56], and using assist gas [57]. Laser cutting can be better characterised and improved with the help of modelling. Second generation laser manufacturing systems became available in European and Japanese market by early 1990's, these systems allowed multi-processing laser manufacturing [58]. With the help of robotics and optical fibres, these systems can manufacture components, subassemblies, and complete products in truly integrated CAD-CAM environment.

New techniques such as use of dual focused lens are also used to improve process performance. Scanning speed is increased by 23% and kerf width reduced by 30% when dual focused lens is used in laser cutting [59], the use of abrasive jet for removal of by-products [60] and laser beam spinning for cutting thicker material [61] have been reported.

2.2. Fibre Reinforced Composites

Composite can be a material that is manufactured by joining two or more materials and each material keeps its own distinctive properties. The resultant material's properties do not match with any of the individual materials. Normally, composites have a bulk phase known as matrix and a discontinuous phase known as reinforcement. Reinforcement can contain small particles or thin fibres. The interface is the boundary where the discontinuity of physical and mechanical properties of these two phases happens. Matrix is the area of interest in the composite materials and mainly serves two purposes. Firstly, it holds the structure together by spreading the load to a larger area and transferring into reinforcement, providing what is known as shear resistance. Secondly, reinforcement provides the material with high stiffness and tension resistance. Therefore, composite structure resists aggregate compression with significant density reduction as compared to other materials.

Composite materials are classified either by matrix or reinforcement or by both depending on material and type as shown in Figure 14. A structure of fibre reinforced laminate consists of numerous layers of woven or unidirectional fibres within the matrix. In transverse direction, the unidirectional fire-reinforced materials have poor properties. Therefore, fibres if not woven are laminated at different angles. Particulate based composite is quasi-isotropic and can be machine uniformly.
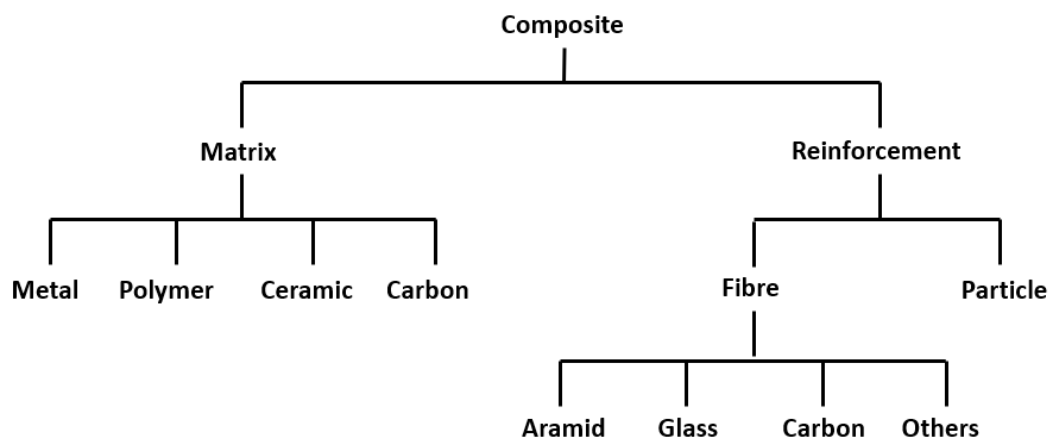
Figure 14: Classification of composites based on constituents.
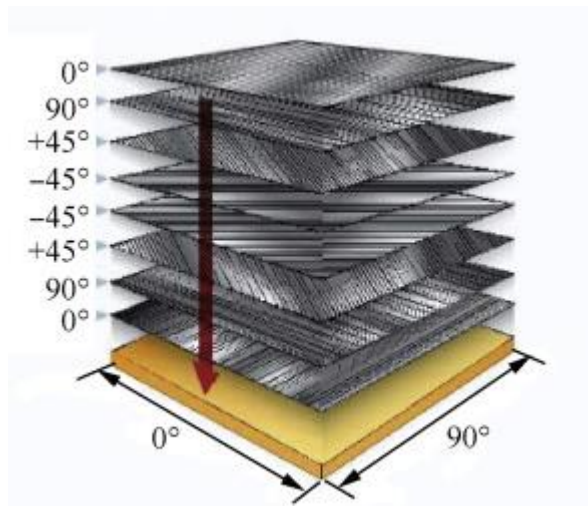
Figure 15: Schematic of fibre-reinforced composite structure [62].

2.2.1. Characteristics

Fibre reinforced composite materials with anisotropic nature can be tailored according to design requirements. This flexibility can be used to reinforce the structure in the direction of major stress concentrations and increases the stiffness in the preferred direction. Another characteristic of fibre-reinforced composites is its their high internal damping, which leads to better absorption of vibrational energy within the material. This reduces the transmission of noise and vibrations to adjacent structures. The assembly requirements can be reduced by joining complex parts as a single cured assembly, either by initial cure or secondary adhesive bonding. With excellent fatigue strength FRPs have developed into major structural material and are used as metal substitution for many weight critical components. Fans with CFRP has saved 180 kg when replaced aluminium in aerospace industry [63].

A 20% reduction in operational cost and 15% reduction of fuel consumption is estimated when CFRP is used in aerospace industry [63]. During the 1980's the composites are modestly used in commercial aircrafts and by 1990's only 10% of the metallic weight is replaced by composites. Airbus's A380 XWB (extra wide body) and Boeing's B787 have used between 30% to 50% composite contents [64]. Figure 16 shows the use of FRPs in Airbus A380 [65].
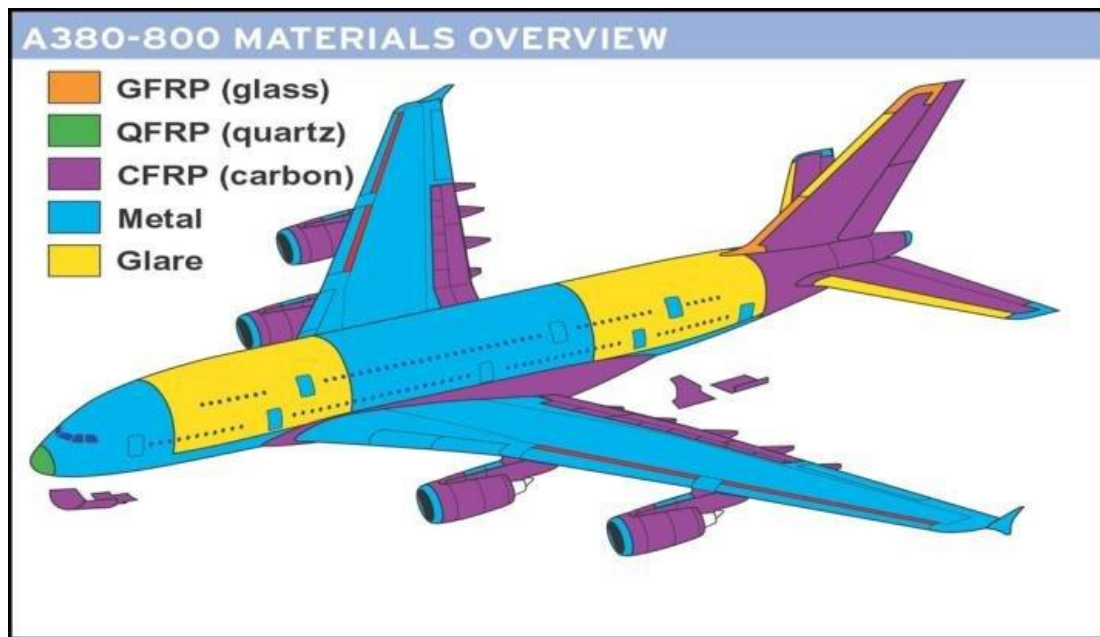
Figure 16: Use of FRPs in Airbus A380 [65]

2.2.2. Properties

2.2.2.1. Specific Strength and Modulus

The characteristics such as diameter, length, orientation, and volume of reinforcing fibres can affect the properties of FRP composites. There are two kinds of fibres used in FRPs, long fibres and short fibres. Long fibres can withstand the load more effectively whereas, short fibres offer better flexibility. As a result, long fibres are bonded easily and offer better properties. Generally, FRPs performance can be ranked by their strength and modulus. A comparison of common FRPs specific strength and specific modulus is shown in Figure 17.
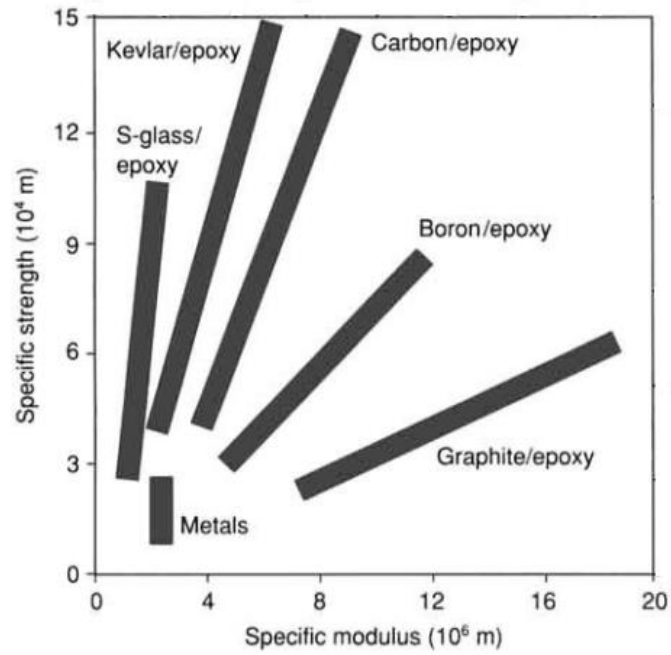
Figure 17: Performance map of FRPs [66]

2.2.2.2. Thermal Conductivity

Fundamentally there are three thermal conductivities in the *x*, *y* and *z* direction for unidirectional FRPs. Generally, thermal conductivity of fibres is higher than matrix, therefore, the heat affected zone (HAZ) is elliptical in shape as shown in Figure 18 [67] .
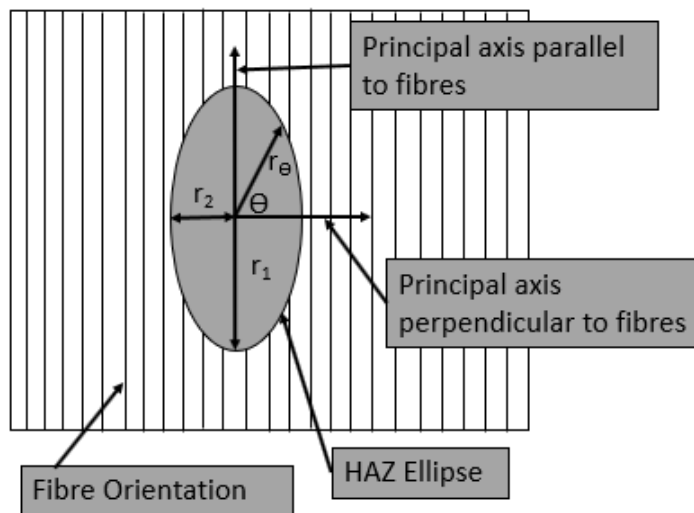
Figure 18: HAZ formation in unidirectional FRPs [66]

The thermal resistance of fibre and matrix can be modelled as thermal resistors, where values are inversely proportional to the thermal conductivity. The expression for the equivalent thermal conductivity, when heat is directed in parallel with the fibre axis is given by:

$$k_{parallel} = V_{fibre}\, k_{fibre} + V_{matrix}\, k_{matrix} \qquad (9)$$

The expression for the equivalent thermal conductivity, when heat is directed in perpendicular to fibre axis is given by:

$$\frac{1}{k_{parallel}} = \frac{V_{fibre}}{k_{fibre}} + \frac{V_{matrix}}{k_{matrix}} \qquad (10)$$

2.2.3. CFRP Composites

2.2.3.1. Constituents

The development of carbon fibre in 1960s has been a revolution in composites industry [68]. Processes such as controlled oxidisation, carbonisation and graphitisation of carbon-rich organic precursors are used to produce carbon fibres. Most commonly used precursor is Polyacrylonitrile (PAN) because it offers best carbon fibre properties, other precursors are pitch and cellulose. Carbon fibre as high strength (~ 2600°C) or high modulus (~ 3000°C), with other types in between can be produced depending on graphitisation process. To improve matrix bonding and chemical sizing, carbon fibre undergoes surface treatment after formation. Carbon fibres characterised as high strength (HS) with modulus greater than 265 GPa, intermediate modulus (IM) (modulus between 265 GPa and 320 GPa), high modulus (HM) (modulus between 320 GPa and 440 GPa) and ultra-high modulus (UHM) [3]. The diameter of most carbon fibres is between 5 – 8 μm. among all commercially available fibres, carbon fibres have highest specific stiffness, very high compression and tension strength and resistance to corrosion and fatigue. The impact strength is lower than glass fibres with HM and UHM fibres exhibits brittle characteristics.

Epoxy and polyester are usually used in CFRP as binders. Epoxy has high temperature properties and polyester offers better resistance to moisture and dielectric

properties. Vinyl ester is a combination of both epoxy and polyester and has excellent water resistance properties and commonly used in marine applications [69].

2.2.3.2. Applications

CFRPs is second most used FRPs lagging only to GFRPs. A comparison chart of GFRPs and CFRPs is shown in Figure 19 [70].
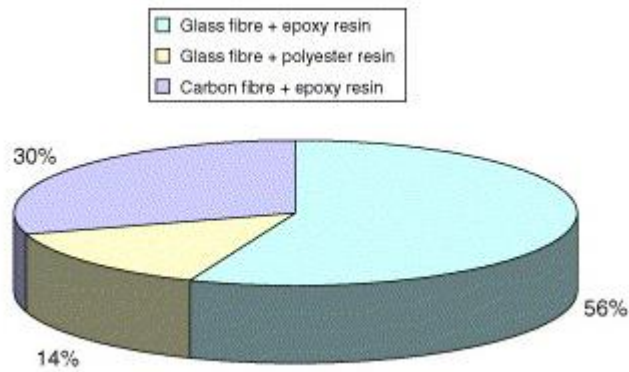
Figure 19: CFRP and GFRP market share [69]

CFRPs are most suitable for high performance and high quality applications for aerospace industry due to its high specific strength up to 4500 MPa stiffness, density of 1.8 g/cm^3, excellent rigidity and low thermal expansion [3,71].

2.3. Summary

CFRP are most commonly used composites and extensively used in industries such as aerospace, automotive and marine industry due to their superior properties. Being anisotropic, inhomogeneous, and abrasive, machining CFRP is a challenge. Laser cutting of CFRP is challenging due to the differences in physical and thermal properties of matrix and reinforcement. This causes an extended HAZ, in laser processing of CFRP reducing HAZ is one of the major challenges. In order to investigate impact of different process parameters in laser processing of CFRP, various studies have been conducted using CO_2, Nd:YAG, excimer and fibre laser. Cutting quality has impacted by laser power, wavelength, laser material interaction time and material properties.

CHAPTER 3

3. Literature Review on Laser Processing of CFRP

This chapter provides a literature review on laser cutting and laser cleaning of carbon fibre reinforced plastics (CFRP)

3.1. Laser Cutting

Conventional methods of cutting CFRP cause extensive tool wear of the machining heads, CFRP delamination and fibre pull out [4]. Cutting technique such as water jet (WJ) and abrasive water jet (AWJ) have several advantages such as increased cutting speed, reduced thermal stress and omission of dust by water jet [72]. However, use of water can cause moisture build up at surface and delamination due to high velocity impact [73]. Osmotic erosion can also occur, and this is a process in which water penetrates the material and causes degradation as investigated by Walter and Ashbee [74]. Due to tool size and its dimension, these methods have failed to cut small or complex shapes [72].

Electro discharge machining (EDM) or wire electro discharge machining (WEDM) are other methods used for cutting CFRP [75]. Small and complex shapes can be cut accurately and good surface finishing using EDM and WEDM. Habib et al. [76] identified that material removal not only depend on tool path and fibre direction but also on process parameters. EDM and WEDM use high current densities which causes polymer melting at cut surface, which increases the heat affected zone (HAZ) at the cut surface. A low current density is required to reduce disproportionate melting, but if low current density is used, the material removal rate (MMR) is very low typically between $2 - 5$ mm^3/min. Slow cutting speed is directly proportional to MMR. An MMR of 4 mm^3/min for a 2 mm thick CFRP sample and 0.1 mm wide worded trench would correspond to 20 mm/min cutting speed [76].

An alternative to traditional process suggested by Abrate and Walton [2] is laser cutting which does not involve mechanical forces and tool wear. Due to it small beam spot, complex shapes can be cut. Narrower kerf widths and faster cutting speeds can

be achieved by lasers compared to abrasive water jet. With lasers it is also possible to cut near the edges of FRPs [27,72,77]. As laser cutting is a thermal process, it causes some damage to CFRP as shown in Figure 20.

Kerf widths, Heat affected zone and Matrix recession

Craters

Delamination

Angle of the cut kerf
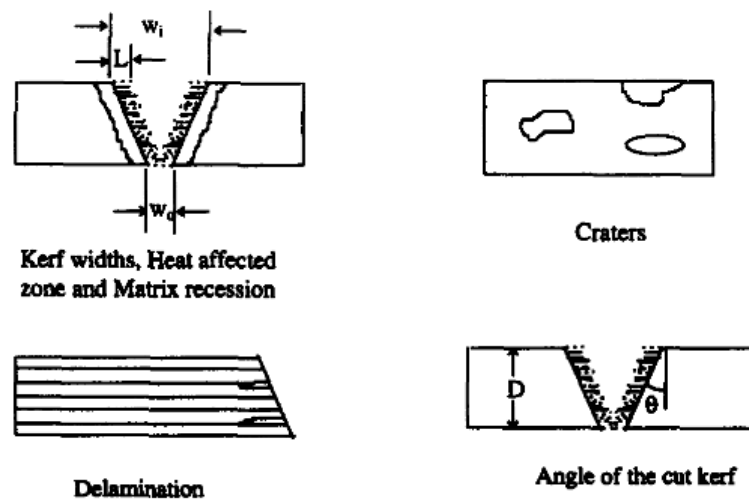
Figure 20: Damage caused by laser cutting [78]

As CFRP is an heterogenous material, the constituents have different thermal properties as material removal depends upon them, shown in Table 1. There are two types of matrix material: thermoplastic and thermoset. Thermoplastic matrix material cut by shearing of localised melt, whereas thermoset matrix is removed by chemical degradation that requires higher temperature and energy compared to thermoplastics.

	Density (g/cm³)	Decomposition Temperature (K)	Thermal conductivity (W/ (m.K))	Specific heat capacity (J/kg.K)	Heat of vaporisation (J/g)
Aramid fibre	1.44	820	0.05	1420	4000
Glass fibre	2.55	2570	1	850	31000
Carbon fibre	1.85	4000	50	710	45000
Polyester	1.25	670	0.2	1200	1000
Epoxy	1.20	700	0.1	1100	1100
Vinyl ester	1.25	650	0.2	1200	1000

Table 1: Thermal properties of FRPs constituents [78–80]

Higher temperature and energy are generally required to desiccate reinforcing fibres as compared to resin. Additionally, the anisotropy of CFRPs develop non-thermal

gradients inside the laminate [81]. These thermal gradients are one of the main factors of HAZ, matrix recession and delamination in laser cutting of CFRP and responsible for performance deterioration in both static and fatigue conditions. The cause effect diagram in Figure 21 shows the factors that has an impact on HAZ.
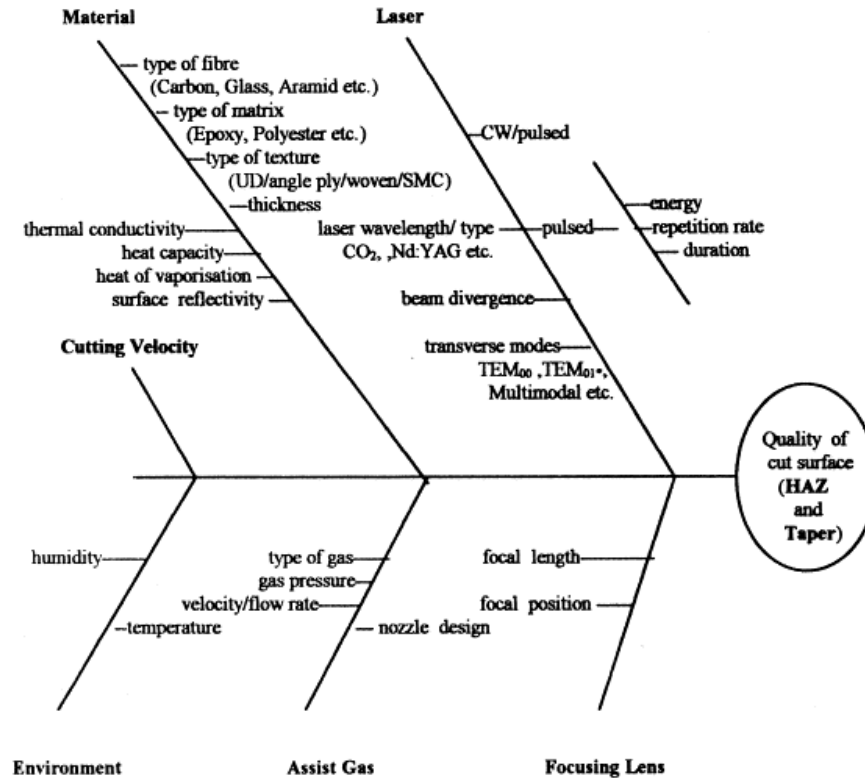
Figure 21: Cause effect diagram showing factors impacting HAZ [82]

In laser processing, the extent of thermal damage is mostly effected by laser power density and interaction time [15]. The relationship between power density and interaction time of common FRPs constituents is shown in Figure 22.
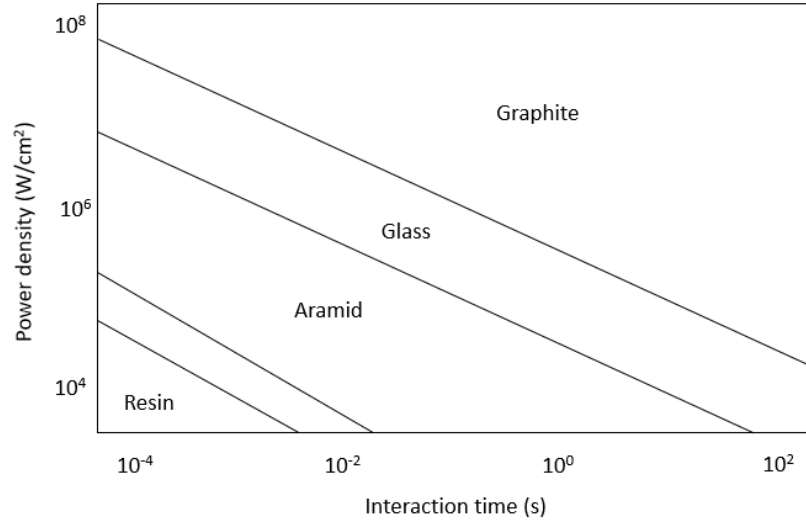
Figure 22: Power density and interaction time relationship for common FRPs constituents.

Dominant factors that influence the laser cutting quality of CFRP are laser power which controls the power density and cutting speed which controls the interaction time. By increasing the cutting speed and reducing the power, the HAZ extent, kerf width and depth and charred material is reduced [78]. This phenomenon is further explained by energy per unit length of laser cut, $\frac{P_0}{V_B}$ ratio, where P_0 is the laser power and V_B is scanning speed. The range of speed for better quality cuts is larger at higher power level when compared with lower power level. The minimum required $\frac{P_0}{V_B}$ ratio is dominated by the fibres with higher reaction temperatures compared to resin [78]. The power per unit length is governed by the speed, there is a minimal energy level at which a through cut is achieved with minimal thermal damage. This maximum speed above which no through cut is achieved depends upon power density and material thickness. A simple one parameter model for the maximum cutting speed for GFRP and CFRP was developed and evaluated by Caprino and Tagliafferi [83]:

$$V_{Bmax} = \frac{P_0}{\delta.D.d_B} \qquad (11)$$

where,

$$\delta = \frac{\pi\rho\lfloor L_v + C_P\ (T_v - T_0\rfloor}{4\eta} \qquad (12)$$

33

V_{Bmax} (mm/sec) is the max cutting speed, ρ (kg/m^3) is density of the material, P_0 (W) in beam power, d_B (mm) is the focal spot diameter, D (mm) is material thickness, L_v (J/kg) is the latent heat of vaporisation, C_p (J/(kg.K)) is specific heat capacity, T_v (K) is the vaporisation temperature, T_0 (K) is the initial temperature and η is the beam absorption coefficient. δ (J/mm^3) is a constant for a given material of given laser. The use of high beam power at max cutting speed reduces the thermal defects in continuous wave (CW) laser cutting of CFRP [83]. Pulsed lasers can also be used for CFRP [84] by delivering higher flux density in short pulses. As an example, 1 ms pulse of ruby glass laser can produce a flux density of 10^9 W/cm^2 [12]. The relationship of the laser pulse parameters for standard rectangular pulses is shown on Figure 23.
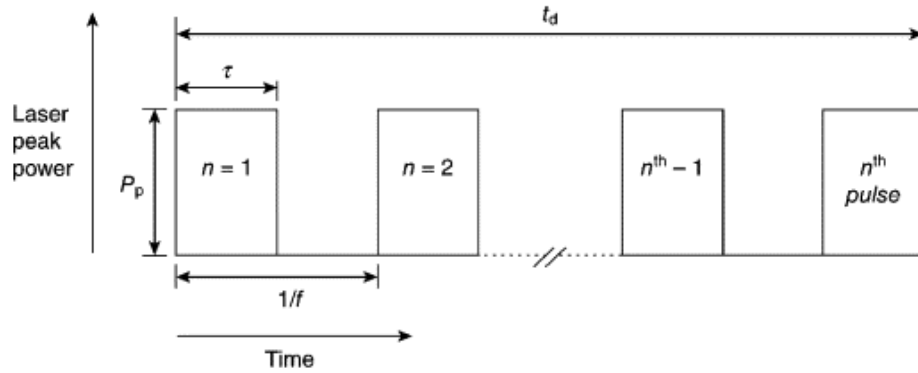
Figure 23: Laser pulse parameters for standard rectangular pulses [85]

Where P_p is the peak power, τ is the pulse width, f is the repetition frequency, t_d is the cutting time, n is the number of pulses and $\frac{1}{f}$ is the period between pulses. All the variables are interrelated to each other. In a laser pulse, the peak power delivered is depends on the pulse energy E_p and pulse duration τ.

$$P_P = \frac{E_P}{\tau} \tag{13}$$

Therefore, the irradiance I_0 in a pulsed laser beam is:

$$I_0 = \frac{E_P}{\tau A_0} \tag{14}$$

The maximum pulse energy is limited by the mean power P_0 delivered by the laser defined as:

$$P_0 = E_P \cdot f \qquad\qquad (15)$$

The average value of the laser irradiance in time and space within each pulse is given by equation 14 [84].

A pulsed Nd:YAG laser with high beam intensity, less interaction time and better focusing behaviour leads to less thermal load and less thermal damage of CFRPs when compared with CW CO_2 laser [84]. A parametric study was conducted by Mathew et al. [82] on laser cutting CFRP using pulsed Nd:YAG laser and observed that pulse energy is directly proportional to HAZ. Higher repetition rate and longer pulse duration combined with low cutting speed gradually increase the interaction time and produce larger HAZ.

Photo-ablation (ablative photodecomposition) is an alternative means to minimise thermal damage. It can be defined as a process of UV laser material interaction in which atomic and /or molecular bonds are broken down [86]. Each material has an ablation threshold which depends on its molecular bond energy. A photo-ablation occurs when a laser beam of photon energy equal to or above this threshold is used [86]. For example, a 193 nm (far-UV) wavelength causes ablative photo decomposition (APD) of organic polymers while 532 nm wavelength can ablate via distortion and melting [87].

Takahashi et al. [88] and Xu et al. [89] investigated the impact of laser wavelength on the cut quality by comparing infrared (IR) and ultraviolet (UV) lasers. Most polymer matrices are highly transparent to near infrared radiation wavelength around 1000 nm with absorptivity less than 15%, whereas carbon fibre has 80% absorptivity [90]. As a result, the bulk of the IR laser beam passes straight through the resin matrix and heats the carbon fibre directly. Therefore, the laser energy in mainly absorbed by carbon fibre and the matrix is heated by hot carbon fibres and not by laser radiation. CFRP is mostly processed by industrial lasers such as CO_2 (10.6 µm), YAG (1.6 µm) and excimer (UV) lasers. Whereas UV wavelength which has fewer thermal characteristics, induced electronic excitation. UV lasers perform much better than IR lasers in this aspect because both polymer and fibres absorb UV light much better

and provides outer shell electrons with enough energy to allow them to escape the organic polymer molecules or to break certain covalent bonds depending on photon energy. The polymer disintegrates faster and more efficiently than heat and promotes evaporation at the same time. Evaporation or ablation whether it has originated from thermal transition beyond gas point or molecular dissociation, contributes to reducing HAZ as the energy absorbed is conveyed away by the gas nozzle, rather than getting trapped in the material and dissipating inside. Hence, UV radiation provides more consistent processing quality than near infrared. However, UV lasers with high average power are not developed. CFRP do not undergo fusion reaction and hence the vapour column is not surrounded by melted material as it is in case of metals [81].

As discussed above small HAZ could be achieved by pulsed laser due to small irradiating time per unit pulse and cooling between pulses [91]. However, CW laser has a faster processing speed due to its high average power. Due to this pulsed industrial lasers lead to low output according to Fujita et al. [7]. With the help of 1-D thermal analysis, Weber et al. [92] determined that maximum cutting speed is influenced by average laser power. Matrix damage extent is typically dependent upon temporal beam intensity, which, can be increased by increasing average laser power, releasing energy in fewer and shorter pulses or by reducing the spot size optically. It was also concluded that if the laser spot size is reduced, the processing depth is also reduced. By reducing the peak power, the energy per pulse and average power is also reduced in pulsed lasers.

Herzog et al. [93] investigated the cut quality of CFRP by using pulsed Nd:YAG laser with pulsed duration between 0.5 ms to 50 ms, CW disk and quasi-CW CO_2 laser and concluded that the smallest HAZ of 0.6 mm was generated by Nd:YAG laser. For CW disk laser and CO_2 laser the HAZ observed was 1.2 mm and 1.4 mm, respectively. For a specimen of 1.5 mm thickness, the optimised cutting speed achieved is 0.1 m/min, 0.1 m/min and 1.5 m/min for pulsed Nd:YAG, CO_2 and disk laser, respectively.

Freitag et al. [94] concluded that with the use of low repetition rate and high pulse energy at same average power, HAZ could be reduced. Leone et al.[95] investigated laser cutting with Yb: YAG (Ytterbium-doped Yttrium Aluminium Garnet) pulsed by using kerf width and HAZ as quality factors and concluded that by using multi-pass technique and increased scanning speed, cut quality was improved. The cutting speed with selected parameters varies between 0.3 – 0.7 m/min. Leonne and Genna [96] use Yb:YAG laser to experimentally investigate the effect of processing parameters on kerf edge, HAZ and cutting region and concluded that pulse energy and cooling effect has an impact on cutting speed, kerf width and HAZ. They also concluded that by using multi-pass technique, HAZ and kerf geometry cold be reduced and improved. Other factors that can affect kerf width and HAZ are scanning speed and direction of fibres. The cutting speed with help of tuned process parameters such as an average power, pulse duration and pulse frequency, for 1 mm thick laminate the cutting speed and HAZ obtained was 0.6 m/min and 170-160 µm respectively.

In comparison to pulsed system with limited average power due to the complexity of their architecture, a CW laser with high power could be used to obtain high processing speed to meet industrial demands. CW lasers are prone to generate larger HAZ than pulsed laser, which can be minimised by using multi-pass technique and higher laser scanning speed [97]. Yb-doped fibre laser was used by Geoke and Emmelmann [8] to investigate laser cutting and confirmed that both kerf width and HAZ were reduced considerably when scanning speed is increased. Using the fibre laser with wavelength of 1.07 mm, the HAZ was between 440 – 450 µm. while using CO_2 slab laser (wavelength 10.6 µm), the HAZ was between 300 – 350 µm for a 1 mm CFRP sample. This may be attributable to high feed rate and higher absorption of CO_2 laser wavelength by polymer and organic material such as carbon fibres, in comparison to moderate absorption to Yb-fibre radiation by polymers.

Klotzbach et al. [9] also confirmed that HAZ is narrowed significantly with multi-pass and increased scanning speed. A 6 kW fibre laser was used by Bluemel et al. [10] to study the impact of processing speed on HAZ, it was concluded that HAZ reduced as the velocity increased and higher scanning speed is possible by using higher laser

power which reduces the HAZ. Jung et al. [98] used 16 kW disk laser to investigate laser cutting at high speed and achieved the best quality smallest HAZ. Additionally, to reduce the thermal effects, a dwell time of 1 s was used between passes. They concluded that cutting speed is inversely proportional to HAZ and kerf width. If the laser power is increased to 5 kW the processing time is reduced without impacting the quality. It was also demonstrated that the tensile strength of laser cut sample does not degrade mechanically and it was in good agreement with virgin CFRP samples.

Laser cutting of CFRP using 400 W fibre laser is used to investigate cut quality by Rao et al. [99] by assessing the effect of laser power, scanning speed and assist gas. Surface response methodology was used to statistically examined these factors on 1.4 mm thick CFRP sample. The laser power of 260 W with cutting speed of 4.5 m/min and gas flow rate of 14.23 l/min were the ideal parameters achieved. With these settings, kerf width of 163.71 μm and HAZ of 573.28 μm was experimentally achieved. Riverio et al. [100] investigated the impact of processing parameters on kerf, HAZ and cross section quality using CO_2 laser in both CW and pulsed modes. It was concluded that using a subsonic co-axial or supersonic off-axial assist gas jet produces similar HAZ. But if off-axis supersonic jet was used there is a tendency of overhanging fibres formation. If the laser power is set at 1.6 kW and cutting speed is between $2 - 4$ m/min, the excessive thermal stress is reduced, and better cut quality is obtained. CW fibre laser is used to investigate cut quality and morphology of cut surface using multi-pass and single-pass strategies by Li et al. [101] and concluded that micro cracks, delamination, holes and over hanging fibres are some of the defects detected using laser cutting of CFRP. Multi-pass strategy without dwell time between passes has a limited improvement in terms of HAZ when compared to single-pass strategy.

Cutting of FRPs in general and CFRPs in particular is a demanding task. The increase in demand of the applications of CFRP materials and absence of alternative cutting technique has led to extensive research and development in mechanical cutting as a dominant method. But mechanical cutting causes material damage and the rate of tool wear is usually high. Thus, proper selection of tool material, geometry and grade

and process data are required for high quality CFRP mechanical cutting. Therefore, for a particular application, a new individual equipment may be needed which is very costly [102]. Therefore, alternatives to mechanical cutting methods of CFRP materials are being investigated. Lasers have shown their potential to be industrially viable methods in the cutting of CFRPs. Lasers are found to be more of use in high speed cutting of thin CFRP laminates [84]. Lasers also benefited from their capability of being transmitted through fibre-optic, robot manipulation and automation. The challenging aspect of laser processing is to reduce thermal damage and maintaining high processing speed. Large HAZ, charring, resin recession and delamination are some of the quality defects, which are major obstacles for industrial applications of laser machining of CFRP composites. Based on previous research, this study used a single mode fibre laser to meet the industrial demands of high rate of cutting speed and low fibre damage (HAZ). The laser cutting experiments investigated the effects of cutting speed, number of passes, nozzle distance from the cut surface, nozzle diameter, double aperture and trenching on the extent of the fibre damage. Double aperture and trenching are a novel technique used to improve the state of the art for both fibre damage extent and cutting speed.

3.2. Laser Cleaning

One of the main reasons for using CFRP are their light weight and excellent strength. Different lightweight materials known as hybrid materials use CFRP and light weight metals such as aluminium to achieve ground breaking light weight manufacturing [103]. However, the joining technology must be suitable and cost effective for the combination of CFP and metals. The current state of the art for joining thermoset CFRP and light weight metals are either bonding using adhesives or mechanical fastening or combination of both technologies [104].

Adhesive joining of CFRP is a better technique as it does not damage load carrying fibres when compared with mechanical fastening by drilling holes, this also does not cause stress building around the joints. Additionally, the adhesive layer acts as an insulator which helps to prevent galvanic corrosion [105]. However, to increase the joining strength of adhesively joined parts, the surface quality of both parts needs to meet extensive requirements. Contaminants such as water or any other impurities from manufacturing process can adversely reduce the bonding strength and these impurities must be removed [106]. Further surface activation of both joining parts is required to increase the number of bonding sites. This increases the final bond strength of adhesives. In industrial manufacturing grinding, grit blasting and use of peel plies are common methods for CFRP treatment [107]. Using these treatment methods has its disadvantages such as low reproducibility of surface properties and fibre damage after mechanical treatment [108]. One method that finally replace peel plies or grit blasting is laser ablation as both former techniques produce water as by product and automation is difficult [109]. It is necessary to remove any mould release agents and other contaminants from previous manufacturing steps to high strength adhesive bond. This is very important as it is well established that adhesive bond strength depends on surface cleanliness before bonding.

A nanosecond, 355 nm Nd:YAG pulsed laser was used on surface of CFRP to ablate patterns without damaging carbon fibres to the depth of 10 – 12 μm investigated by Palmieri et al. [110]. They concluded that using laser ablation, an efficient, precise, and reproducible surface is prepared for adhesive bonding by eliminating physical

waste, reduction of process variability due to increased precision and surface preparation automation. Hartwig et al. [111] investigated treatment of epoxy-resin by excimer laser, the results showed that epoxy resin is decomposed at wavelength of 248 nm. The process also caused surface layer to become porous, which aided bonding. The strength of surface layer is high at low intensity treatment to get adhesively bond of high strength. The use of laser for cleaning surface enhances the reproducibility of strength. However, if high energy density is used, the surface became degraded, whereby the porous top layer's inner strength decreases resulting in decreasing bond strength.

The use of excimer laser treatment to control the adhesion performance of CFRP has been investigated by Fois et al. [112]. It was concluded that surface treatment using excimer laser can provide removal of organic material in selective manner without any damage to fibre reinforcement. It was also noted that fibre reinforcements were not degraded when intensive treatment conditions were used.

Wolynski et al. [113] systematically investigated the influence of the wavelength on CFRP ablation in terms of quality and process throughput using a pulsed picosecond laser using 355 nm, 532 nm and 1064 nm wavelengths. Using laser power of 10 W all three laser wavelengths shown similar ablation rates. The maximum HAZ observed at 1064 nm which was doubled when compared with HAZ at 523 nm. This also shows the liner dependency on the applied laser power. It was recommended to conduct further investigations on UV wavelength for focusing condition and ablation threshold.

Kamara et al. [114] investigated technical feasibility of low power CW CO_2 laser for ablating top resin layer of CFRP without damaging the carbon fibres with laser power of 14 W and scanning speed of 880 mm/s. Using a three 3D FEA model it was concluded that with proper control of the maximum temperature, without damaging the substrate, a top layer of resin can be removed.

The previous investigations on surface pre-treatment of CFRP for adhesive bonding using excimer laser radiation [115] concluded that by application of UV laser, the full

potential of the joint can be exploited. SEM micrographs and XPS spectra confirms the direct correlation between the quality of adhesive bonding and the removal of adhesives investigated by Kerling et al. [116]. It was also concluded that further investigations of the discrete release agent, the pure epoxy resin via XPS is required. Furthermore, mechanical tests such as peel-test and ageing behaviour of excimer laser treated CFRP are required for process reliability.

As a contactless method, one of the advantages of laser ablation is cleaning and activating surfaces in single step process. For laser ablation CFRP, different types of lasers must be examined [117]. In the case of IR laser, they have high transmission coefficient to epoxy resin which causes the laser energy to pass through resin polymer and absorbed [118]. This energy caused the removal of epoxy matrix and unintentional recoil pressure ejecting parts of the matrix [119]. Due to this the use of IR lasers are usually dismissed for laser ablation [120]. However, some researchers suggested that bonding strength could be increased by stripped fibres due to IR radiation [121]. Recently further investigations were carried out using UV lasers. The fibre damage can be completely avoided using a UV laser due to its higher absorption coefficient. Furthermore, ablation is more controlled and occurred by breaking molecular bonds [122]. Laser ablation can be used to etch selectively without damaging fibres underneath unlike a nonselective process such as mechanical abrasion [123].

In other applications laser surface cleaning is a proven method, avoids all the disadvantages of other techniques and clean all contaminant residue [124]. Laser cleaning did not require any surface preparation, unlike mechanical techniques and if correct parameters were used, avoids further fibre damage. Additionally, laser processing is suitable for preparing large surface area, can be automated and delivers consistent results. Laser cleaning process is readily used in metals and non-metals for surface treatment. However, this study uses a novel approach which uses lasers to clean the glue remained on separated CFRP parts that were previously joined with adhesives. Although lasers are used to clean metals and composites alike, however, the technique developed in the study was never attempted before to clean the glue

from the damaged composite components and contribute to net zero remanufacturing of composites.

3.3. Summary

Cutting CFRP in particular is a challenging task, the increase in demand and absence of alternative cutting methods has led to extensive research in mechanical machining. However, in mechanical machining, tool wear and material damage is usually high, which may require secondary work or part rejection. Therefore, alternative methods of cutting CFRP are being investigated. Amongst them are EDM and WEDM. These methods are limited due to very low material removal rate, high tool wear and thermal damage.

Abrasive waterjet has shown to be industrially viable method in cutting of thicker CFRP laminates. AWJ is associated with low thermal and mechanical forces, high jet pressures, low stand-off distances, small abrasive particle size and small nozzle diameter. This makes AWJ ideal for cutting CFRP. However, use of water can cause moisture build up at surface and delamination due to high velocity impact. Osmotic erosion can also occur, and this is a process in which water penetrates the material and causes degradation. Due to tool size and its dimension, these methods have failed to cut small or complex shapes.

Lasers cutting benefits from their capability of being transmitted through fibre optic, ability of robot manipulation and automation. However, the challenge for laser processing is to reduce HAZ and maintain high cutting speed. Major obstacle for industrial applications of laser cutting of CFRP composites are large HAZ, charring, resin recession and delamination due to intense thermal effects.

CHAPTER 4

4. Laser Cutting of CFRP

New opportunities have been created by high power fibre lasers for application that requires high beam quality, smaller focused beam size and low power usage. Therefore, fibre lasers are being used for high speed and high quality cutting [125]. Particular application of the fibre laser in laser cutting and its success in metal cutting [125] drives the investigation in its capabilities of CFRP laminates. This chapter presents the experimental findings of laser cutting of CFRP using a single mode fibre laser and results were studied on process window defined in terms of cutting speed, no of passes, nozzle distance from surface and nozzle diameter. Thermal effects were analysed using scanning electron microscope (SEM) and optical microscope (OM). The HAZ was further optimised using double aperture and trenching. Regression analysis was carried out and five models for CAD/CAM interface were developed.

4.1. Overview

Laser cutting process can produce high quality cuts consistently mainly due to the high control of processing parameters. The significant factors in laser cutting of composites are [126]:

- Laser power
- Cutting speed
- Standoff distance cutting head and work piece
- Linear speed
- Number of passes
- Nozzle diameter
- Cooling gas pressure

Major disadvantages associated with laser cutting are the changes in the material and its strength due to HAZ, decrease in cutting efficiency with increase in thickness of the composite work piece and kerf taper formation [127]. Laser cutting also produces

hazardous chemical by-products such as fragmented powders of fibres, molecular organic compounds and formation of CO and CO_2 at high concentrations [91].

4.2. Equipment and Methodology

4.2.1. Description of Material

The type of CFRP investigated is 12k standard modulus carbon supplied by INVENT GmbH (www.invent-gmbh.de). The samples were in the form of 100 x 100 x 2 mm flat plates and consisted of 8 thin layers. The fabric layout is detailed in Table 2. The matrix type used in the material is medium viscosity epoxy resin. The resin is designed to use in mass production of structural automotive parts such as frame, chassis, floor panels, firewalls and monocoque structure.

Layer	Fibre description
1	150 gsm 0^0/90^0 12k standard modulus carbon
2	148 gsm $+45^0$/-45^0 12k standard modulus carbon
3	148 gsm $+45^0$/-45^0 12k standard modulus carbon
4	150 gsm 90^0/0^0 12k standard modulus carbon
5	150 gsm 0^0/90^0 12k standard modulus carbon
6	148 gsm -45^0/$+45^0$ 12k standard modulus carbon
7	148 gsm -45^0/$+45^0$ 12k standard modulus carbon
8	150 gsm 90^0/0^0 12k standard modulus carbon

Table 2: 2mm CFRP fabric layout

The weaving pattern was wider than the readily available CFRP material. The fabric layers were weaved using transparent or semi-transparent textured polyester thread.

4.2.2. Measured Characteristics

The definition of measured features on samples after laser cutting is provided below:

- **Surface profile** – This measurement performed by Elcometer E123A, examines the local depth of surface features on the edge of the kerf. The depth is measured against a plane defined by at least three of the highest peaks of the surrounding area defined by the reference flange diameter of the

tool. An average is taken as a final characteristic value by repeating the measurement on the various points of the edge of the cut.

- **Fibre damage (HAZ)** – The measurement represents the extent of damage and broken fibres individually or in small batched of 2 to 5. Loose fibres are not counted as broken or damaged.

- **Epoxy removal** – It is a measurement of how far the top sealing epoxy has been removed from the edge of the cut on the irradiated side.

- **Top delamination** – The measurement of the thickness / depth of a layer which detached from the bulk body of the sheet, measured on the irradiated side and on the edge of the cut.

- **Bottom delamination** – The measurement of the thickness / depth of a layer which detached from the bulk body of the sheet, measured on the beam exit side and on the edge of the cut.

4.2.3. Experimental Equipment and Setup

The laser cutting trials were performed using a SP-1500-CW diode pumped single mode fibre laser. The specifications of the laser are shown in Table 3.

Characteristics	Values	Units
Power	1500	W
Wavelength	1080 ± 2	nm
Pulse duration	10	µs
M^2 (beam quality factor)	1.3	-
Beam divergence	82	mrad
Spot size	28	µm

Table 3:Laser characteristics used in cutting trials.

The laser beam was delivered into a laser processing station containing an XY motion stage that holds the CFRP sample (Figure 24). A process viewing window with laser filtration protection was used to view the laser processing station. A 200 mm focal length fibre was attached in a collimation and refocusing optical system and a 1:1 height adjustable demagnification ratio (Figure 25). Manual adjustment of the

focussing optics is allowed for the optical system, this brings the focal position in reference to the purge gas jet nozzle and the rest of the mechanics. Through an exchangeable gas jet nozzle of different aperture / orifice, an argon jet gas was coaxially delivered with a beam. A single aperture and double aperture were the two types of gas jet nozzles used in the trials. A single aperture was a standard gas jet nozzle, whereas in double aperture, an internal ring is inserted in the nozzle forming a second aperture. The double aperture was used for delivering more collimated jet gas for deeper cuts.
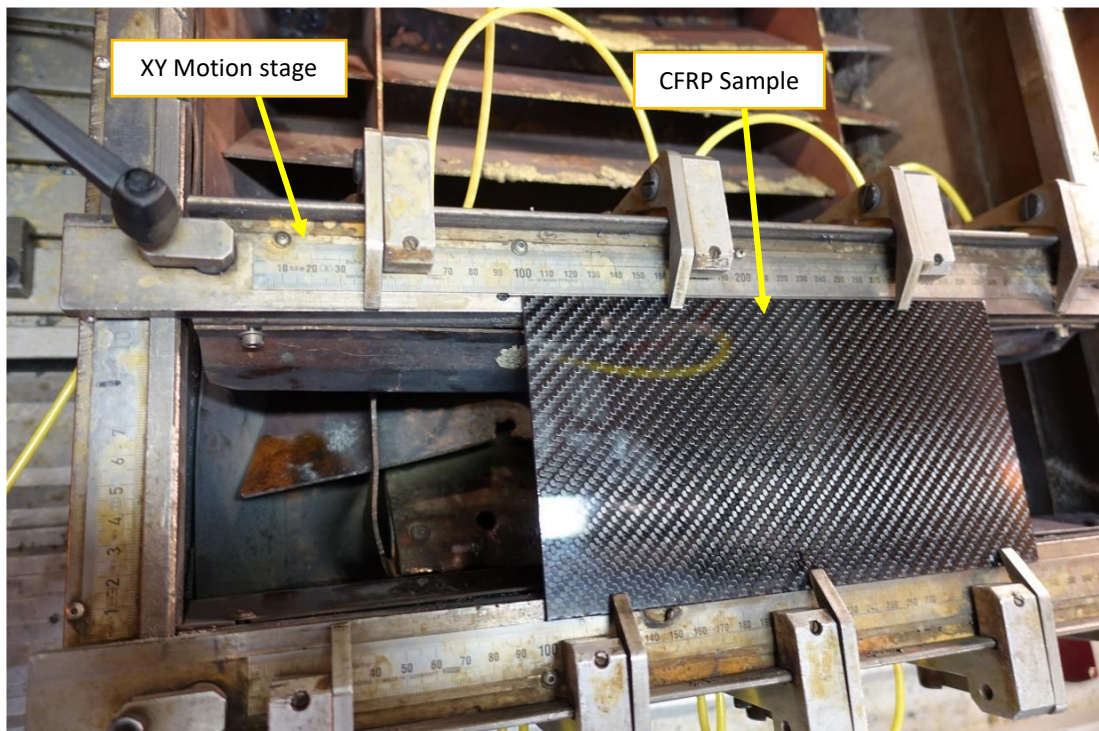
Figure 24: Sample clamped in XY stage of processing station.
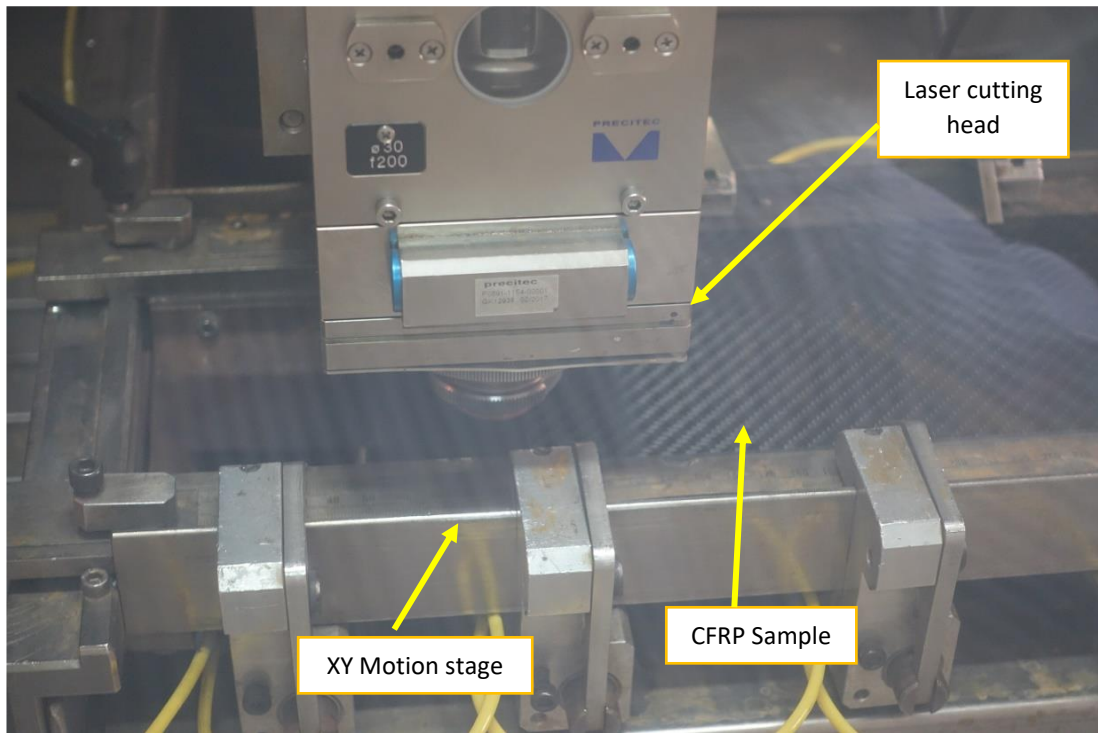
Figure 25: Focussing optics system placed over a sample.

For microscopic analysis, a 10x magnification eyeloop with 100 μm graduation reticule, 60 to 100x magnification compact microscope with 10 μm graduation reticule and 50x magnification USB microscope with 50 μm graduation reticule was used.

For process monitoring, a Sony RX100 IV high frame rate camera at 1000 FPS, with Exmor RS 4k sensor in Cyber-shot configuration and a Zeiss Vario-Sonnar F1.8 lens was used. The camera was used to record videos of the process through the station's viewing window. A Flir digital thermal imaging camera with recording capability of 320 x 240 pixels and thermal sensitivity of 0.1 ^{0}C with manual focussing was used for recording thermal images and videos during processing. For surface depth measurements assessment, Elcometer E123A-M with a tungsten 60 ^{0}C full angle conical pin ending to a 50 μm diameter tip was used.

4.2.4. Design of Experiments

The quality in laser cutting composites is assessed by response to variation of one process parameter in time. This process required an extensive experimental run which could be lengthy and expensive in terms of process and materials required.

Using this approach, it is very difficult to investigate the interaction effects between two parameters. Statistical analysis has been diversly accepted in experimental research studies to minimise the experimental runs and optimise the quality during the process [82], [128], [129]. This allows the main effects and interactions to be evaluated with minimum experiments. The statistical experimental design can be customised depending on the desired number of experiments and suitable order of experimental runs. For laser cutting in CFRP, these effects both material usage and research time [82]. 30 laser cuts were made for the investigation, all parameters and measured characteristics describing each cut are listed in Appendix A. Regression analysis using the laser cutting parameters and results was carried out in Appendix B. Images of laser cut surface are in Appendix C and Appendix D. SEM images of laser cut surfaces are in Appendix E.

A total of 7 test sets were conducted, process parameters are shown in Table 17, Table 18 and Table 19 of Appendix A. Cuts 46b to 50, replication of process parameters for comparison and assessment of speed effects. Cuts 51 to 54, investigation of multi-pass effect, cuts 51 to 54, investigation of stand-off distance, cuts 59 to 63 investigation of large diameter aperture and multi-pass, cuts 64 to 68, investigation of trenching, cuts 68 to 72, investigation of double aperture and cuts 73 to 75, verification of good results. Trials 1 to 46 have not mentioned since they were for initial trials and testing purposes only.

4.3. Results

For the investigation, a total of 6 test sets were conducted. The purpose of these sets was as follows:

- Assessment of cutting speed
- Investigation of multi-pass effects
- Investigation of stand-off distance
- Investigation of large diameter aperture
- Investigation of double aperture
- Investigation of trenching

4.3.1. Assessment of Speed

Several experiments were carried out to investigate the impact of cutting speed. The averaged results of measured parameters with power kept constant at 1.5 kW, number of passes at 1, 1.0 mm nozzle aperture and 16 bar gas pressure are shown in Table 4. With these conditions, it was possible to split the CFRP sample completely. It was also observed that the cutting speed is inversely proportional to HAZ (fibre damage) but directly proportional to epoxy removal and top delamination.

Trials	Cutting speed (m/min)	Fibre damage (µm)	Epoxy removal (µm)	Top delamination (µm)	Bottom delamination (µm)
Multi-pass	3.3	89	400	128	60
Stand-off	2.8	48	312	120	53
Large nozzle	3.2	99	283	134	88
Trenching	9.4	31	196	135	102
Double aperture	3.8	59	157	142	100

Table 4: Averaged laser cutting characteristics of measured parameters.

Significant fraying was observed in the experiment from the top of the material as shown in Figure 26 . This behaviour is associated with the loose weaving of the sample with large distance between weave knots. The fraying fibres belong to the bottom and top layers and can be seen in the microscope images of the edge as shown in Figure 27. Scanning electron microscope (SEM) micrographs also confirmed the results shown in Figure 28.
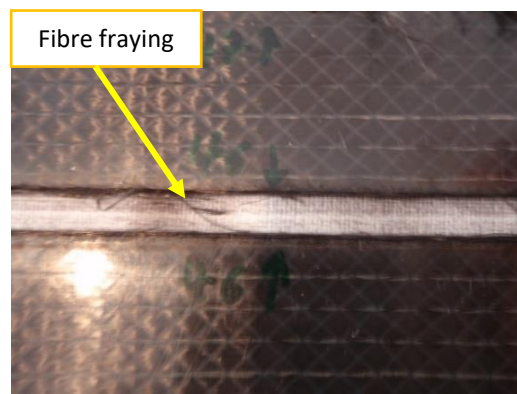
Figure 26: Test cut at cutting speed of 2.5 m/min.
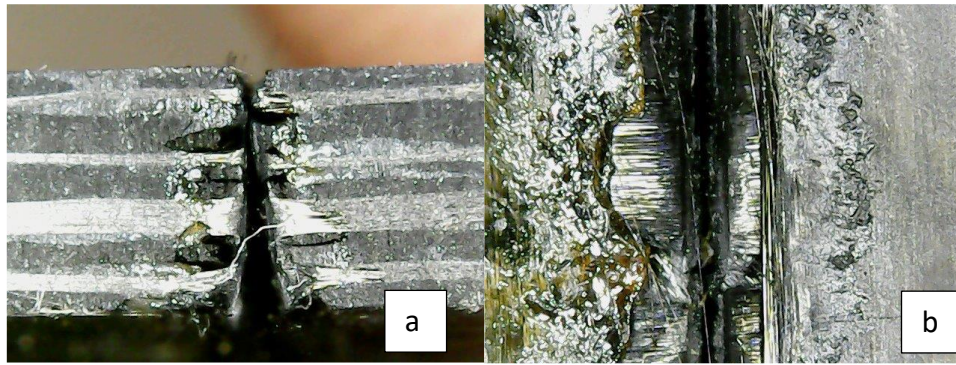
Figure 27: Microscopy images of trials using 1 pass, 2.5 m/min cutting speed and 16 bar gas pressure and 1 mm gas nozzle. (a) side view, (b) top view.
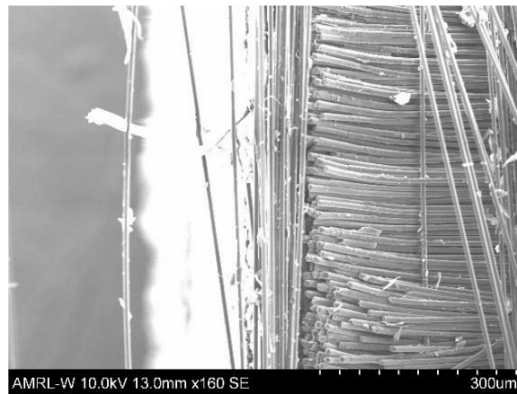
Figure 28: SEM micrograph showing significant fraying.

4.3.2. Investigation of Multi-pass Effects

The multi-pass effect was investigated by increasing the number of passes from 1 to 3, with every incremental step the speed was also proportionally increased to maintain the cutting speed at 2.5 m/min, e.g., 2 and 3 passes were performed with scanning speed of 5 and 7.5 m/min, respectively. It was noticed that by increasing the number of passes fibre damage and top delamination was reduced. As the linear speed further increased to 10 m/min, fibre damage, top delamination and epoxy removal is further reduced but the bottom delamination increased by 60 μm. This damage was probably induced during the 3rd pass where pressurised gas and excess laser radiation forces the lower layer of fibres out of position.

Executing at high scanning speed of 10 m/min but with 2 passes, the quality of measured characteristics decreases apart from epoxy removal which reached 180 μm. The sample cut at cutting speed of 2.5 m/min and 3 passes showed no fraying (Figure 29) and SEM micrograph showing fibre damage at 65.6 μm (Figure 30). The

51

effect of multi-pass technique on measured characteristics as averaged valued are shown in Table 4.
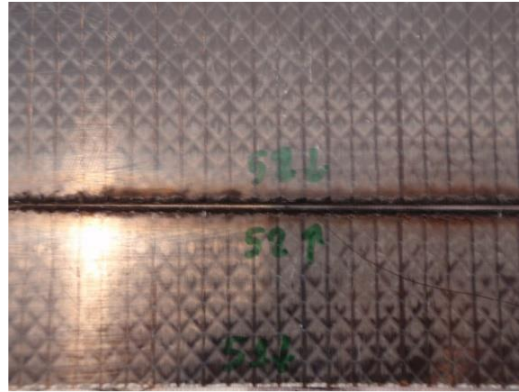
Figure 29: Test cut with no fraying.

AMRL-W 10.0kV 12.4mm x351 SE   100um
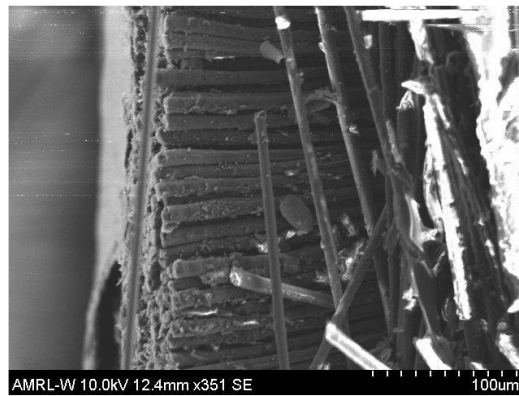
Figure 30: SEM micrograph showing HAZ at 65.6 μm.

4.3.3. Investigation of Stand-off Distance

The optimisation of stand-off distance did not show any noticeable improvements in measured characteristics. There was some visual improvement observed in terms of fibre orientation and delamination. The stand-off distance was eventually set to 1.3 mm as a compromise between tested values.

4.3.4. Investigation of Large Aperture Diameter

There was not any significant improvement of measured characteristics and quality aspects once the nozzle aperture increased from 1.0 mm to 2.0 mm. The fibre damage and bottom delamination was increased by a factor of 1.5 and 2, all other characteristics remained within the average range. Table 4 shows the measured

characteristics of nozzle aperture at 2.0 mm. Photograph of test sample using 2.0 mm nozzle and 3 passes with significantly less fraying is shown in Figure 31.
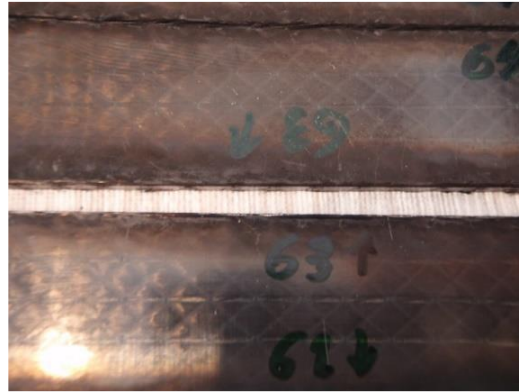
Figure 31: Test sample using 2 mm diameter nozzle and 3 passes.

4.3.5.Investigation of Double Aperture Nozzle

The double aperture nozzle resembles the normal single aperture nozzle. The difference in the double aperture is in the cone insert which has a smaller aperture itself. The radial blades are used to suspend the cone insert, this draws air flow annularly through a large aperture and axially through the centre of the smaller aperture. The cross-section schematics of the double aperture is shown in Figure 32. Double aperture nozzle was mainly used to cut thicker material by generating a thin flow of air that maintains its size after exiting the nozzle. The double aperture has an outer diameter of 2.0 mm and an inner diameter of 1.5 mm.
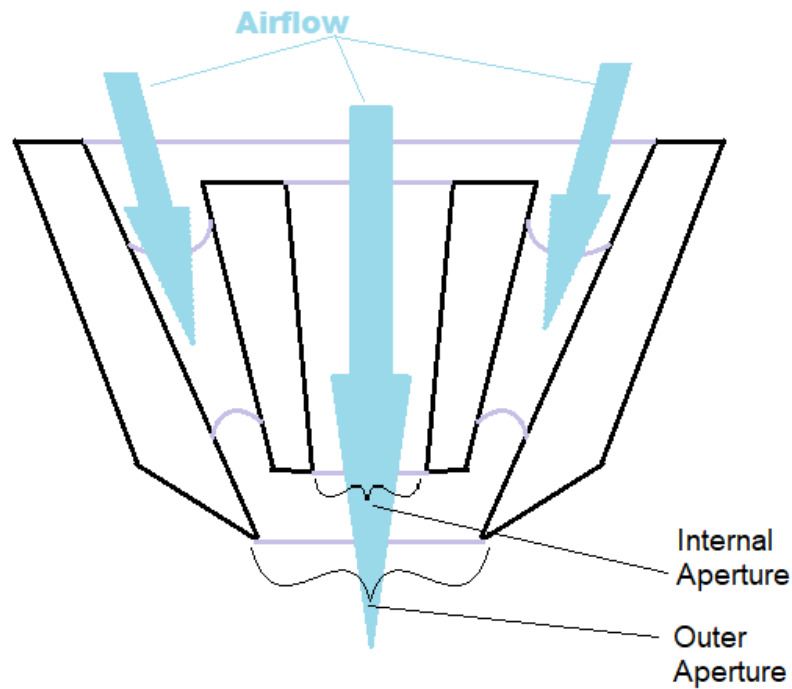
Figure 32: Schematic of an inductive cross-section of the double aperture nozzle, also showing the direction of air flow.

Averaged measured characteristic using double aperture are shown in Table 4. Fibre damage between $30 - 80$ µm was obtained using double aperture. Notably the epoxy removal was reduced to an average of 157 µm. This is comparatively less than the average of 341 µm for cuts using a 2.0 mm aperture and 345 µm using a 1.0 mm aperture nozzle. The double aperture nozzle works by generating a flow of high-pressure air directed downwards on the surface and less air is directed radially. This reduces the pressure that forces the top epoxy layer away from the laser radiation or gas flow during processing.

4.3.6. Investigation of Trenching

While using the multi-pass technique, it was observed that measured characteristics were still high. To overcome this issue, an approach to widening the kerf was investigated. Trenching is obtained by traversing three parallel lines besides each other. The purpose is to open a channel or trench which is wider than the channel opens by a single beam. Once the trench gap is defined, the centre of the beam is placed at either edge of the defined trench gap, i.e., the trench achieved is expected

to emerge wider than this gap. Once the gap was opened by 2 passes, a beam passes the third time through the centre of the trench. This approach provides better means of entry to the deeper levels of the material without impacting the edges with laser power that may be required to process these levels (Figure 33).
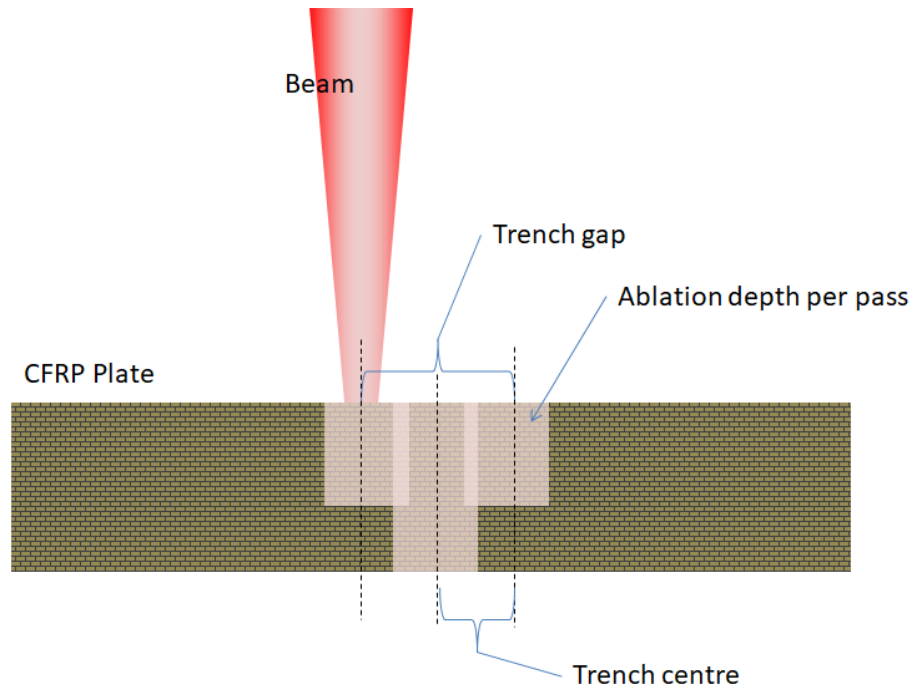
Figure 33: Schematics showing the position of the trench cut lines in relation to the kerf / trench centre.

The results of the cutting characteristics for trenching are shown in Table 4. Two trench gap settings of 50 µm and 100 µm were used for trials at high scanning speed of 15 m/min. However, this failed to separate the sample. Full cuts were achieved at comparatively less scanning speed of 7.5 m/min. Best results were achieved with a 1.0 mm nozzle and a 100 µm trench gap. A trench gap of 50 µm achieved better results in terms of epoxy removal of 55 µm. Most of the results were good with negligible fraying.

An exceptional overall performance of trenching compared with single-pass and multi-pass approaches is shown in Figure 34. With trenching, an average fibre damage of 31 µm and epoxy removal of 196 µm was obtained when compared with other techniques (Table 4).
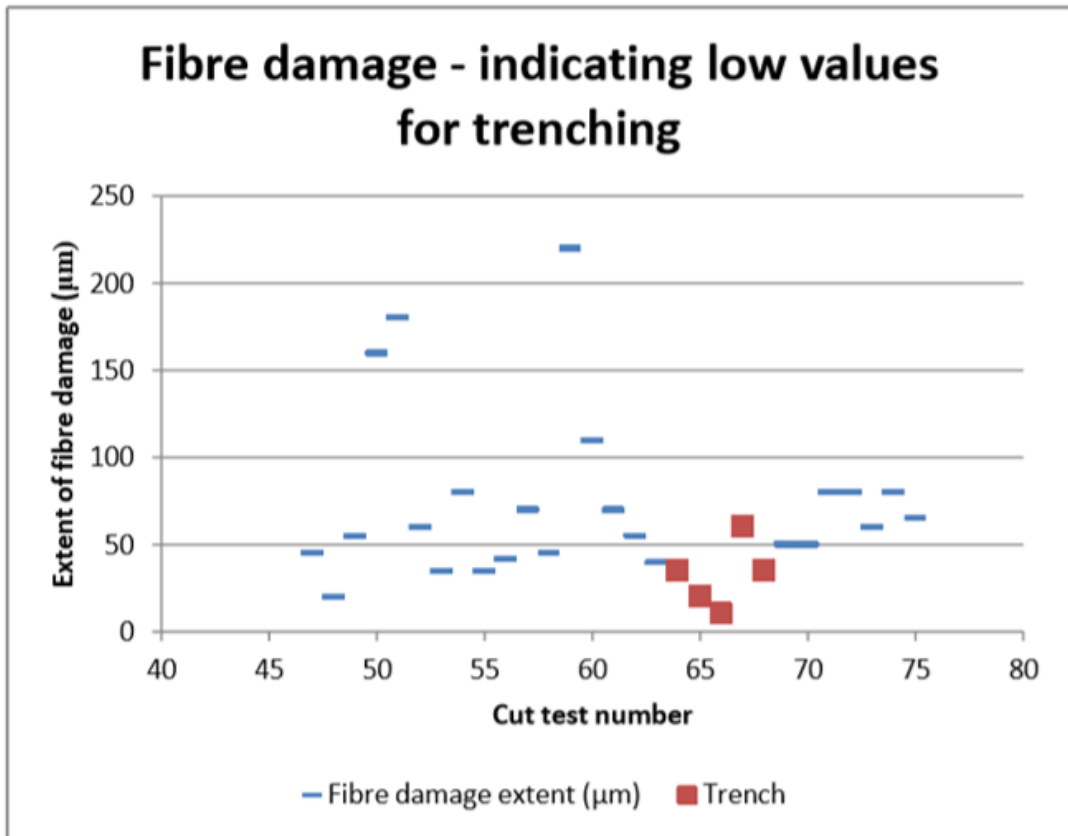
Figure 34: Extent of fibre damage per cutting test and emphasizing the test results obtained with the use of trenching.

4.4. Discussion

4.4.1. Optimisation and Thermal Guidelines

The epoxy removal was improved using a double aperture, achieving an average of 157 µm from the overall average of 308 µm without double aperture. With trenching the lowest epoxy removal obtained was 110 µm but without trenching it was 130 µm. Figure 35 shows the average of epoxy removal and top delamination per test speed.
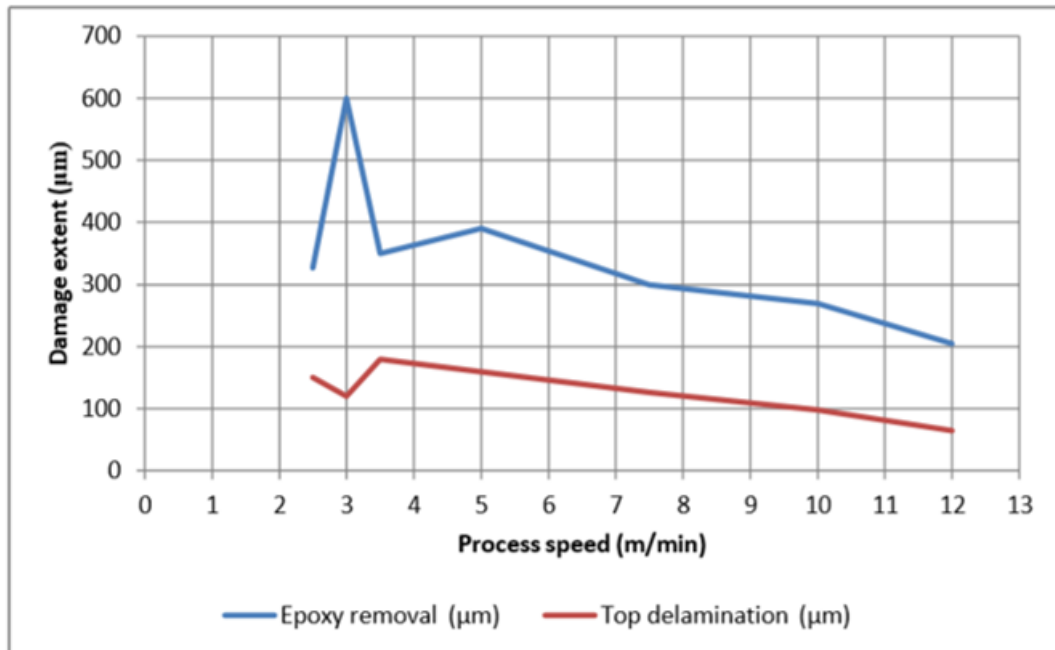
Figure 35: Measurement of epoxy removal and top delamination per test speed.

The plot indicated that increasing the processing speed by adding number of passes can improve epoxy removal and top delamination, this is due to low beam dwell time (dwell of a beam over the area that needs to be irradiated), during the process. This allows the material to dissipate before causing further damage with the next pass. Hence, the multi-pass technique delivers the same amount of energy per irradiated area over a longer time scale, which reduces the temporal energy density during each pass. This process has a greater impact on the top surface of the material as it is exposed to higher levels of direct optical energy resulting in greater localised thermal energy build-up.

Fibre damage extent remains below 100 μm apart from cut 50, 51, 59 and 60 when fibre damage was 160, 180, 220 and 110 μm respectively. Cut 51 was made using gas pressure of 8 bar and flow rate of 83 lt/min. Cuts 59 and 60 were made using large aperture nozzle and as mentioned in section 4.3.4 there was not any improvement of measured characteristics. With trenching (cuts 64 – 67), better-quality cuts and good characteristics have been achieved when compared with other process parameters. Highest epoxy removal extent of 740 μm was obtained for cut 73 using multi-pass technique. Cut 59 has epoxy removal extent of 560 μm and highest top delamination of 260 μm using large aperture nozzle. Highest cutting speed of 15 m/min was achieved for cut 64 (Table 18) and cuts 65 to 68 has second highest cutting speed of 7.5 m/min (Table 18) using trenching. The chart of performance improvement comparison with measured values are shown in Figure 36.
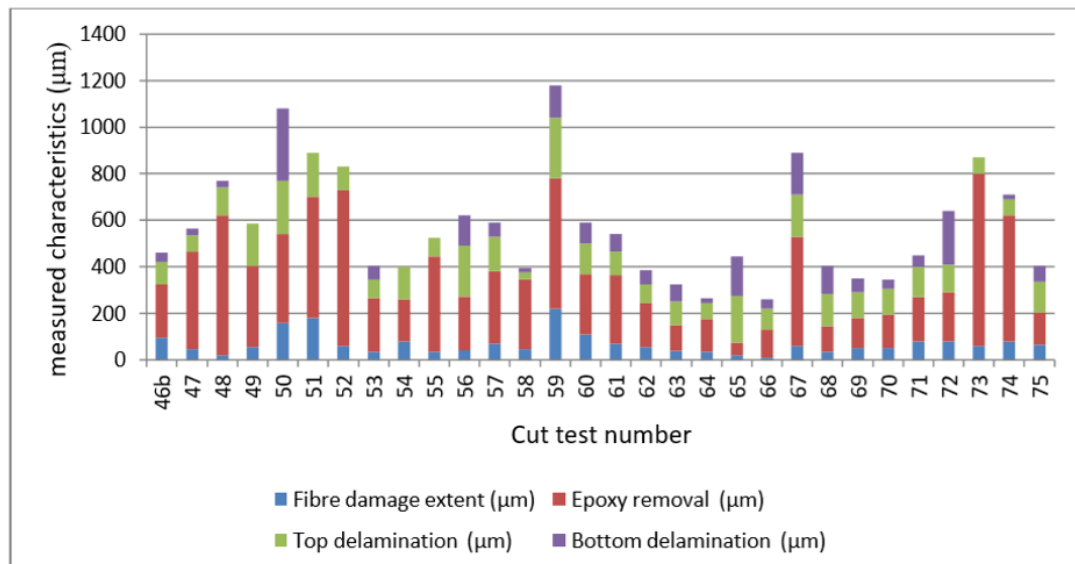
Figure 36: Chart showing the measured cut quality characteristics of each cut.

Cuts from 67 to 71 were carried out using trenching by maintaining the beam intensity whereas, the overall energy per unit area delivered through out multi-pass process is reduced. This causes sudden shuttering of the material.

4.4.2.Shuttering of Fibre Bundles

In materials such as steel and polymer, laser cutting can leave behind striations along the cutting length, with parallel orientation to the beam emission direction. This has

only been observed on samples which was subjected to multi-pass at higher speeds (Figure 37). These striations are presumed to have occurred from a possible small misalignment of the multiple beam passes. It is highly unlikely that the beam can bend, deflect, and cut individual weaving layers at different vertical positions with a distance between them of several hundred of microns. Instead, the phenomenon resembles the behaviour of a glass, when shattering or being subjected to thermal cleaving techniques with laser or other methods. The behaviour, which is observed in most trials conducted and explained as a layer-by-layer shattering effect. The layers corresponding to the weaved bundles, behaving as material of a glassy or crystalline nature.
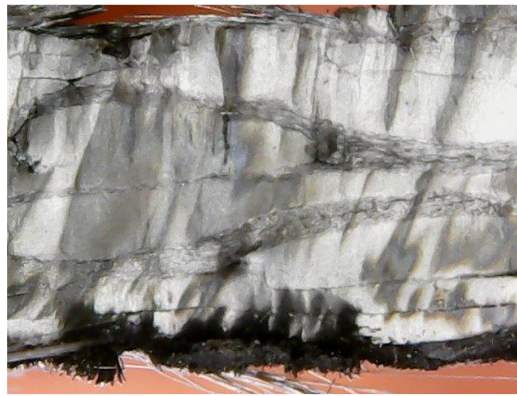
Figure 37:Surface undulations lengthwise for multi-pass cut.

As the carbon fibres are expected to demonstrate large tensile and yield strength, but very litter plastic deformation, it is likely that the weaving bundles behave as extremely rigid strands of material that instead of melting or plastically deforming when subjected to very high temperatures, they shatter at the weakest point of the bundle. These weak points can be distributed randomly along the bundle. Additionally, considering that temperature conduction is also affected significantly by the weaving direction and contact of the fibres in the bundle, the thermal gradient is not homogenous across the bundles in the material and thus the points prone to shattering are expected to be scattered at the microscopic scale.

Considering the above, two scenarios are proposed to explain the shattering behaviour of the material under intense laser irradiation with a small beam, in conjunction with the large surface level variations.

The first scenario assumes that the material is semi-transparent to the beam's wavelength. Presently, this was not the case as the material appears black to the visible spectrum, thus fully absorbent. The binder may or may not be black coloured as most polymers and epoxy binders are transparent in the visible spectrum and much more transparent in the near IR wavelength of laser emission. If optically absorbent, the assumption is that it vaporises instantly around the beam or is displaced between the fibres, thus allowing the beam to propagate through the fibres. Fibres were assumed to originate from poly-arcylonite (PAN) however, it was not certain whether they have been just oxidised, stress graphitised or carbonised at high temperature and inert atmosphere.

This plays a significant role in the optical absorption characteristic of the fibres. A full carbonised at high temperature generates true graphite rings, whose pi-bonds absorb a very wide spectrum of light. The other two methods do generate ring-based polymer fibres; however, the electronic absorption band of those rings is limited due to the inclusion of nitrogen and oxygen atoms in the circular monomers.

Near IR radiation may well be transmitting or partially transmitting through these molecules. Therefore, in this first scenario, the beam heats up the layers by transmitting through them, either due to inherent transmittance or induced transmittance via photonic transformation. Heat conduction and thermal gradients across the weave bundles is different for each one, thus, the breakages can follow a jiggered line through the thickness of the material (Figure 38 (a)), defined by the points of higher temperature gradient as well as local material weakness in each bundle.
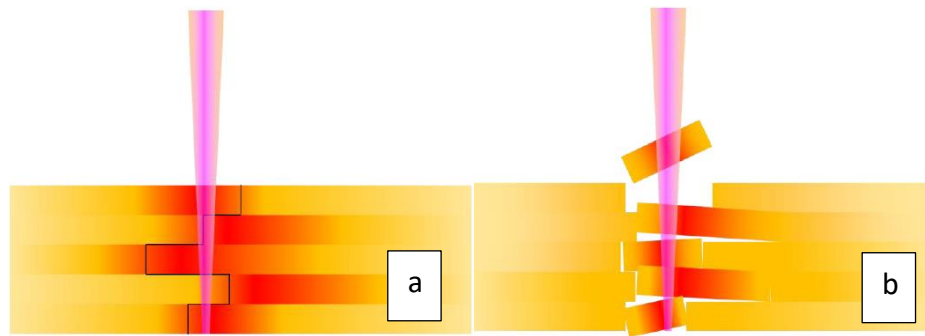
Figure 38: (a) First scenario, a crack propagating through the points of greatest thermal gradient in each bundle, (b) Second scenario, blocks of material from each bundle, snapping off, either side of the axis of the highest temperature.

The second scenario still considers that bundle breakages occur at points of highest temperature gradients and thus temperature induced stress (Figure 38 (b)). Nonetheless, these happen around the beam and thus forcing pieces to be ejected from the material's body during irradiation. They are then propelled away from kerf, most likely from the evaporation of binder matrix. In this scenario, the beam shatters and removes block by block of the material in the area being irradiated and thus manages to penetrate all the way down to the bottom of the material. The scenario is applicable with the fibres being absorbent at 1 μm or having any degree of transparency. The block removed are uneven in size, through the depth of the cut due to variations in the weaving direction and other material inhomogeneities.

Both scenarios explain surface level variations on the kerf edge and accept the glassy behaviour of the bundles under thermomechanical stress and large temperature gradients. Consequently, a higher average power by few kW and corresponding beam intensity at the target, will not result in a much smoother kerf edge, unless if transgressing of several tens of GW/cm^2 of beam intensity.

Higher power can be used to increase processing speed proportionally, with more or less the same finish being achieved. Better control of the surface finish at the kerf can be obtained via a much higher photon energy, e.g., by green, blue or UV photons, or by processing with ultrashort laser pulses and thus peak intensities of several GW/cm^2 towards TW/cm^2.

4.4.3.Thermographic Analysis

Thermographic analysis was carried out to characterise the trenching technique using a remote thermal camera that provides information of the highest recordable temperatures. A maximum temperature reading of 71.2 ^{0}C was recorded during the first trench pass; for the second and third passes the temperature recorded was 44.2 ^{0}C and 96.7 ^{0}C, respectively (Figure 39). These temperature recordings show the maximum temperature that the material reaches during the cutting process. Also, the material does not undergo any significant thermal loading that may distort its shape as the maximum temperature recorded was below 100 ^{0}C in all tests, which was few hundred degrees of Celsius below the melting temperature of the CFRP material.
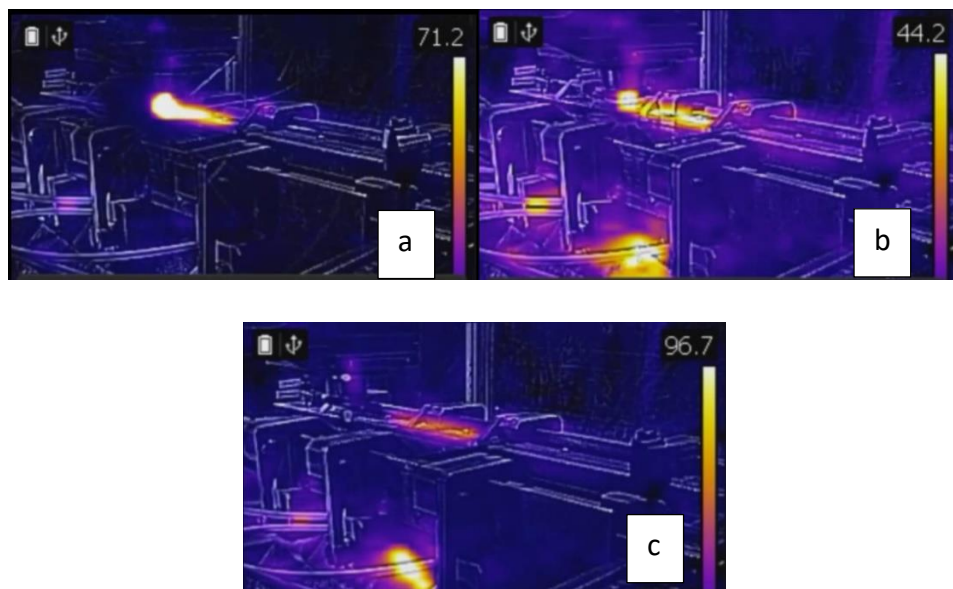
Figure 39: Thermal images of Trenching, (a) First pass, (b) Second pass, (c) Third pass.

4.5. Regression Analysis

For regression analysis, Response Surface Methodology (RSM) was used. RSM is widely used in statistics to find best operating conditions to increase the efficiency of the process and used when several input parameters having an impact on the performance or on the output of the model. RSM allowed an appropriate mathematical equation between dependent and independent variables. In this study

RSM is used to develop mathematical models behind the CAD/CAM interface for quick adaptation of the process parameters.

Five models have been developed to different variations in properties and are presented in Appendix B. One of the models is presented in equation 16, this defines the causes of fibre damage between 55 to 95 μm. the input and output control parameters are shown in Table 5, whereas the parameter definitions, contour plots and coefficients are presented in Appendix B.

$$y_{55-95}(\mu m) = \epsilon_2 + \beta_9 x_{SZ} + \beta_{10} x_{CS} + \beta_{11} x_{ND} + \beta_{12} x_{NP} + \beta_{13} x_{SZ}^2 + \beta_{14} x_{CS}^2 + \beta_{15} x_{NP}^2 \qquad (16)$$

Contour plot of fibre damage between 55 to 95 μm with respect to cutting speed and stand-off distance is shown in Figure 40.

Parameters	Units	Annotation
Standoff Z	mm	x_{SZ}
Cutting speed	m/min	x_{CS}
No of passes	-	x_{NP}
Nozzle diameter	mm	x_{ND}
Fibre damage	μm	y_{FD}

Table 5: Input and output control parameters
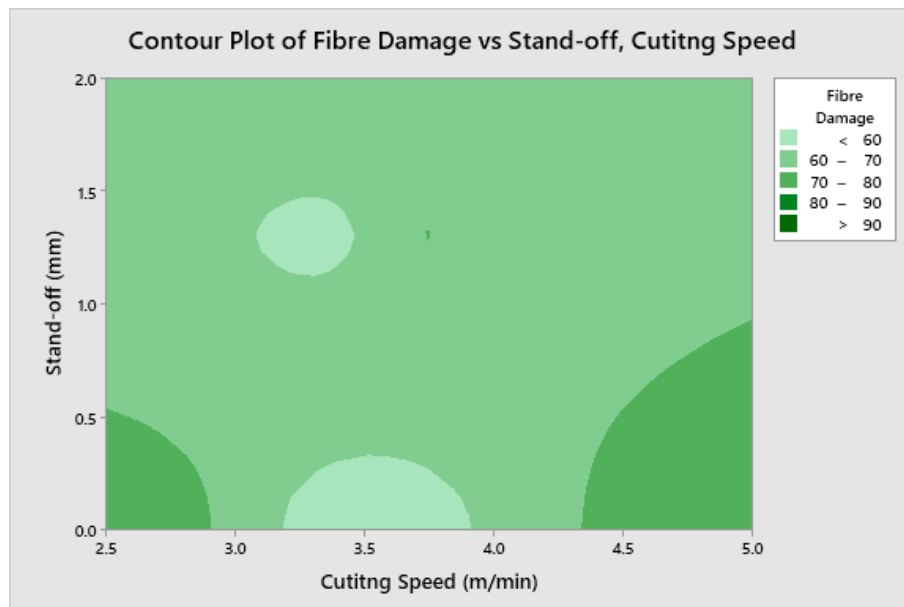
Figure 40: Contour plot of fibre damage (55 – 95 μm) w.r.t cutting speed and nozzle stand-off distance in z direction.

4.6. Summary

In the experimental study, the effects of different laser cutting process parameters on the surface quality of the CFRP were analysed. It was concluded that the behaviour of the material during cutting is attributed to the wide weaving, specifically on the top and bottom layers, where the material suffers significant amounts of fraying when processed. It is possible to compensate multiple passes with processing each pass at an equivalent higher speed. In fact, an overall speed advantage can be gained when taking such an approach and making larger than proportionate speed increments. Multi-pass with 3 passes is found to be significantly supressing top and bottom fraying and improving the cut quality, whether processed with large, small, or double aperture nozzles. Cuts performed using single pass exceeds the target performance in terms of cutting speed and fibre damage. Trials 46b to 49 were performed using single pass and fibre damage below 100 μm was achieved. Further single pass trials were conducted with different laser stand-off distances in trials 55 to 57 and fibre damage below 70 μm was achieved as shown in Appendix A. For trials 46b to 49, the cutting speed achieved were between 2.5 m/min to 3.5 m/min and for trials 55 to 57 the cutting speed achieved was 2.5 m/min as shown in Appendix A. all the trials mentioned above are conducted using single pass and achieved equivalent or better target cutting speed of 2.5 m/min and below target fibre damage of 100 μm. trenching returns more consistent quality of cuts. Trenching (trials 64 to 67) or double aperture processing (trials 69 to 72) achieves low extent of fibre damage, below 100 μ and averaging around 50 μm. it was also observed that plate temperature does not exceed 100 °C. furthermore, regression analysis was carried out and five models for the CAD/CAM interface was developed.

CHAPTER 5

5. Laser Cleaning

The objective for these tests was to investigate whether pulsed laser cleaning can be applied on separated CFRP samples. These samples were initially joined with epoxy based (EP) and polyurethane based (PU) adhesive. The aim was to understand if the laser process can be tuned into limiting damage to the fibres and the composite material substrate as a whole.

5.1. Methodology

5.1.1. Spectroscopic Analysis

The aim of the study is to determine the best approach in laser cleaning of the two different adhesives being considered for CFRP. The tests are expected to determine the transmissivity of the adhesive materials at typical wavelengths of the industrial lasers in UV, visible and NIR spectrum. If the adhesive demonstrates adequate transmissivities at the wavelength of interest, then the process can be turned towards detachment. If the material is mostly opaque at the laser wavelength, then laser ablation or material degradation approach can be followed.

5.1.1.1.   Material Preparation

For measurement purposes, four samples were used. Sample 1 was a piece of CFRP base material measuring approximately 2.5 x 2 x 0.2 cm and was used as reference representing the substrate (Figure 41 (a)). Sample 2 was a CFRP material measured approximately 5.6 x 2 x 0.2 cm and was coated by 2.7 mm thick PU based adhesive (Figure 41 (c)). Sample 3 was a CFRP material measured approximately 9.3 x 3.1 x 0.2 cm and was coated by 0.13 to 0.18 mm thick EP based adhesive (Figure 41 (d)). Sample 4 was a piece of EP based adhesive as a bulk material measuring 2.4 x 1.2 x 2 cm (Figure 41 (b)).
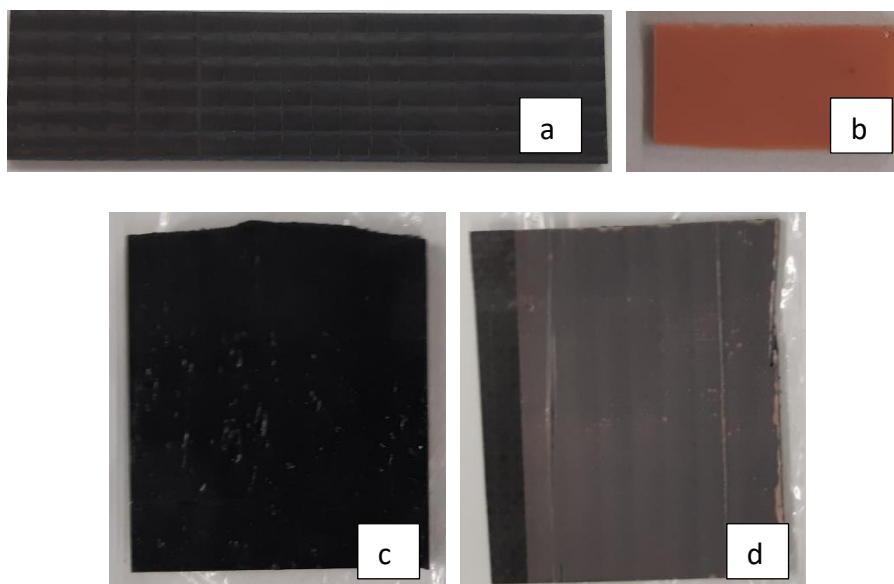
Figure 41: (a) Sample 1 CFRP base material, (b) Sample 4 EP-based bulk material, (c) Sample 2 CFRP material coated with PU adhesive and (d) Sample 3 CFRP material coated with EP adhesive.

Thin filament of thickness 0.1 mm of EP and PU filaments were obtained from samples 3 and 2, respectively. Mixed sealant and carbon fibre filaments were obtained from sample 1. These filaments were set into 8 mm diameter vials, suitable for testing material with the spectrometer.

5.1.1.2. Experimental Setup

A multipurpose analyser (MPA) Fourier transform NIR (Near Infra-Red) spectrometer from Bruker (Karlsruhe, Germany) was used, in combination with Photonics Instrument CCS200 diffraction grating spectrometer to collect UV-Vis part of the spectrum. A quartz beam splitter and InGaAs (Indium Gallium Arsenide) detector was used for tor the NIR transmission measurements. For UV-Vis transmission measurements, a quartz beam splitter with a combined incandescent – fluorescent emission source was used. The samples were placed in cylinders of 8 mm external diameter and 6 mm optical pass as measurement cells. The spectra measurements, instrument control and data acquisition, were performed by using the OPUS 6.5 software from Bruker.

5.1.2. Laser Cleaning Trials

The objective of laser cleaning trials was to understand if the laser process can be tuned into limiting the damage to the fibres and the composite material substrate as a whole. An initial investigation was conducted to assess the impact of laser pulses on the rate of ablation for the two adhesives and the top surface of the composite. Then, the irradiation is applied over the whole area coated with adhesives to further optimise the process. After optimisation, 3 samples of each of both adhesives were processed using optimised parameters.

5.1.2.1.   Material Description

The samples used in the experiment were rectangular coupons of approx. 100 x 25 mm. One end of the sample is coated with adhesive layer of an approx. area of 12.5 x 25 mm. The adhesives were black PU based and coral EP based adhesive (Figure 42). PU adhesive had a maximum thickness of 2 mm, whereas the EP adhesive layer had a thickness of 1 mm.

Figure 42: (a) CFRP sample with PU based adhesive, (b) CFRP sample with EP based adhesive.

Five quantities were measured for each processed area shown in Table 6. Debonding quantity was not possible to measure for PU and EP sealant test.

Measured characteristic	Definitions
Damaged fibres	The count of damaged fibres per 0.25 mm^2 of exposed fibre area only. The measurement was taken from 5 different processed sites if adequate exposed area exists. Optical microscope with 60x to 100x magnification was used to count damage fibres.
Adhesive debonded	This defines the percentage of area debonded from the sealant surface with adhesive layer still present and appears as light colour than the sealant debonded area. This happens due to internal reflections above the sealant and thus light does not transmit far enough to be absorbed by the darker carbon fibre bulk material
Sealant debonded	Defines the percentage of area which has debonded at the at the boundary of the sealant and fibres. The adhesive layer and sealant are still present and possibly still adhere to each other and behave as one layer.
Adhesive detached	The site area which has detached from the bulk material at the adhesive to sealant interface with sealant and sub layer exposed.
Sealant detached	The percentage of area debonded from the bulk material at the sealant to carbon fibre and dark binder boundary with carbon fibres exposed.

Table 6: Definition of measured characteristics

5.1.2.2. Experimental Setup

A flash-lamp pumped Nd:YAG laser was used as the light source for the laser cleaning trials. The laser was manufactured by Litron Lasers UK Ltd to a proprietary specification. The characteristic of the laser is shown in Table 7.

Parameter	Value	Units
Average power	25	W
Wavelength	1064	nm
Pulse duration	10	ns
Pulse energy	2.5	J
Free space beam delivery	16 (Full Width Half Maximum)	mm
Focusing lens	500	mm

Table 7: Litron laser characteristics

The schematic of the laser beam setup is shown in Figure 43. The beam was focused via the focusing lens onto the sample. The samples were moved against the focussed beam by an automated XYZ platform, while held vertically to the direction of the incoming beam. The spot size and thus laser fluence per pulse was adjusted by changing the focus position along the beam propagation axis.
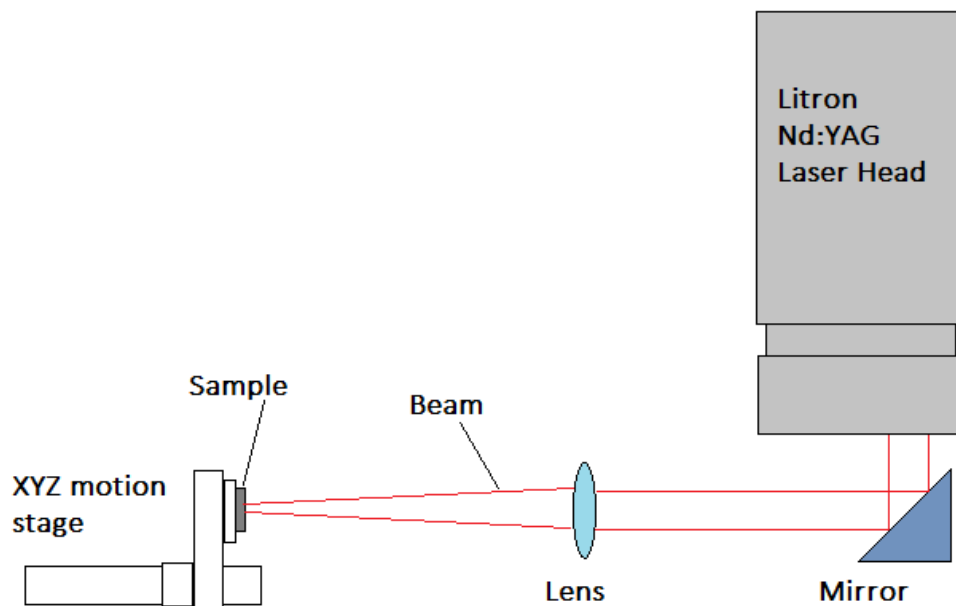
Figure 43: Test setup of flash-lamp pumped Nd:YAG laser

For microscopic analysis, a 10x magnification eye loop with 100 μm graduation reticule, a 60x to 100x magnification compact microscope with 10 μm graduation reticule and 50x magnification USB microscope with 50 μm graduation reticule were used. For process monitoring, a Sony RX100 IV high frame rate camera at 1000 FPS

(frames per second), with an Exomor RS 4K sensor in Cyber Shot configuration and a Zeiss Vario Sonnar F1.8 lens camera were used. For surface depth measurement Elcometer E123A – M with tungsten 60^0 full angle conical pin ending to a 50 µm diameter tip was used.

5.1.3. Thermographic Analysis

The thermographic analysis was carried out using a Flir digital thermal imaging camera with recording capability of 320 x 240 pixels and thermal sensitivity of 0.1 ^{0}C with manual focussing, for both adhesives. During the video recordings, the samples were held on a XYZ motion stage in front of a stationary beam. For time – resolved or space - resolved thermography during laser processing, thermal cameras are not recommended for 2 to 5 mm spot size. For accurate measurement, a commercial precision pyrometer with precision of < 1 ms is required.

5.1.4. Re-joining and Testing

Once the adhesive was cleaned from CFRP samples, the samples were then glued with another virgin CFRP joining partner sample and tested for tensile shear in accordance with DIN EN 1465. A universal testing machine (Figure 44) was used for the destructive test, which enables testing in the load range of 20 kN. It is important that the sample is clamped as vertically as possible to initiate a straight load path.

Figure 44: Exemplary representation of the clamping of a sample using a device.

5.1.5. Design of Experiments

6 tests were performed on PU covered sample, 7 tests were performed on the surface sealant of the uncoated material of the practice samples. 15 tests were performed on the EP covered samples, listed in Appendix F. The process parameters for cleaning EP and PU adhesive are shown in Table 32 and Table 33 respectively. The information detailed in Appendix F are:

- Test performed on PU covered samples.
- Tests performed on EP covered samples.
- All parameters and measured characteristics describing each processed area.

The following information is detailed in other appendices:

- Images of the processed samples in Appendix G.
- SEM images of laser cleaned area of PU and EP in Appendix H and Appendix I respectively.
- Re-joining and tensile shear testing of laser cleaned samples in Appendix J.

Two thermography videos, one for PU and one for EP coated samples. There were also four high frame rates videos of samples EP 3.2 – first pass, EP 11.2 – second pass, PU 3.2 – first pass and PU 11.1 – second pass, to control the process parameters.

5.2. Results and Discussion

5.2.1. Spectroscopic Analysis

5.2.1.1.   Epoxy-based (EP) Adhesive

The transmission spectrum obtained from the EP adhesive is shown in Figure 45. Epoxy based adhesives are transparent in the red and NIR regions and expected to have absorption bands beyond 2000 nm. The spectrum exhibits a wide absorption band between 2200 and 2700 nm, a double band at around 1750 nm and another double band of smaller absorption at around 1400 nm. These are typical absorption bands featured in two-part clear epoxies used in sealing and potting applications. The specific material also exhibits a drop in transmission below 600 nm, which corresponds to the coral hue of the material. As expected for this type of material, it

shows significant transmission in the 1064 nm laser emission wavelength, measured at 0.89. This indicates that it should be possible to approach the removal of the adhesive with a detachment or hybrid detachment method.
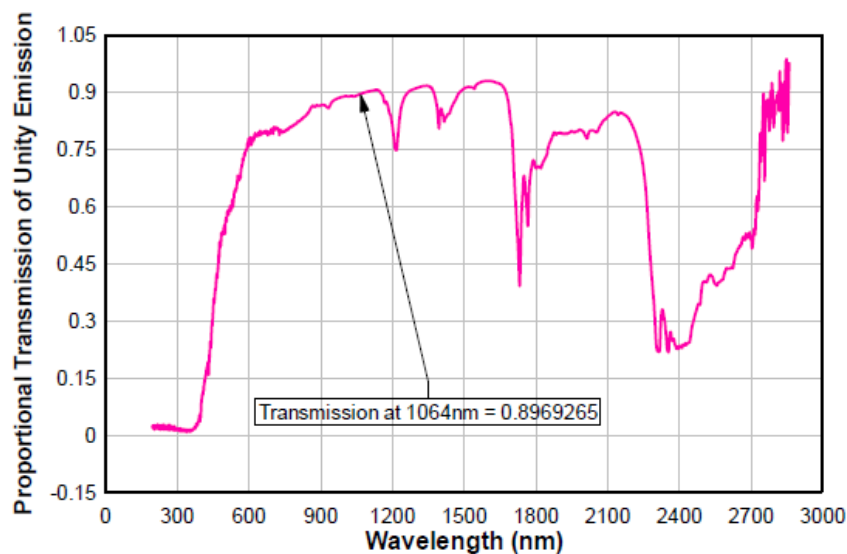
Figure 45: Transmission spectrum for EP based adhesive.

5.2.1.2.   Polyurethane-based (PU) Adhesive

The PU based adhesive is mostly absorptive across the whole examined spectrum, with maximum absorption occurring closer to the medium IR between 2700 nm to 3000 nm, where most polymers have sharp transmission to absorption transition. The transmission spectrum is shown in Figure 46. The rest of the spectral response is governed by less than 1% transmission, which corresponds with the very dark, nearly black appearance of the material. It exhibits some small increase in transmission at around 1000 nm and possibly a harmonic at 500 nm, which offers very slight dark blue opaque hue to the material. The transmission at 1064 nm is less than 1%. This implies that detachment will not be possible at this wavelength. The low transmission across the entire examined spectrum confirms that detachment or hybrid detachment will not be possible with laser.
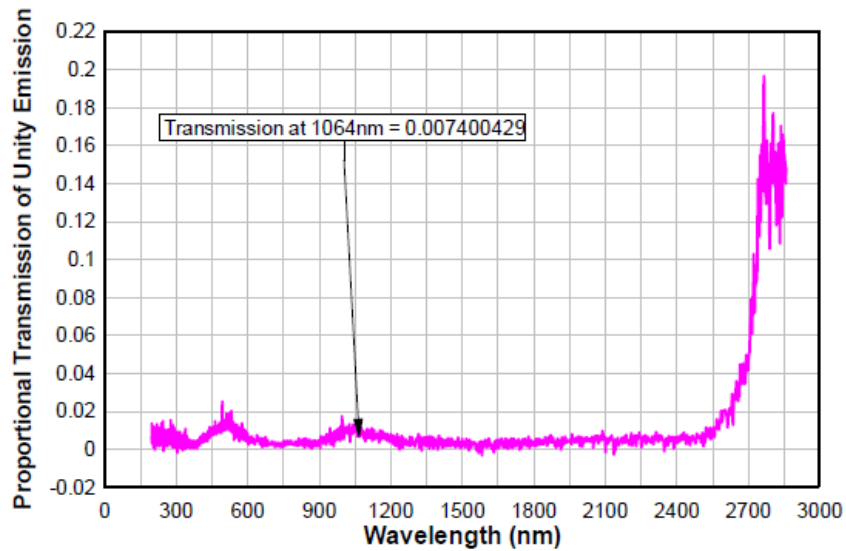
Figure 46: Transmission spectrum of PU based adhesive

Thus, the recommended approach is by photo-thermo-acoustic degradation of the adhesive layer and subsequent removal by shock pulsing, or pulse by pulse ablation against 3D topographic data. The wide band absorption is most likely due to inorganic additives or organic additives with long alkene chains.

5.2.1.3. CFRP Sealant

The mixed sealant-fibre filament shows a moderate to high transmission across most of the examined spectrum. Small absorption points exist around 800 to 2700 nm, while transmission remains high until UV region (Figure 47). The few carbon fibres included in the filament absorbs some percentage of the radiation across most of the spectrum collected. The measurement implies that the radiation may continue through the sealant and reach the fibres. This can endanger the fibres to some extent. Therefore, higher energy pulses are required for low impact detachment. A hydrogen fluoride chemical laser tuned at around 2700 nm or ns pulses from direct diode emission at 808 nm may offer some advantages in detaching at the adhesive-sealant interface, though these lasers are expensive and not available as industrial sources. The refractive index difference between the adhesive and sealant may also aid in detachment that occurred at the adhesive – sealant interface instead of sealant – fibre interface. However, there is still a risk that transmission can reach highly absorbing carbon fibres.
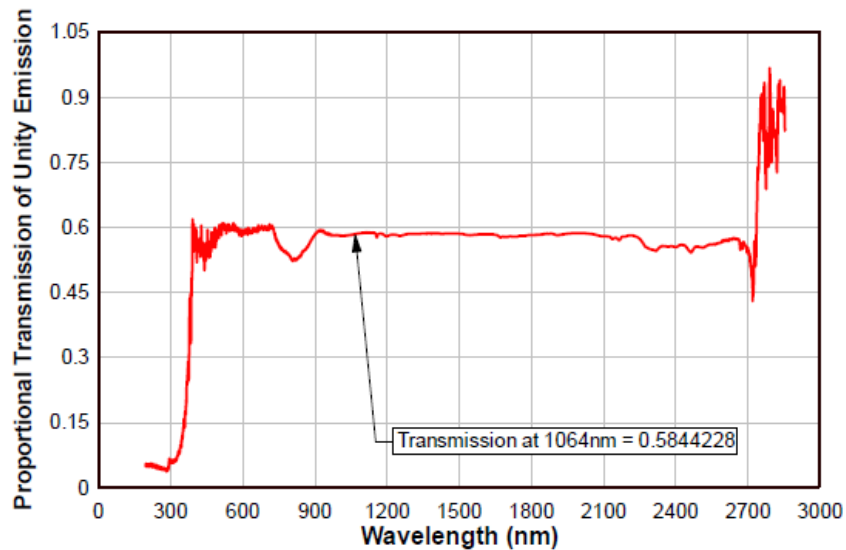
Figure 47: Transmission spectrum of CFRP sealant and CFRP fibres.

It was considered beneficial to approach EP adhesive by NIR pulsed radiation with the aim to detach the material degradation instead of ablation. For PU adhesive, initially material degradation was recommended before the final laser removal with shock pulsing. Alternatively, a pulse-by-pulse ablation approach may be used over a known topography of the adhesive layer thickness. Finally, the sealant used on the CFRP is mostly transmissive across most laser wavelengths. Consequently, some damage to the highly absorbing fibres that are located on the surface may occur. As a result, high pulse energy ns pulses were used for best results and for supressing the fibre damage occurrence.

5.2.2. Laser Cleaning

5.2.2.1. Rate of Ablation

The rate of ablation investigation on the epoxy sealant surface of the substrate material was inconclusive due to the high transparency of the wavelength used (Figure 48). The process of the material removal is governed by the interaction of the laser with the underlying carbon fibres and binder and with the interface of fibre strands that exists on the CFRP epoxy interface. Most processing parameters do not have any impact on the surface lying material. These conclusions confirm the use of NIR laser to clean EP adhesive.
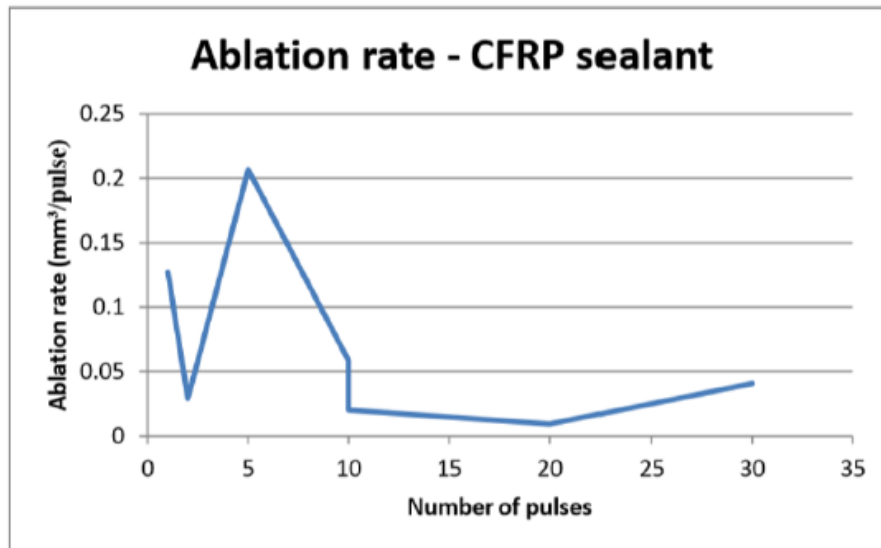
Figure 48: Ablation rate of CFRP sealant material.

Initially, defocus position was assessed on the test sample, this defocus provides a larger spot size to activate debonding at adhesive – sealant interface with as little ablation as possible. Figure 49 shows the spot size of approx. 4.2 mm in diameter from defocus of 110 mm.
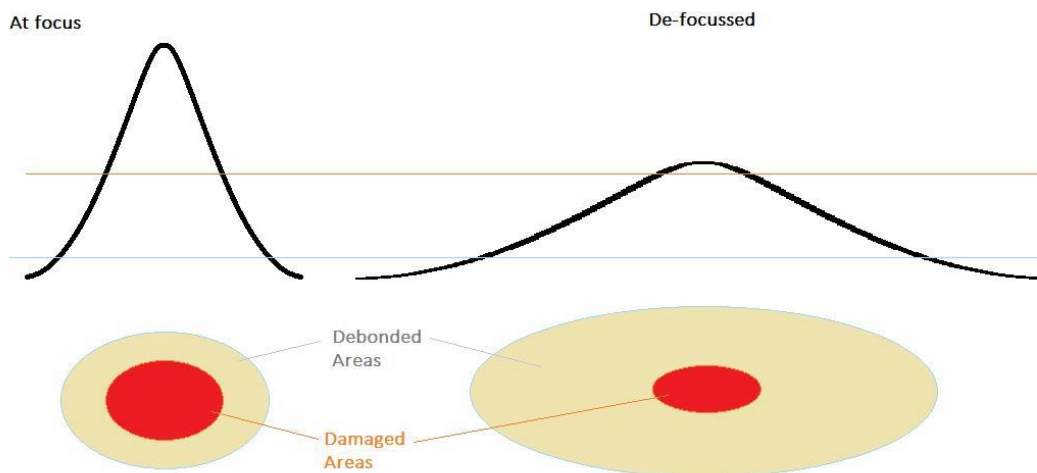
Figure 49: The difference in how an irradiated area is affected by a focused and defocused beam.

There was some damage caused by the irradiated beam at the corner of each area, this is due to small part of the beam still above ablation threshold. However, most of the beam caused debonding. Debonding might not immediately cause detachment but can result in further mechanical and/or acoustic stimulus, reducing the possibility of substrate impact. The ratio of damaged can be impacted by simple debonding

using defocusing high pulse energy beam. An attempt on trials 6, 7 and 8 was made to manually arrange the irradiated area in order to observe the impact or overlapping lines using similar parameters. The result showed a possibility of attaining linear pulse train without causing unnecessary damage to the material at overlapping region. Hence, overlapping was automated.

For trials 10 and 11, the automated laser of the beam was used across the area. The coverage area was good, but a damage field exists at the centre of each pulse where it outpaces the ablation or damage threshold of the coating. The damage spot observed had a shape that resembles an arrowhead, or a T shape as shown in Figure 50.

Figure 50: An irradiated area with 5 successive pulses in linear transverse sequence. The damaged areas resembling a T or an arrowhead to an upper – left direction occurred by the central and more powerful part of the beam.

The shape in Figure 50 demonstrate that the beam from the laser source is rather misaligned due to non – radial diffraction such as coma. To stop the damage a beam profile homogenizer would be ideal for the central part of the beam and helps in better tuning of the pulse within the debonding threshold. For homogenous coverage, the parameters are tuned for the total irradiated are per test. For test 12 and13, the total fluence was distributed into two passes, then off-setting one pass the other, diagonally by 0.5 mm, this was necessary to verify that the stronger part of the beam did not fall on the exact same part as its predecessor in test 14 and 15. During tests 12 to 15, the area percentage of debonded adhesive was increased, treated as optimal condition with minimal impact on the substrate for a layer of uninterrupted thickness as shown in Figure 51.
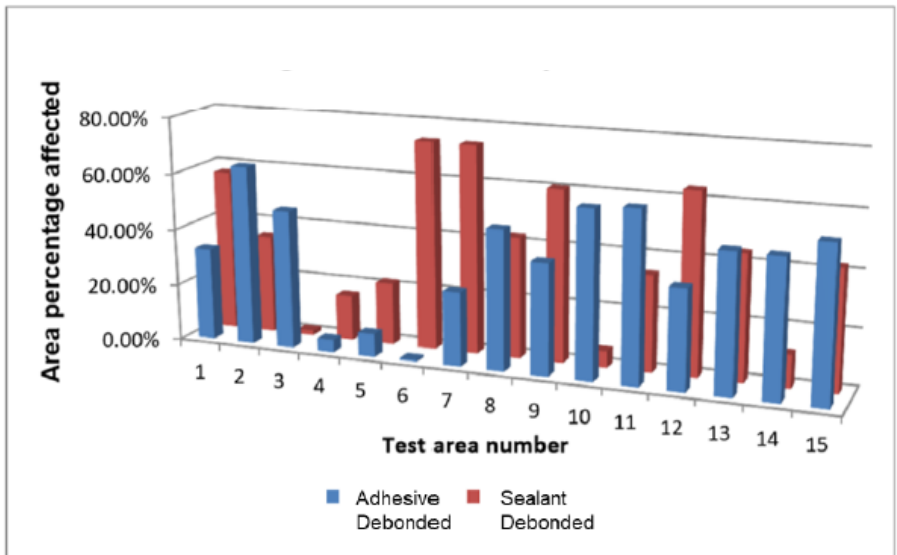
Figure 51: Chart indicating the percentage area, for each test, that has been debonded at the adhesive to sealant interface or at the sealant interface. The measurement has been normalised against the observed irradiated area.

The investigation for the initial trials for the pulse material degradation and ablation under the laser irradiation was fixed focus position with the only change being the number of pulsed pointed on the targeted area. The difference in the depth of removed material is very small, the only increase in the affected area where the number of pulses increased to 10. With 5 pulses, the surface shown significant damage and degradation to the third carbon fibre layer (Figure 52).
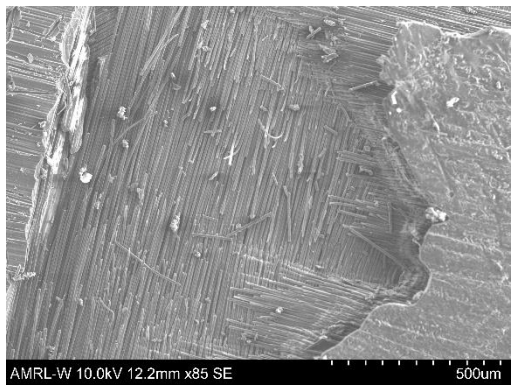
Figure 52: SEM micrograph of surface degradation with 5 pulses.

This degradation was intensified when irradiated with 10 pulses. However, it was difficult to rotate the number if pulses and total energy released with very small variation in penetration depth on specific area (Figure 53).
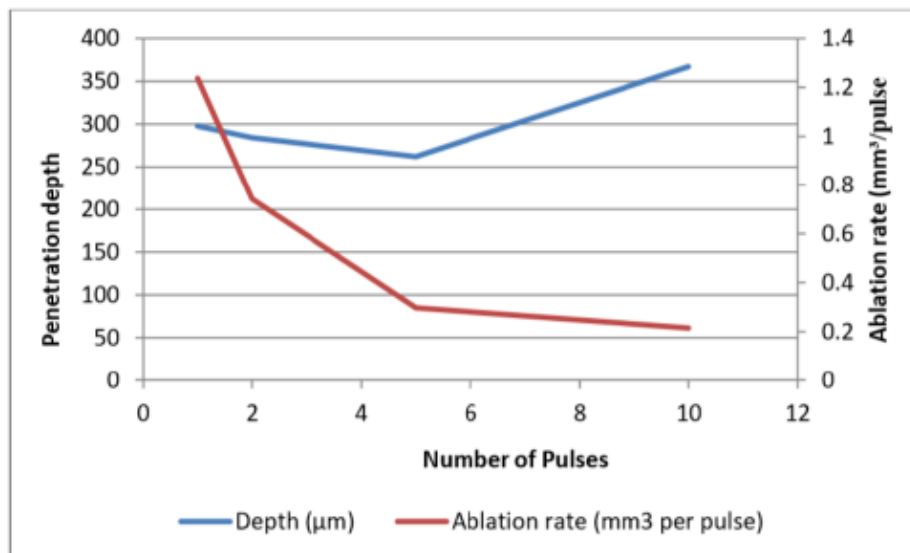
Figure 53: The plotted graph indicates penetration depth against number of pulses and ablation rate against number of pulses.

As ablation is guided by peak power, this was somewhat expected. The ablation rate reduces exponentially with the number of pulses when ablation rate was observed in this irradiation regime. Radiating in ablation regime using a small spot of same energy, with very high peak power density over irradiated area was linearly dependent on the number of pulses. However, the sample was deliberately irradiated with wider spot and induce material degradation in order to increase the process window for processing composite substrate and PU adhesive.

The PU adhesive will absorb the same amount of radiation as the substrate and individual carbon fibres. However, by moving to degradation regime, the fibres and binder material should prove more flexible than the PU adhesive. The PU adhesive started to disintegrate with accelerated degradation and removal occurs by pulse acoustic shock. Debonding was not investigated for PU adhesive due to its high absorptive nature for laser wavelength, proven in spectral investigation of the adhesive material. The material layer was very thick, and it was very difficult to examine the whole depth without damaging the substrate material.

5.2.2.2.   Parameter Optimisation

For samples with EP adhesive, higher fluence was provided by changing the focus to a smaller spot size. The spot size was changed from 4.24 mm to 3.05 mm and a

fluence of 5.6 J/cm^2. This change was adapted because of the aim to remove the whole thickness of the coating. The pulse repetition rate (PRR) was set at 5 Hz and rastering at 2 passes and 0.5 mm diagonal offset for the second pass to maintain homogenous irradiation over the duration of processing.

Defocus and pulse energy were adjusted to the energy density and energy distribution of the pulse energy within the adhesive detachment window, since beyond two pass processing, no additional stimulus was further applied for sample cleaning. The parameter set that removed the extensive area and kept the count of damaged fibres reasonably low is shown in Figure 54. The defocus was at 55 mm, giving a nominal spot size of 2.86 mm with energy setting of 40%, these setting return 0.95 J of pulse energy and 14.8 J/cm^2 fluence.
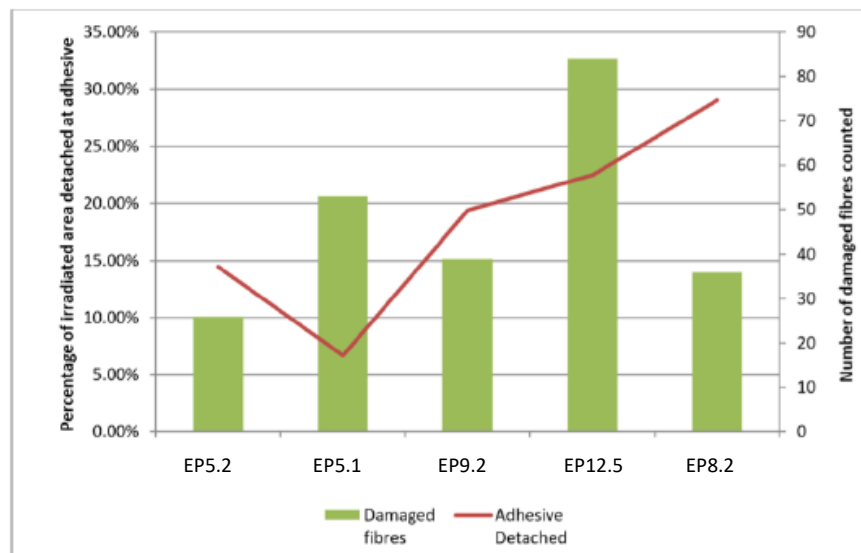
Figure 54: Area percentile that has detached at the adhesive to sealant boundary for each of the optimisation samples, and the number of damaged fibres measured across different points on the irradiated area.

The 3 repeat reference samples were processed with these parameters; however, the results were not the same for repeated samples because due the thickness of the adhesive varies from sample to sample significantly, as shown in Figure 55. The adhesive was mostly cleaned from the samples while a small amount of surface of the composite may be affected due to the beam reaching the fibres and substrate. However, the fibre count was relatively low.
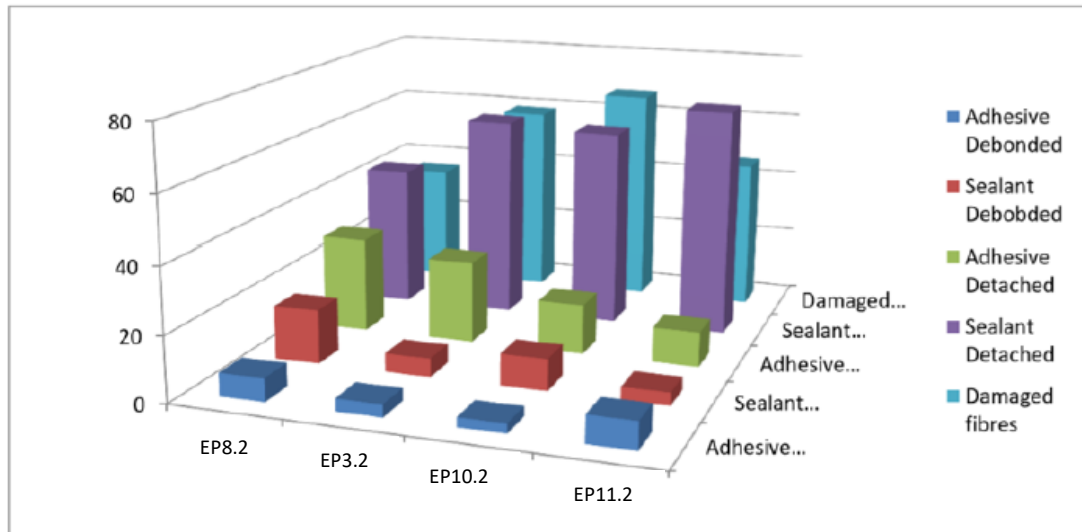
Figure 55: Chart depicting the area percentile that have been debonded at the two boundaries, for the EP coated samples.

For PU adhesive optimisation, the lasers were not able to process the sample effectively due to adhesive thickness. However, the laser with average power of 800 W or higher would be capable to remove thick absorptive adhesive. The thickness of adhesive layer on sample varies from few hundred microns to a few millimetres. This process would remove the absorbing substrate to a significant depth which was not required. A way around the problem is to trim the coating with sharp blade to an approx. consistent thickness of 350 – 150 μm. This thickness is more attainable by the degradation method and protects the substrate effectively. The defocus was set to achieve a 2.86 mm diameter spot and pulse energy of 1.493 J and fluence of 23.33 J/cm^2 was achieved.

For EP adhesive, a similar scattering pattern was used which provided a surface irradiation regime of homogenous nature. For optimal performance, the speed was tuned between 6 mm/s to 5 mm/s.

Due to high absorption of PU material, there was no evidence of debonding, hence no further tuning is required due to high absorptivity of PU adhesive. An adequate level of coating removal was being achieved and only dependent on the coating thickness. Coated or irradiated area up to 70% of PU coating was removed by the process as shown in Figure 56. The process also removed a sealant over a good proportion of the area. The removal of sealant results in the exposure of substrate

80

and fibres in relatively small numbers. This suggest that the impact on substrate is only contained to a shallow substrate level, indicating that some degree of protection is achieved by the coating degradation regime due to the variation of coating thickness reduced to 200 μm peak to valley, however, the substrate of composite is not affected more than 2 to 3 fibre depth.
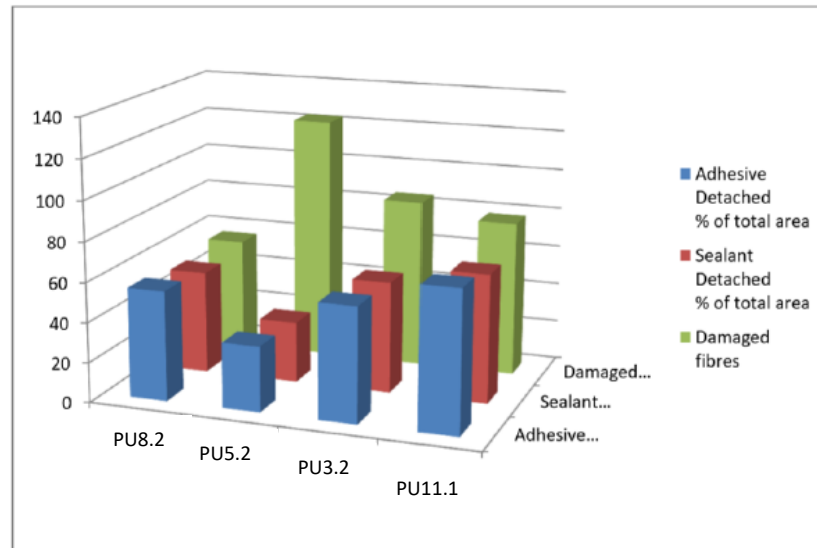
Figure 56: Measured characteristics of processed area on the PU adhesives.

Thickness variation of highly absorptive PU adhesive adversely impacted the process. An automated system that monitors the adhesive thickness and consequently adjusts the pulses per surface area that depend in number and energy on the thickness of the coating would be beneficial to the process. Using this approach allows the laser to remove material in mechanically controlled fashion and protect against the damage. Therefore, surface damage would not exceed 5 to 7 μm. This was measured using optical microscope with high magnification.

5.2.2.3. Fibre Damage on Samples

The fibre damage measured within the area of investigation of 0.25 mm^2 shows that the damage was caused on the substrate with average of 14 to 170 fibres damaged over 5 investigated area. The bulk material with unaffected fibres embedded in the composite material and its binder is visible through most of the surface exposed underneath the detached sealant. The fibre count for EP adhesive sample ranged

from 24 to 84 fibres which is relatively small when compared with fibre counts of PU samples which were 56 to 123 fibres. This was expected as debonding of EP adhesive is much more effective than that of PU adhesive.

The estimated depth of damage caused on the substrate was between 5 to 36 µm considering the thickness of the fibres between 8 to 12 µm. This includes the error margin in the definition of fibre diameter and status of unbroken fibres visible at processed area. The broken fibres were observed over 0.25 mm^2 area section. To better understand the actual damage depth, material could be divided into sections and investigated across the section and through the depth under the microscope. However, the mechanical sectioning must not distort the fibres and material.

The fibre damage can further reduce, firstly, by adjusting the process even further to a debonding process during which the laser wavelength is explicitly selected to only penetrate through the adhesive layer and must be absorbed by the sealant layer. This process requires the development of a laser with wavelength identified by spectroscopic studies. For EP adhesive the wavelength is expected between 1.5 µm to 5 µm and for PU adhesive, the wavelength may occur in the far IR region of 11 µm to 25 µm.

Secondly, the process can be turned into purely ablative using an automated feedback loop using control electronics. This process required a precision measurement device of 1 µm or better, this device will determine the variations in thickness of the coating and release-controlled pulses per surface area. With this approach, the removal process stops at a depth assumed to be useful therefore, limiting further damage to less than 10 µm. A far IR or UV region may be useful and would guarantee better absorption by all materials involved.

Thirdly, a less M^2 (beam quality factor) ns-pulsed laser with energy range between 12 to 30 mJ and a small spot size and long focal length to target a interface of separation at glazing angle, together with a mechanical tool to lift the coating being removed away from the substrate.

5.2.2.4. Interaction at Adhesive – Sealant Interface

On EP adhesive samples, better deboning interaction was observed specially the 15th processed area (Figure 51) where adhesive layer was still attached to the sealant, only possible on samples with consistent adhesive layer. Therefore, to clean the samples, these parameters reduce the differentiation between EP and sealant. Thus, the process stopped at the substrate and sealant interface, with optical absorption 78 times higher than the EP and sealant layer.

As the EP adhesive thickness on the sample varies significantly, due to this the process window tuning was problematic due to the substrate damage threshold being closer to the debonding threshold of EP – sealant interface for thicker EP coating. Therefore, the power density required to debond thick EP layer of several hundred microns was higher than the density required to debond low thickness area. This causes the interaction with highly absorbing composite fibres resulting in surface damage. Removal of EP at adhesive – sealant would be much more effective, and substrate could be further protected if the adhesive is of consistent thickness.

5.3. Thermographic Analysis

The overall surface temperature of the EP adhesive sample does not exceed 76 ^{0}C during processing (Figure 57) and the overall surface temperature of PU adhesive sample does not exceed 32.5 ^{0}C (Figure 58). During video calibration, the camera sets to highest temperature level monitored in the required image sequence. In both cases the video was calibrated, therefore, general indication of the surface temperature in each case is considered as valid measurement.

It is anticipated that the local temperature within the laser spot of 10 ns emission time, reached thousands of degree kelvin. But this heat can rapidly dissipate as heat loss into the evaporated material, the residual heat in the material adds to the average surface temperature.
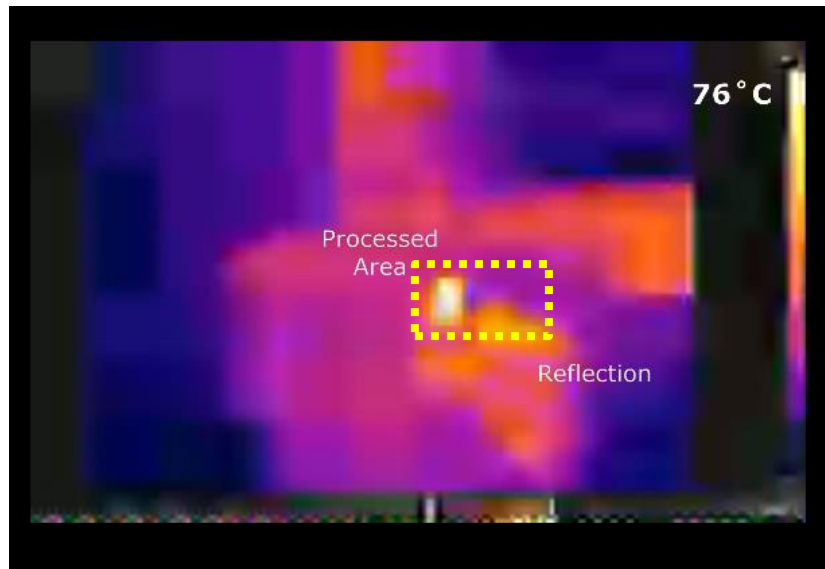
Figure 57: Thermographic image of EP adhesive sample
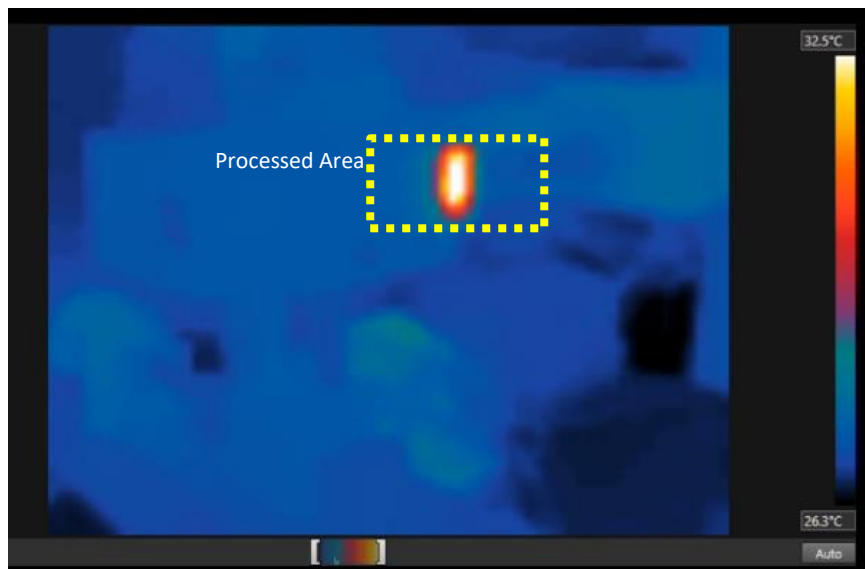
Figure 58: Thermographic image of PU adhesive sample

The debonding process was successfully demonstrated below 50 ^{0}C with the local temperature kept within 300 to 500 ^{0}C during irradiation in other materials [130], however this was not the case with EP adhesive due to varying thickness of the adhesive and the process was not tuned to pure debonding process. Therefore, the excess energy was accumulated at the substrate material and caused higher temperature reading when comparing to the PU adhesive. The low average temperature recorded was encouraging in adopting a short-pulsed laser process for the cleaning of these materials as it implies low heating and thermal modifications of

the substrate. Only surface localised effects are taking place within a maximum of 36 µm considering fibre breakage counts.

5.4. Re-joining and Testing

After laser cleaning of the glue from CFRP samples, the samples were then glued with another virgin CFRP joining partner sample and tested for tensile shear accordance with DIN EN 1465. Details of the equipment and test conditions are set in Appendix J. Tests of virgin CFRP samples were also taken for comparison.

The adhesive joint between two virgin CFRP samples with PU adhesive failed at a force of 1100 N and average length of 2 mm, whereas, when the same test carried out using laser cleaned samples failed at an averaged force of 850 N and averaged length of 2.6 mm (Figure 59). Similar tests were repeated for EP adhesive. The adhesive joint between two virgin CFRP samples, failure averaged at 5900 N and average length of 0.83 mm, whereas the joint between virgin CFRP sample and laser cleaned sample, the failure averaged at 5950 N and average length of 1.2 mm (Figure 60). These results showed that EP based laser cleaned samples were in better agreement with the benchmark virgin samples.
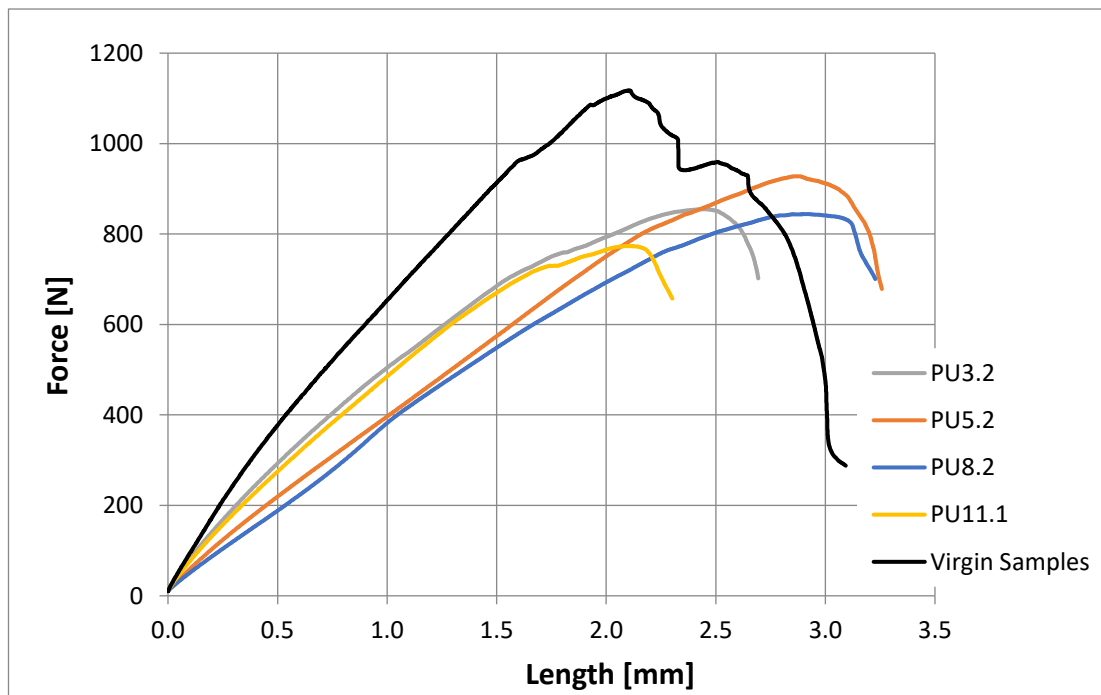
Figure 59: Experimental results of the samples glued with PU adhesive.
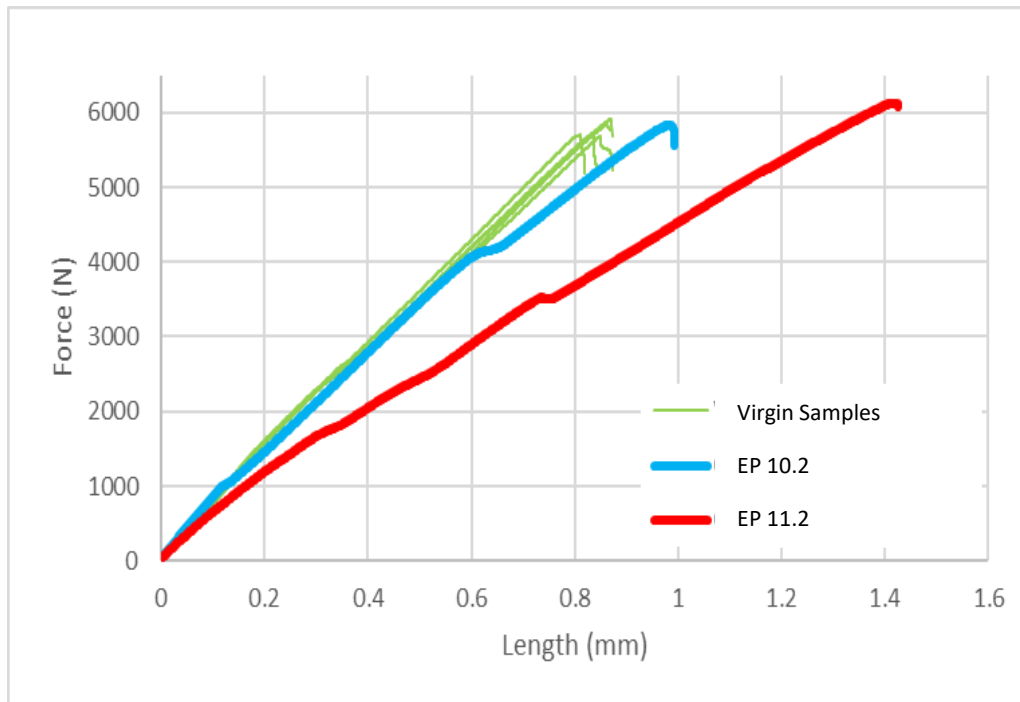
Figure 60: Experimental results of the sample glued with EP adhesive.

For PU samples the failure has been mostly due to adhesive failure, whereas for the EP there were mixed failures. In both cases there was some adhesive remaining after the laser cleaning process and as expected the failure occurred on the samples that were laser cleaned. This was expected as most of the glue was removed from EP samples and the cleaning process was not as aggressive as the PU cleaning. The difference in results could also be due to separation of samples before laser cleaning that may have caused severe damage to the samples.

5.5. Summary

It is possible to laser clean both EP and PU adhesives from CFRP substrates using pulsed NIR laser. There seems to be some natural process window that limits damage on the substrate, in comparison to that induced on the coatings, however, this does not shield the substrate completely. The EP material can undergo debonding from the fibres and binder as well as the sealant if the layer thickness is consistent over the irradiated area. For layers with non-consistent thickness, this is not possible, and irradiation reaches the substrate and damages the surface fibres. For the PU material an ablation process is used. when promoting material degradation, the surface is

expected to suffer less damage on the surface fibres, while a purely ablative process would not differentiate between the materials, especially considering the very high optical absorption of both materials.

The damage occurred on the CFRP from removing PU adhesive was greater than removing EP adhesive since EP required less energy to be removed. However, for both adhesives, the damage on the substrate was less than the maximum surface abrasion of 0.1 mm. a concerning damage that could occur on the substrate is the damage caused by overall heating during laser cleaning process. The developed process managed to control the temperature of polymers involved in the bulk composite structure. For tensile tests of the cleaned samples, the substrate with EP adhesive performed better than PU when compared with virgin samples.

CHAPTER 6

6. Caser Study: Laser Cleaning of CFRP Internal Curved Surfaces

The case study was conducted to assess the feasibility of employing a laser cleaning process in removing adhesive residue from internal curved 3D CFRP components. The study also evaluates the use of a LIBS (Laser Induced Breakdown Spectroscopy) method, for process monitoring and control.

6.1. Laser Induced Breakdown Spectroscopy (LIBS)

In atomic emission spectroscopy (AES), Laser induced breakdown spectroscopy (LIBS) uses a laser generated plasma as the hot vaporisation, atomisation, and excitation source. LIBS has many advantages over conventional AES technique because the plasma is formed by focused optical radiation and uses an adjacent physical device to form vaporisation / excitation source. LIBS has an ability to examine samples in situ and remotely. Basically, measurements are achieved by forming a plasma laser on or in the sample and collecting and spectrally analysing the plasma. By monitoring emission line positions and intensities, qualitative and quantitative analyses can be carried out. Prior to 1980, the interest in LIBS was mainly on basic physics and plasma formation. After the 1980's LIBS analytical capabilities became more noticeable and few instruments have been developed mainly due to the significant technological development in components such as lasers, spectrograph and detectors used in LIBS instruments and also to perform measurements under conditions not possible using conventional analytical techniques [131].

6.2. Description of Materials

Two types of samples were used in the case study. Different types of CFRP material were used in both. The differences are highlighted in Table 8: **Composite properties of CFRP profile** and Table 9.

The first sample was a shaped insert (Figure 61) with profile planned for use in automotive car seat structure with a right-angle triangle cross section, rounded corners and sides measuring approximately 4.5 cm and 2.5 cm. The carbon fibre used to manufacture profile was produced by the treatment of an acrylic fibre precursor, with pyrolysis, surface treatment and sizing process. Both openings of each sample had a layer of EP adhesive, measured thickness of 150 to 600 µm and approximate width of 40 mm, on inside walls reaching all the way down to a porous white filler foam material. The composite properties of the cylinder are shown in Table 8.

Property	Unit	Nominal value
Tensile strength	MPa (kgf/mm^2)	2060 (210)
Tensile modulus	GPa (10^3kgf/mm^2)	130 (13.5)
Tensile strain	%	1.4
Compressive strength	MPa (kgf/mm^2)	1570 (160)
Flexural modulus	GPa (10^3kgf/mm^2)	125 (13.0)
ILSS (Interlaminar shear strength)	MPa (kgf/mm^2)	110 (11)

Table 8: Composite properties of CFRP profile
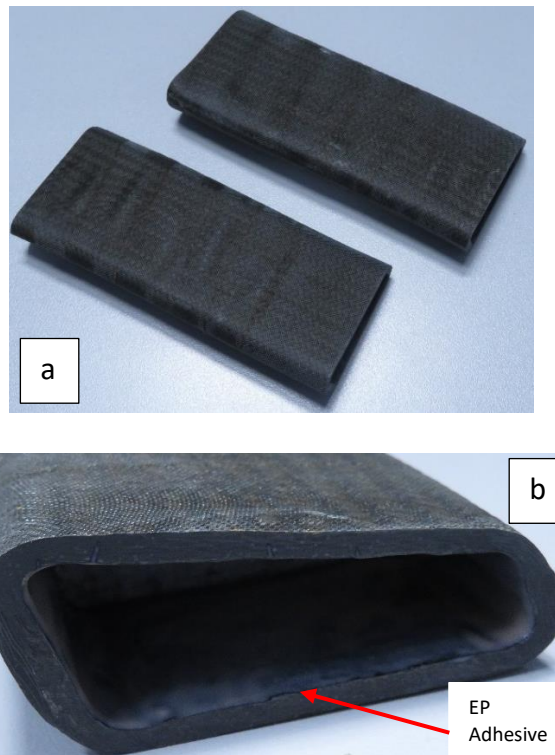
Figure 61: Rectangular shaped samples (a) Top view, (b) side view .

The second sample was a cylinder with internal diameter of 9.5 cm and wall thickness of 4 mm (Figure 62). The carbon fibre used in manufacturing the cylinder was produced by treatment of an acrylic fibre precursor, with pyrolysis, surface treatment and sizing process. The cylinder was cured by hot curing epoxy matrix system, suitable for high performance composite parts. The inside wall on either side covered by a layer of EP adhesive with similar thickness as the shaped insert. The composite properties of the cylinder are shown in Table 9.

Property	Unit	Nominal value
Tensile strength	MPa (kgf/mm^2)	2550 (260)
Tensile modulus	GPa (10^3kgf/mm^2)	135 (14.0)
Tensile strain	%	1.7
Compressive strength	MPa (kgf/mm^2)	1470 (150)
Flexural modulus	GPa (10^3kgf/mm^2)	120 (12.3)
ILSS (Interlaminar shear strength)	MPa (kgf/mm^2)	69 (7)

Table 9: Composite properties of CFRP cylinder
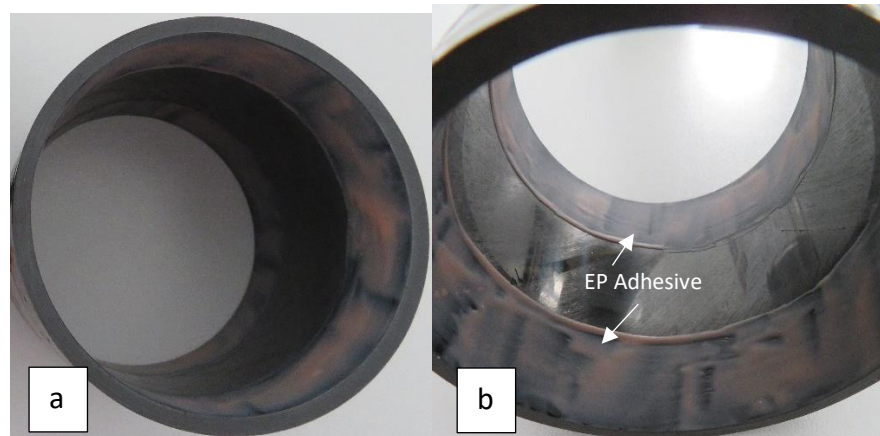
Figure 62: Cylindrical sample (a) Top view, (b) Side view

Due to the different nature of the composite CFRP material, the behaviour of this material under laser radiation was different from each other.

6.3. Measured Features and Characteristics

There were 7 quantities measured for each processed area. The definition of the measurement for each quantity is provided below. The Figure 63 shows the unprocessed area of CFRP.
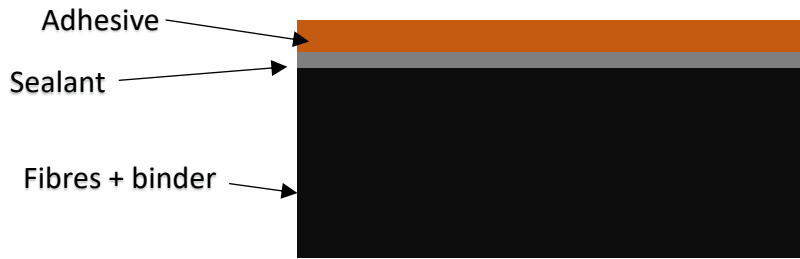
Figure 63: Unprocessed area of CFRP.

- **Damaged fibres** (Figure 64) – The fibres damaged per 0.25 mm^2 of exposed fibres. These are averaged measurements from different areas of the processed site and was performed using optical microscope with 60x to 100x magnification.
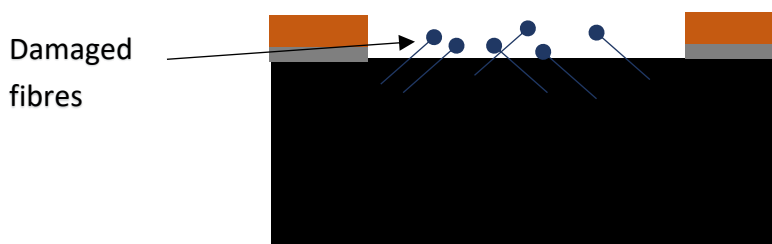
Figure 64: Schematic of damaged fibres on CFRP sample.

- **Adhesive debonded** (Figure 65) – Percentage of processed area which has debonded from the sealant surface, but the adhesive layer is still present with desert sand colour appearance, then the sealant debonded area. This is caused by the internal reflection that happens above the sealant and thus light does not transmit far enough to be absorbed by the darker carbon fibre bulk material.

Figure 65: Schematic of adhesive debonded on CFRP sample.

- **Sealant debonded** (Figure 66) – Percentage of processed area which has debonded at the boundary of the sealant and the fibres, but the adhesive layer and sealant are still present and possibly still adhere to each other and

91

behaving as one layer. The area appears somewhat darker with as ash grey or pastel grey colour as the continuity of material with similar optical properties in the visible range permits the transmission of some light towards the dark carbon fibres and their binder which absorbs more of this light.
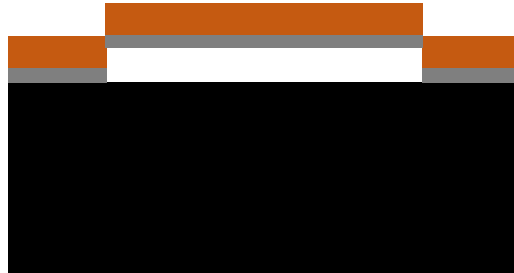
Figure 66: Schematic of sealant debonded on CFRP sample.

- **Adhesive detached** (Figure 67) – Percentage of processed area which has detached from the bulk material at the adhesive to sealant interface. The sealant or sub-layers are exposed.

Figure 67: Schematic of adhesive detached on CFRP sample.

- **Sealant detached** (Figure 68) – Percentage of site area which has detached from the bulk material at the sealant to carbon fibre boundary. The carbon fibres are exposed.

Figure 68: Schematic of sealant detached on CFRP sample.

- **Burnt area** – Percentage of processed area where an active oxidation reaction initiated during processing has modified or fused the individual

fibres or fibre bundles. This was calculated from estimates of fibre condition across 60 sites in the processed area, distributed over 3 depths.

- **Surface roughness** – This assesses the deviations in the direction of the normal vector of a real surface from its ideal form. Surface roughness corresponded to large deviations and varied with an increasing number of passes.

6.4. Laser Process Parameters

During the trials there were 5 process parameters used defined below:

- **Defocus** – The distance in cm by which the processing tool was intentionally moved away from the nominal effective focus distance of the optical system. Defocus is positive when the material surface lies between the effective focus point and the focusing lens.

- **Energy percentage** – The percentage of pulse energy released controlled by optical attenuator system adjustment.

- **Energy setting** – The nominal pulse energy released by the laser under operating conditions for each test. Optical losses have not been considered.

- **Pulse repetition rate** – The number of pulses occurred per unit time at a particular point in a propagation medium.

- **Passes** – The number of passes per unit area. For handheld test, it is an approximate value.

6.5. Experimental Setup

The following types of laser source was employed manufactured by Powerlase Ltd, were used for these trials. For CFRP rectangular shape inserts, Rigel i1600, diode-lamp side pumped q-switched Nd:YAG laser was used. The laser emission characteristics are shown in Table 10. The beam was delivered via an 800 μm core diameter fibre, collimated with 180 mm FL lens and focussed with a 210 mm EFL F-Theta lens. The F-Theta lens was mounted on a Scanlabs Hurryscan of 25 mm aperture, which was suspended on an automated z-axis, actuated by a stepper motor with a ballscrew, providing focus adjustment or z-axis motion of 230 mm. 12 tests were performed in total, 4 on the shaped inserts and 4 on the cylinder samples. T

Characteristics	Values	Units
Average power	1600	W
Wavelength	1064	nm
Pulse duration	45 - 130	ns
Pulse energy	200	J

Table 10: Laser characteristics for processing rectangular shape insert.

For CFRP cylinder, a Vulcan 500c, Nd doped ns pulsed fibre laser was used. The laser emission characteristics are shown in Table 11. The beam was delivered via a 400 μm core diameter fibre on to a single axis handheld scanning tool with a focusing lens system of 180 mm.

Characteristics	Values	Units
Average power	500	W
Wavelength	1064	nm
Pulse duration	45 - 150	ns
Pulse energy	45	mJ
Pulse repetition rate	11 - 50	kHz

Table 11: Laser characteristics for processing CFRP cylinder.

In conjunction with Rigel i1600 laser source, a digital spectrometer was used to monitor the emission spectrum of the laser induced breakdown of atomic electrons, thus generating a LIBS spectrum while processing the various materials involved. The process returns different spectra depending on the material that is being processed. A 60 mm collection lens was used to target the plasma area. The spectrometer was monitoring continuously and transmitted accumulated spectra every 20 ms. The spectra were communicated to an electronic controller which monitored specified emission frequencies and issued control signals to the z-moto controller. The schematics of the test setup is shown in Figure 69.
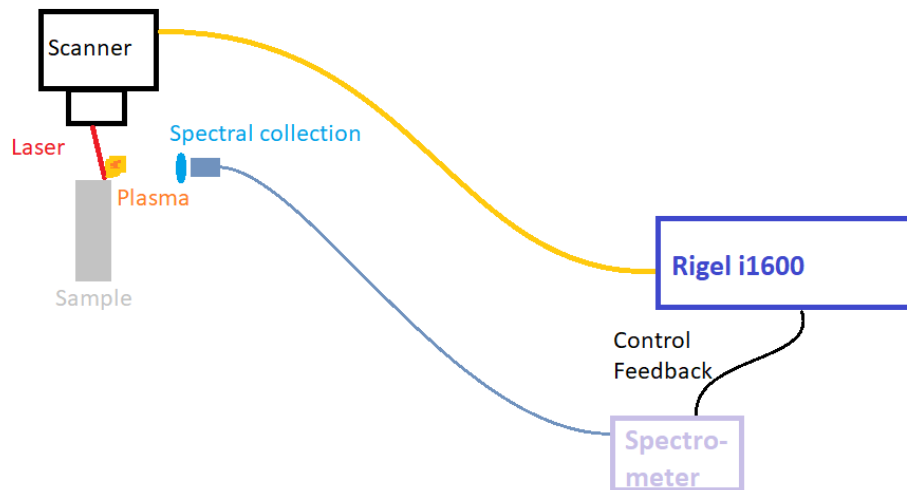
Figure 69: Test setup of Rigel i1600 laser with automated scanner and z-motion controller.

For microscopic sample analysis, 10x magnification eyeloop with 100 μm graduation reticule, a 60 to 100x magnification compact microscope with 10 μm graduation reticule and 50 x magnification USB microscope with 50 μm graduation reticule was used.

6.6. Results and Discussion

6.6.1. Approach

For the shaped inserts, the cross-section shape was loaded as a step file on the Scanlabs scanner program. The system repeats scanning on the side of the opening, across the perimeter of the cross-section. The scan started on the top of the components and when spectra representing ablation on the surface was observed, a signal was issued by the controller to the z-axis motion system to move further down into the sample. This sequence was repeated until scanning reached the programmed bottom of the insert (Figure 70).
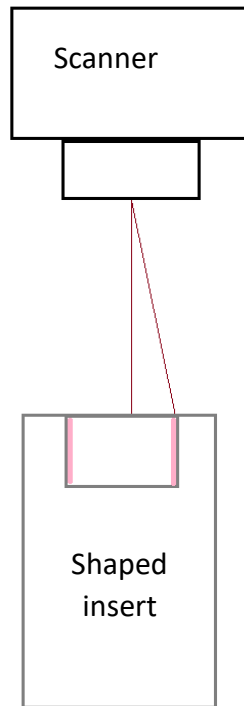
Figure 70: Schematic of using the scanner to irradiate the internal surface.

The fluence of 14.8 J/cm^2 was used which was proven in the experiments using a high pulse energy q-switched laser of flat samples to ensure correlation and continuity of results. Lines were scribed on the samples at normal angle of incidence. The results were recorded, and the sample was then tilted at a set angle until the smallest angle of incidence for the insert was reached. The laser attenuator setting was increased at each step until the same result was observed for each angle. A plot of energy required at each angle is shown in Figure 71.
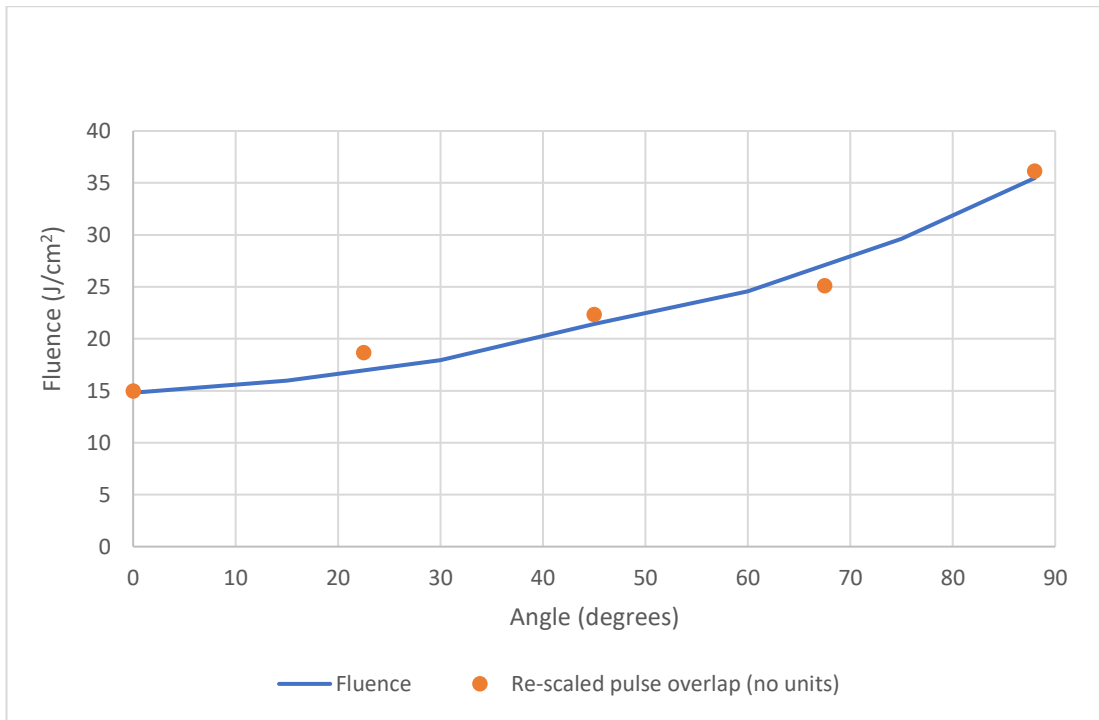
Figure 71: Fluence required to effectively detach EP adhesive from CFRP at different angle of incidences.

6.6.2. LIBS Spectra

LIBS spectra were initially obtained from the exposed CFRP materials and the EP adhesive, without allowing penetration down to the substrate. The EP adhesive served as a reference in order to avoid designating the wrong peaks as indication to move. The CFRP spectra was used to identify a characteristics peak which will indicate that the beam has reach the substrate and motion is requested in order for the process to move ahead. As the spectra collection system was continuously collecting data during the repeating circulation of the beam around the sample's cross section, the signal was an average of 1 or more circulations and thus contained mixed spectral signals. When the signal on a specific peak during one collection of data exceeded a set limit, this means that enough adhesive was being ablated in order to validate the control instruction and move deeper. The spectra recorded on the EP adhesive and CFRP is shown in Figure 72.
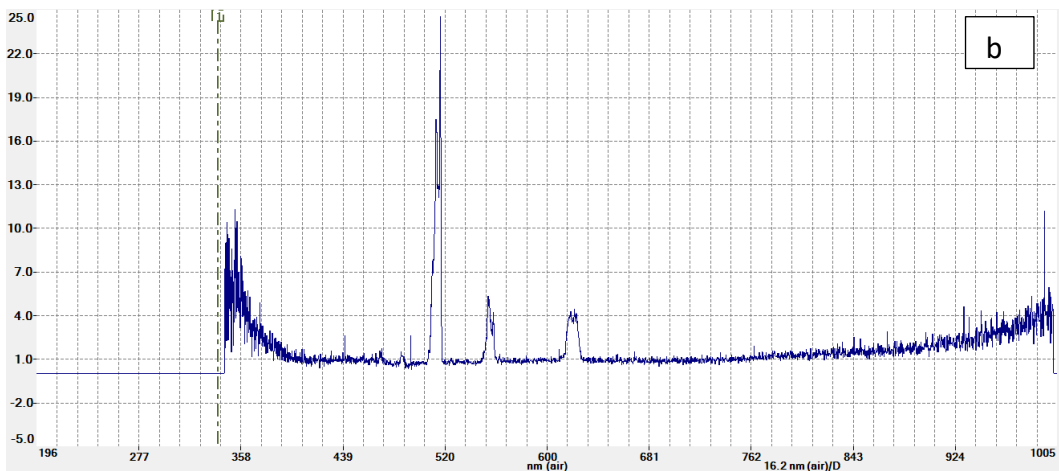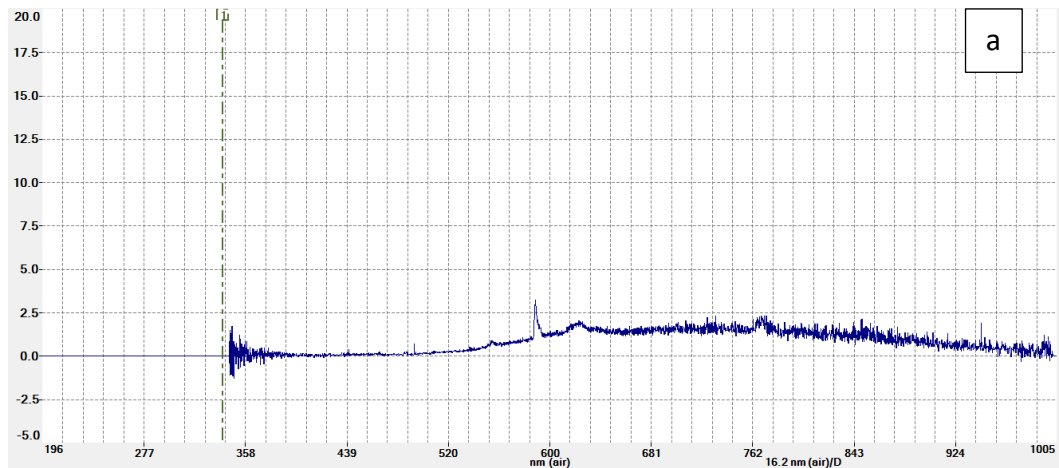
Figure 72: LIBS spectra (a) EP adhesive, (b) CFRP material.

The ablation breakdown of EP adhesive emits a small peak at around 589 nm. In contrast, the CFRP substrate emits mainly at 515 nm with smaller peaks at 548 nm and 622 nm. The controller was programmed to monitor the 515 nm emission peak. When the peak reached an intensity of 2.5, it issued a motion instruction to the z-axis motor which is propagated to the next depth of processing.

6.6.3. Processing of Shaped Inserts

The parts were lined up under the laser scanner connection to the Rigel i1600 laser. They were aligned with the trajectory of the scanner which was propagated based on cross-section design of the part. As processing progressed, spectra were continuously being collected and the depth of scanning propagated every time the CFRP emission line was detected (Figure 73). Moreover, considering that more than half of the radiation was now being reflected away from the surface due to the very sharp angle

of irradiation (30 mJ against 15 mJ for every square cm), it was inevitable due to high flammability of the filler foam, it passed its flash point and catch fire during processing.
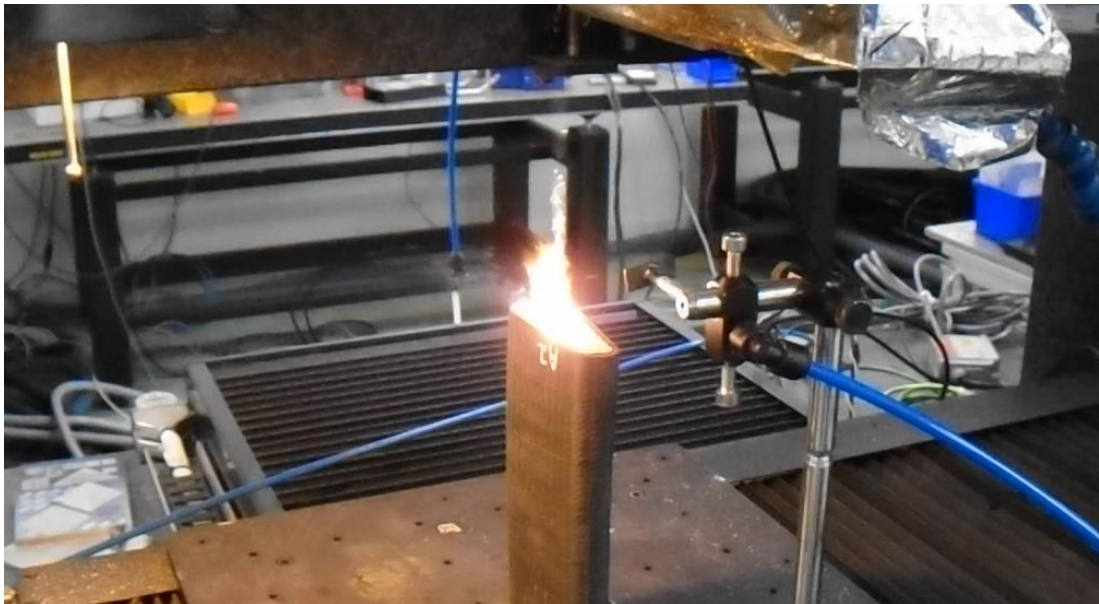
Figure 73: Shaped CFRP insert processing using a scanner and close loop control automated process depth control.

This cause fire degradation to the rest of the material and ignition of CFRP areas (Figure 74). The tendency of this particular CFRP material to ignite and catch fire indicates that the binder material does not exhibit optimum fire retardance properties and hence not suitable for laser processing. All sides of the shaped inserts have suffered significant fire damage.

Figure 74: Sustained flame inside the insert, fuelled by the existence of the filler foam material (left), Aluminium foil placed inside the shaped insert to cover the flammable material form laser irradiation (right)

Two main contributors were determined to promote fire damage. The first contributor was processing at very sharp angle, this induced significant energy losses due to high reflectivity of all materials when irradiating at grazing incidence. This raised the temperature of the surrounding structures and materials, thus increasing their temperature to the flash point. The process also becomes unstable, as small roughness features can suddenly absorb large amount of this excess energy that is otherwise reflected away, results in local over processing. Similarly, very smooth and reflective surface areas enhance reflections further and thus results in severe local reduction of process effectiveness. Consequently, the risk of fire and thermal loading on material increased significantly. This problem could be solved by inserting a processing tool into the profile's opening. These send the beam inside the material using a fibre and redirect the beam towards the side walls, by reflection. The beam then impinges on the material at a near normal angle of incidence, thus reducing the risks.

The second contributing factor was the type of material used for filler foam and the binder. These materials increase the risk of fire when some power is dissipated onto them due to inefficiencies stated in first factor. Covering the filler material with aluminium foil to reflect the impinging energy did not solve the problem. This problem could be solved by increasing peak intensity to promote more immediate ablation of the adhesive, can help to reduce the risk, if materials cannot be changed due to design. Process parameters and results for shape insert is shown in Table 12 and Table 13.

Test	Defocus (cm)	Energy (%)	Energy Setting (J)	Pulse Rep	Passes
A1	0	91	0.2427	6000	1
A2	0	91	0.2427	6000	1
A3	0	91	0.2427	6000	1
A4	0	91	0.2427	6000	1

Table 12: Process parameters of shape inserts.

Test	Adhesive debonded (%)	Sealant debonded (%)	Adhesive detached (%)	Sealant detached (%)	Damaged fibres	Burnt area (%)	Spot size (μm)	Fluence (J/cm²)
A1	1.61	2.27	9.06	11.76	560	76.20	93.3	35.47
A2	1.48	2.09	3.67	13.10	600	93.00	93.3	35.47
A3	3.14	2.36	38.48	14.50	510	36.00	93.3	35.47
A4	4.67	26.77	39.42	57.31	480	24.00	93.3	35.47
Average	2.73	8.37	22.66	24.17	537.5	57.30	-	-
Std Dev	1.30	10.62	16.41	19.16	49.03	28.26	-	-

Table 13: Process results for shaped inserts.

6.6.4. Processing CFRP Cylinder

A different approach was used with the cylindrical pieces. Due to its larger size, it was possible to irradiate its internal surfaces using a handheld laser tool, without the need of precisely aligned or depth controlled mechanised irradiation system. The Vulcan 500c laser system with a single axis handheld scanning toll was used (Figure 75 a). The minimum angle of incidence deviation from the normal the surface was approx. 14 degrees, which is within the typical process condition for most laser manufacturing methods. The maximum angle from the normal was 30 degrees to allow human positioning error and good clearance from the component's wall opposite to one being processed. The beam scanning speed was adjusted to 2 m/s in order to assimilate the required process conditions for detachment of the EP adhesive. It was noted that during single pulse tests, the detachment was not effective. The scanning speed was increased to 7.5 m/s. The process effectiveness was a such that a single raster scan of the beam was achieving a full detachment (Figure 75 b).

Figure 75: (a) Handheld laser detachment of EP adhesive, (b) EP adhesive peeled from the cylinder surface.

The laser detachment or peeling effect takes place because of the optimum combinations of adhesive and substrate material properties with EP adhesive shown good transmission in spectral analysis. The substrate has a very good absorbance of light. Particularly one of the layers of the substrate has very high absorption at 1064 nm. During the examination it was noticed that several of the top layer fibres have been exposed under the processed area and somewhat elevated. It was assumed that sealant is transmissive, but the binder and possibly the fibres themselves are highly absorptive at that wavelength.

Consequently, the laser light reaches with high intensity at the top layer of binder or fibres and releases all layers residing above that level by eliminating the adhesive bond (Figure 76).
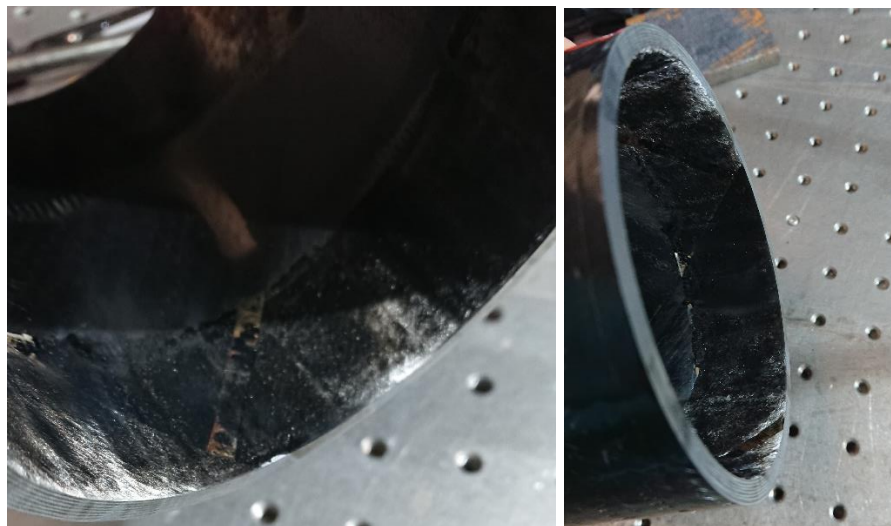
Figure 76: EP adhesive removed from inside the cylinder.

Due to high process efficiency and ability of high intensity pulses to interact with critical bond level, thermal dissipation into the materials involved is kept minimum. Hence, the process ensures the lowest possible thermal or mechanical impact on the component. Process parameters and results for CFRP cylinder is shown in Table 14 and Table 15. The detachment and debonding measurements show that the majority of the phenomena occurred with sealant and adhesive detachment to almost an average of 50% each. The burnet area is very small and therefore it was acceptable. The surface roughness was measured on the remaining surface of about 50% of

sealant and 50% of surface of cylinder. The average value of surface roughness was 32.45 µm which was below the surface abrasion of 100 µm.

Test	Defocus (cm)	Energy (%)	Energy Setting (J)	Pulse Rep	Passes
A1	0	45	0.048	15000	2
A2	0	45	0.048	15000	2
A3	0	45	0.048	15000	2
A4	0	45	0.048	15000	2

Table 14: Process parameter of CFRP cylinder.

Test	Adhesive debonded (%)	Sealant debonded (%)	Adhesive detached (%)	Sealant detached (%)	Damaged fibres	Burnt area (%)	Surface roughness (µm)
A1	0.32	3.84	33.93	59.21	94	0.00	32.28
A2	0.11	4.92	64.42	29.78	78	0.33	29.43
A3	0.64	5.19	39.92	54.36	107	0.00	34.54
A4	0.34	6.24	47.84	43.08	89	0.00	33.56
Average	0.34	5.05	46.53	46.61	92	0.08	32.45
Std Dev	0.19	0.85	11.45	11.34	10.42	0.14	1.92

Table 15: Process results for CFRP cylinder.

6.7. Summary

The study confirms the possibility of transferring of process developed for detaching EP adhesive using q-switched pulsed laser onto industrial grade laser with high repetition rate and high throughput processing capability. Whilst cleaning the internal cavity through small aperture, where standard laser processing tools does not fit, irradiation angle had to be reduced to near grazing incidence angles. Whereas, when processing internal areas through much larger apertures, the angle of incidence was closer to 90 degrees, the process was much more efficient with good results demonstrated.

A LIBS based in-line process-controlled method has been successfully deployed and demonstrated for the first time on CFRP material processing. However, the material flammability has caused problems with the overall result of the process.

CHAPTER 7

7. Conclusion

7.1. Laser Cutting

The experimental study investigated and analysed the effects of different laser cutting process parameters on the cut surface quality of CFRP composites. Based on the findings it was concluded that the behaviour of the material during cutting is attributed to the wide weaving, specifically on the top and bottom layers, where the material suffers significant amount of frying when processed. It is possible to compensate multiple passes with processing each pass at an equivalent higher speed. In fact, an overall speed advantage can be gained when taking such an approach and making larger than proportionate speed increments. Multi-pass with 3 passes was found to be significantly supressing top and bottom fraying and improved the cut quality, whether executed with large, small, or double aperture.

Double aperture or large aperture combined high linear speed of 10 to 12 m/min returned some of the best results with laser cutting speed of 2.5 m/min and over was achieved.

Cuts performed using a single pass technique exceeds the target performance in terms of cutting speed and fibre damage. Trials 46b to 49 were performed using single pass and fibre damage below 100 μm was achieved. Further single pass trials were conducted with different laser stand-off distances in trials 55 to 57 and fibre damage below 70 μm was achieved as shown in Appendix A.

For trials 46b to 49, the cutting speed achieved were between 2.5 m/min to 3.5 m/min and for trials 55 to 57 the cutting speed achieved was 2.5 m/min as shown in Appendix A. All the trials mentioned above are conducted using a single pass and achieved equivalent or better target speed of 2.5 m/min and fibre damage of 100 μm. Trenching returns more consistent quality of cuts. Trenching (trials 64 – 67) or double aperture processing (trials 69 – 72) achieves low fibre damage, below 100 μm and averaging around 50 μm . It was also observed that sample temperature does not

exceed 100 ^{0}C and was thus considered safe for the material in macroscale. Furthermore, regression analysis (appendix B) was carried out and five models for CAD/CAM interface were developed. In addition, contour plots have been developed for effective analysing of the behaviour of process parameters on the fibre damage.

7.2. Laser Cleaning

The study concluded that it is possible to clean both EP and PU adhesives from CFRP samples using pulsed NIR laser. There seems to be some natural process window that limits the damage on the sample, in comparison to that induced on the coatings, however, this does not shield the sample completely. This effect is best exploited at this NIR wavelength of around 1 µm by releasing pulses of high energy over a large spot size. The EP adhesive can undergo debonding from the fibres as well as the sealant if the layer thickness is consistent over irradiation area. For layers with non-consistent thickness, that was not possible as irradiation reaches the substrate and damages surface fibres.

For the PU adhesive, an ablation or material degradation process was used. when promoting material degradation, the substrate is expected to suffer less damage on the surface fibres, while a purely ablative process would not differentiate between the materials, especially considering the very high optical absorption of both materials. Surface topography is more of a concern for PU adhesive due to its nature and large changes (around 1.5 mm) in topography as in Figure 159 and Figure 160 of Appendix K that shows a photograph and 3D X-ray computed tomography (XCT) scan, respectively was removed with laser using an ablation process. Whereas EP adhesive had a more uniform thinner (0.3 mm) spread and due to its nature (semi-transparent) it was removed by the laser in more effective debonding manner. Figure 161 and Figure 162 of Appendix K shows the EP adhesive on the CFRP sample photograph and 3D XCT scan, respectively. The damage occurred on the CFRP sample from removing PU adhesive was 60% greater than removing EP adhesive since EP adhesive required less energy to be removed.

A concerning damage that could occur on the substrate is the damage caused by overall heating during the laser cleaning process. The developed process managed to control the temperature at any time below 76 ^{0}C in thermography imaging of both adhesives maintaining the integrity of polymers involved in the bulk composite structure.

Tensile shear test of virgin CFRP samples joined using PU adhesive was performed, the adhesive joint failed around 1100 N. Whereas, tensile shear test of laser cleaned samples, when joined using PU adhesive, failure occurs around 800 – 1000 N (Figure 59). Similar test was repeated for EP adhesive. The adhesive joint of EP adhesive failed around 5000 – 6000 N. The test was repeated on laser cleaned samples, the joint failed around 5000 – 6000 N (Figure 60). Therefore, the numerical results of the tensile shear test showed that laser cleaned samples of EP adhesive were in close agreement to the corresponding benchmark virgin samples than the PU cleaned samples tested and this was to be expected as most of the glue was removed from EP samples and the laser cleaning was not as aggressive as PU cleaning. The difference in results could also be due to the separation of the samples before laser cleaning that may have caused severe damage to the samples.

7.3. Case study: Laser Cleaning Curved Surfaces.

The study showed that it was possible to transfer the process developed for detaching EP adhesive using q-switched laser pulses, onto industrial grade lasers with high repetition rate and throughput processing capability. The process was also employed in removing adhesive from internal surfaces of curved 3D shapes.

Cleaning internal cavities through small aperture where standard laser processing tools do not fit was challenging, especially when the irradiation angle had to be reduced to near grazing incidence angles. Specialised bore reaching tools are recommended for this type of processing. When processing internal areas through much larger apertures, that allow angle of incidence closer to 90 degrees, the process can become much more efficient and good results were demonstrated.

The performance of the process depends significantly on the types of materials being used and their optical and thermo-chemical characteristics. Performance varies from very high thermal and fire damage to nearly inexistent thermal damage or material degradation, apart from some surface fibre exposure on the irradiated area which may aid the adhesion and bond strength of future adhesive layers applied to the material. A LIBS based in-line process -controlled method has been successfully deployed and demonstrated for the first time on CFRP material processing. However, the material flammability has caused problems with the overall results of the process.

7.4. Key Performance Indicators (KPI)

7.4.1. Laser Cutting

Current state of the art for cutting speed is 0.1 m/min to 1.5 m/min [132] for 1.5 mm thick sample. The cutting speed of 2.5 m/min was achieved for trials using 1 mm nozzle gap for gas flow, with single pas cutting process shown in Table 18 Appendix A. cutting speed between 3 – 5 m/min was achieved for trials using a mixture of 1 mm, 2 mm, and double aperture nozzle (2.0; 1.5 mm) nozzle, with single and multi-pass cutting process. Enhanced cutting speed of 7 – 15 m/min was achieved for trials 64 – 68, which was carried out using trenching and double aperture technique as shown in Table 18 Appendix A. All the trials were conducted on 2 mm CFRP flat plates.

The state of the art for fibre damage is between 300 to 350 μm for 1 mm thick sample [133]. The fibre damage of 100 μm and lower was achieved. Fibre damage extent between 10 – 50 μm was achieved for trials 47, 48, 53, 55, 56, 58, 63, 64, 65, 66, 68, 69 and 70 (Table 20 Appendix A).

7.4.2. Laser Cleaning

The laser cleaning process of separated CFRP parts was never attempted before as damaged parts joined using adhesives were considered as waste. The developed process successfully cleaned the adhesive from the separated CFRP parts for remanufacturing purposes. PU and EP were two adhesives that were cleaned from separated CFRP flat plates using NIR laser.

Tensile shear test of virgin CFRP samples joined using PU adhesive was performed. The adhesive joint failed around 1000 – 1600 N. Whereas, tensile shear test of laser cleaned samples, when joined using PU adhesive, failure occurs around 800 – 1000 N (Figure 59). Similar test was repeated for EP adhesive. The adhesive joint of EP glue on virgin CFRP samples failed around 5000 – 6000 N. The test was repeated on laser cleaned samples, the joint failed around 5000 – 6000 N (Figure 60). The results show that EP adhesive laser cleaned samples are in better agreement with virgin samples.

The PU bonded samples have been found to mainly exhibit cohesive failure, whereas EP bended samples exhibit mixed failures. PU bonded samples featured an area percentile covered by adhesive after laser cleaning which is greater than EP bonded samples. This difference is considered a major contributor to the cohesive failure of PU bonded samples. It is likely that the laser radiation alters and degrades the high optical absorption PU adhesive to depths of 5 to 50 μm, thus reducing the joint's cohesive strength when re-using any post cleaning remaining adhesive in the bond layer volume.

In contrast, EP joint failures post laser cleaning show limited cohesive failure, as the transmission ratio of the two materials at 1064 nm stands at approximately 20.8 dB, hence most of the laser energy in EP adhesive cleaning has acted on the adhesive to sealant or sealant to fibre level. This is represented in Figure 15 above where the adhesive to sealant detachment or debonding area percentiles are typically close to or above 80%.

CHAPTER 8

8. Future work

8.1. Laser Cutting

Although the results achieved with cuts using single pass technique exceeds the target performance, if further improvements are required in terms of faster cutting speed and reduced fibre damage then the implementation of trenching and multi-pass using double aperture is recommended using a high precision robot, and a processing tool containing 2D beam scanner or rotation optics. A 100 µm positional repeat precision will be required across the whole cut trajectory that the robot will follow.

8.2. Laser Cleaning

For further improvement in the quality of the surface left behind, it is recommended that an automated feedback system is used to return information of coating thickness and surface topography and possibly even density, to central controller that will then adjust laser processing parameters accordingly in order to control the depth of penetration. PU adhesive which is an ablation-based process would then be better suited with a green UV or far-IR laser. This will have a good interaction and optical absorption on most of the material. Some examples of the measurement device are a laser beam deflection surface profiler or distance measurer, an acoustic monitor, a T-Ray monitor, interferometric topographer, or a confocal sensor.

Another approach would be to design and build a laser at a wavelength specifically selected possibly in the near to middle IR region for the EP adhesive, which would transmit through the adhesive and become absorbed by the sealant surface. As polymers have very sharp absorption peaks in the region, characteristics of their chemical constituency, a wavelength can be identified there. The laser would however need to reach sufficient peak intensities per pulse for necessary debonding and typically a laser of at least a few Watt in average power and a short or ultra-short pulse durations would meet these conditions.

8.3. Laser Cleaning Curved Surfaces

The small aperture of the shaped inserts can be processed by a low repetition rate high pulse energy laser and open beam optical components with a last small turning mirror inside the aperture. This will raise other engineering problems on beam delivery and system handling.

An absorbent layer may be applied between EP and most CFRP composite substrate, in order to enhance the detachment process and promote similar low impact results like the one demonstrated on the cylindrical components. An example of such absorbent layer or additive colourant is Clearweld^{TM}. Other pigmentation or colouring additives with specific absorption bands at 1064 nm can also be used.

It would be very helpful to conduct spectral studies on the cylindrical material fibres, binder and sealant materials in order to understand and validate the laser absorption and debonding process observed in the study.

References

[1]   Ravishankar SR, Murthy CRL. Characteristics of AE signals obtained during drilling composite laminates. NDT E Int 2000;33:341–8. https://doi.org/10.1016/S0963-8695(99)00059-6.

[2]   Abrate S, Walton DA. Machining of composite materials. Part I: Traditional methods. Compos Manuf 1992;3:75–83. https://doi.org/10.1016/0956-7143(92)90119-F.

[3]   Jacobs, J.A., Kilduff TF. Engineering materials technology, structures, processing, properties and selection. 3rd ed. London: Prentice-Hall; 1997.

[4]   Teti R. Machining of composite materials. CIRP Ann - Manuf Technol 2002;51:611–34. https://doi.org/10.1016/S0007-8506(07)61703-X.

[5]   Selzer R, Friedrich K. Mechanical properties and failure behaviour of carbon fibre-reinforced polymer composites under the influence of moisture. Compos Part A Appl Sci Manuf 1997;28:595–604. https://doi.org/10.1016/S1359-835X(96)00154-6.

[6]   Campbell FC. Chapter 1 - Introduction to Composite Materials and Processes: Unique Materials that Require Unique Processes. In: Campbell FC, editor. Manuf. Process. Adv. Compos., Amsterdam: Elsevier Science; 2004, p. 1–37. https://doi.org/https://doi.org/10.1016/B978-185617415-2/50002-2.

[7]   Fujita M, Somekawa T, Miyanaga N. Micromachining of CFRP with ultra-short laser pulses. Phys Procedia 2013;41:636–9. https://doi.org/10.1016/j.phpro.2013.03.127.

[8]   Goeke A, Emmelmann C. Influence of laser cutting parameters on CFRP part quality. Phys Procedia 2010;5:253–8. https://doi.org/10.1016/j.phpro.2010.08.051.

[9]   Klotzbach A, Hauser M, Beyer E. Laser cutting of carbon fiber reinforced polymers using highly brilliant laser beam sources. Phys Procedia 2011;12:572–7. https://doi.org/10.1016/j.phpro.2011.03.072.

[10]   Bluemel S, Jaeschke P, Wippo V, Bastick S, Stute U, Kracht D, et al. Laser machining of CFRP using a high power fiber laser - Investigations on the heat affected zone. ECCM 2012 - Compos Venice, Proc 15th Eur Conf Compos Mater 2012:24–8.

[11]   National Aeronautics and Space Administration. No Title 2010. http://science.nasa.gov/ems/01_intro (accessed January 13, 2021).

[12]   Ready JF. Chapter 1 - Fundamentals of Lasers. In: Ready JF, editor. Ind. Appl. Lasers (Second Ed. Second Edi, San Diego: Academic Press; 1997, p. 1–30. https://doi.org/https://doi.org/10.1016/B978-012583961-7/50003-X.

[13] Ashby MF. Materials Selection in Mechanical Design. Design 2005:624. https://doi.org/10.1016/B978-1-85617-663-7.00011-4.

[14] Ion JC. Chapter 3 - Lasers. In: Ion JC, editor. Laser Process. Eng. Mater., Oxford: Butterworth-Heinemann; 2005, p. 41–103. https://doi.org/https://doi.org/10.1016/B978-075066079-2/50006-4.

[15] Steen WM, Mazumder J. Laser Material Processing. 2010. https://doi.org/10.1007/978-1-84996-062-5.

[16] Weber J. Amplification of microwave radiation by substances not in thermal equilibrium. IRE Trans Prof Gr Electron Devices 1953;3:1. https://doi.org/10.1109/IREPGED.1953.6811068.

[17] Slusher RE. Laser technology. Rev Mod Phys 1999;71:471–9. https://doi.org/10.1103/revmodphys.71.s471.

[18] Schawlow AL, Townes CH. Infrared and optical masers. Phys Rev 1958;112:1940–9. https://doi.org/10.1103/PhysRev.112.1940.

[19] MAIMAN TH. Stimulated Optical Radiation in Ruby. Nature 1960;187:493–4. https://doi.org/10.1038/187493a0.

[20] Javan A, Bennett WR, Herriott DR. Population inversion and continuous optical maser oscillation in a gas discharge containing a He-Ne mixture. Phys Rev Lett 1961;6:106–10. https://doi.org/10.1103/PhysRevLett.6.106.

[21] Bromberg JL. The laser in America, 1950-1970 1991.

[22] Gefvert B, Wallace J, Overton G, Nogee A. Annual Laser Market Review & Forecast 2020. Laser Focus World 2020:46–56.

[23] O'Neill W, Sparkes M, Varnham M, Horley R, Birch M, Woods S, et al. High power high brightness industrial fiber laser technology. Int. Congr. Appl. Lasers Electro-Optics, Laser Institute of America; 2004, p. 301. https://doi.org/10.2351/1.5060263.

[24] Eberly JH, Milonni PW. Quantum Optics. In: Meyers RABT-E of PS and T (Third E, editor., New York: Academic Press; 2003, p. 409–39. https://doi.org/https://doi.org/10.1016/B0-12-227410-5/00627-X.

[25] Silfvast WT. Lasers. In: Meyers RABT-E of PS and T (Third E, editor., New York: Academic Press; 2003, p. 267–81. https://doi.org/https://doi.org/10.1016/B0-12-227410-5/00363-X.

[26] Kim J, Moon DG. Basic Principles of Laser for Prostate Surgery. Korean J Androl 2011;29. https://doi.org/10.5534/kja.2011.29.2.101.

[27] Chyrssolouris G. Laser Machining: Theory and Practice. Springer; 1991.

[28] Ready JF, Farson DF, Feeley T. LIA Handbook of Laser Materials Processing. 2001.

[29]   Steen WM. Laser material processing — an overview. J Opt A Pure Appl Opt 2003;5:3–7. https://doi.org/10.1088/1464-4258/5/4/351.

[30]   Mickelson A, Guenther BD. Fiber and guided wave optics: overview. Encycl. Mod. Opt., 2005, p. 425–32.

[31]   Town GE. Lasers, Optical Fibres. Encycelopedia Phys. Sci. Technol., 2004, p. 419–41.

[32]   MacFadyen AJ, Jennings BR. Fibre-optic systems for dynamic light scattering — a review. Opt & Laser Technol 1990;22:175–87. https://doi.org/10.1016/0030-3992(90)90105-d.

[33]   France PW. Optical Fibre Lasers and Amplifiers. British Telecom Research Laboratories; 1991.

[34]   Yincan Y, Xinmin J, Guofu P, Wei J, editors. Chapter 1 - Introduction. Submar. Opt. Cable Eng., Academic Press; 2018, p. 1–27. https://doi.org/https://doi.org/10.1016/B978-0-12-813475-7.00001-1.

[35]   Basting D, Marowsky G. Excimer Laser Technology. Berlin, Heidelberg: Springer Berlin Heidelberg; 2005. https://doi.org/10.1007/b137894.

[36]   Tseng AA, Chen YT, Chao CL, Ma KJ, Chen TP. Recent developments on microablation of glass materials using excimer lasers. Opt Lasers Eng 2007;45:975–92. https://doi.org/10.1016/j.optlaseng.2007.04.003.

[37]   Bass M, Kar A. Laser–Materials Interactions. Encycl. Phys. Sci. Technol., Elsevier; 2003, p. 247–65. https://doi.org/10.1016/B0-12-227410-5/00361-6.

[38]   Chryssolouris G, Tsoukantas G, Salonitis K, Stavropoulos P, Karagiannis S. Laser machining modeling and experimentation: an overview. In: Carabelas A, Baldacchini G, Di Lazzaro P, Zevgolis D, editors., 2003, p. 158. https://doi.org/10.1117/12.513593.

[39]   Dutta Majumdar J, Manna I. Laser processing of materials. Sadhana - Acad Proc Eng Sci 2003;28:495–562. https://doi.org/10.1007/BF02706446.

[40]   Ghany KA, Newishy M. Cutting of 1.2 mm thick austenitic stainless steel sheet using pulsed and CW Nd:YAG laser. J Mater Process Technol 2005;168:438–47. https://doi.org/10.1016/j.jmatprotec.2005.02.251.

[41]   Belforte DA. Laser Cutting. Encycl. Mater. Sci. Technol., Elsevier; 2001, p. 4399–402. https://doi.org/10.1016/B0-08-043152-6/00770-1.

[42]   Belforte DA. Laser Cutting. Encycl. Mater. Sci. Technol., Elsevier; 2001, p. 4399–402. https://doi.org/10.1016/B0-08-043152-6/00770-1.

[43]   Ivarson A, Powell J, Kamalu J, Magnusson C. The oxidation dynamics of laser cutting of mild steel and the generation of striations on the cut edge. J Mater Process Tech 1994;40:359–74. https://doi.org/10.1016/0924-0136(94)90461-8.

[44] Rao BT, Kaul R, Tiwari P, Nath AK. Inert gas cutting of titanium sheet with pulsed mode CO2 laser. Opt Lasers Eng 2005;43:1330–48. https://doi.org/10.1016/j.optlaseng.2004.12.009.

[45] Man HC, Duan J, Yue TM. Design and characteristic analysis of supersonic nozzles for high gas pressure laser cutting. J Mater Process Technol 1997;63:217–22. https://doi.org/10.1016/S0924-0136(96)02627-1.

[46] Quintero F, Pou J, Lusquiños F, Boutinguiza M, Soto R, Pérez-Amor M. Comparative study of the influence of the gas injection system on the Nd:yttrium-aluminum-garnet laser cutting of advanced oxide ceramics. Rev Sci Instrum 2003;74:4199–205. https://doi.org/10.1063/1.1597953.

[47] Quintero F, Pou J, Fernández JL, Doval AF, Lusquiños F, Boutinguiza M, et al. Optimization of an off-axis nozzle for assist gas injection in laser fusion cutting. Opt Lasers Eng 2006;44:1158–71. https://doi.org/10.1016/j.optlaseng.2005.10.001.

[48] Di Pietro P, Yao YL. An investigation into characterizing and optimizing laser cutting quality - A review. Int J Mach Tools Manuf 1994;34:225–43. https://doi.org/10.1016/0890-6955(94)90103-1.

[49] Dubey AK, Yadava V. Laser beam machining-A review. Int J Mach Tools Manuf 2008;48:609–28. https://doi.org/10.1016/j.ijmachtools.2007.10.017.

[50] Tabata N, Yagi S, Hishii M. Present and future of lasers for fine cutting of metal plate. J Mater Process Technol 1996;62:309–14. https://doi.org/10.1016/S0924-0136(96)02426-0.

[51] Meijer J. Laser beam machining (LBM), state of the art and new opportunities. J Mater Process Technol 2004;149:2–17. https://doi.org/10.1016/j.jmatprotec.2004.02.003.

[52] Kaplan AFH. Theoretical Analysis of Laser Beam Cutting. 2002.

[53] Yilbas Z. Study into the measurement and prediction of penetration time during COz 1990;204:105–13.

[54] Kaplan AFH. An analytical model of metal cutting with a laser beam. J Appl Phys 1996;79:2198–208. https://doi.org/10.1063/1.361098.

[55] Yilbas BS, Kar A. Thermal and efficiency analysis of the CO2 laser cutting process. Opt Lasers Eng 1998;30:93–106. https://doi.org/10.1016/S0143-8166(97)00060-2.

[56] Wee LM, Li L. An analytical model for striation formation in laser cutting. Appl Surf Sci 2005;247:277–84. https://doi.org/10.1016/j.apsusc.2005.01.143.

[57] Farooq K, Kar A. Removal of laser-melted material with an assist gas. J Appl Phys 1998;83:7467–73. https://doi.org/10.1063/1.367509.

[58] La Rocca A V. Second generation laser manufacturing systems. In: Panchenko

VY, Golubev VS, editors., 1996, p. 202. https://doi.org/10.1117/12.234190.

[59] Powell J, Tan WK, Maclennan P, Rudd D, Wykes C, Engstrom H. Laser cutting stainless steel with dual focus lenses. J Laser Appl 2000;12:224–31. https://doi.org/10.2351/1.1324718.

[60] Li L, Kim JH, Abdul Shukor MH, Jennings H. Abrasive laser machining. Laser Inst Am Proc 1997;83. https://doi.org/10.2351/1.5059623.

[61] Arai T, Riches S. Thick plate cutting with spinning laser beam. Laser Inst Am Proc 1997;83. https://doi.org/10.2351/1.5059632.

[62] Altin Karataş M, Gökkaya H. A review on machinability of carbon fiber reinforced polymer (CFRP) and glass fiber reinforced polymer (GFRP) composite materials. Def Technol 2018;14:318–26. https://doi.org/10.1016/j.dt.2018.02.001.

[63] Shyha I, Soo SL, Aspinwall D, Bradley S. Effect of laminate configuration and feed rate on cutting performance when drilling holes in carbon fibre reinforced plastic composites. J Mater Process Technol 2010;210:1023–34. https://doi.org/10.1016/j.jmatprotec.2010.02.011.

[64] Hexcel corporation n.d. https://hexcel.com/Markets/Commercial-Aerospace/Commercial-Aircraft.

[65] Shivi Kesarwani. Polymer Composites in Aviation Sector. Int J Eng Res 2017;V6. https://doi.org/10.17577/IJERTV6IS060291.

[66] Ishai O, Daniel I. Engineering Mechanics of Composite Materials. 2005.

[67] Pan CT, Hocheng H. Evaluation of anisotropic thermal conductivity for unidirectional FRP in laser machining. Compos - Part A Appl Sci Manuf 2001;32:1657–67. https://doi.org/10.1016/S1359-835X(00)00093-2.

[68] Ashby AMF, Bush SF, Swindells N, Bullough R, Ellison G, Lindblom Y, et al. Technology of the 1990s : Advanced Materials and Predictive Design [and Discussion] Source : Philosophical Transactions of the Royal Society of London . Series A , Mathematical and Physical Sciences , Vol . 322 , No . 1567 , Technology in the 1990s : Th 2019;322.

[69] Marsh G. Vinyl ester -the midway boat building resin. Reinf Plast 2007;51:20–3. https://doi.org/10.1016/S0034-3617(07)70248-5.

[70] Abrão AM, Faria PE, Rubio JCC, Reis P, Davim JP. Drilling of fiber reinforced plastics: A review. J Mater Process Technol 2007;186:1–7. https://doi.org/10.1016/j.jmatprotec.2006.11.146.

[71] Shyha IS, Aspinwall DK, Soo SL, Bradley S. Drill geometry and operating effects when cutting small diameter holes in CFRP. Int J Mach Tools Manuf 2009;49:1008–14. https://doi.org/10.1016/j.ijmachtools.2009.05.009.

[72] Abrate S, Walton D. Machining of composite materials. Part II: Non-

traditional methods. Compos Manuf 1992;3:85–94.
https://doi.org/10.1016/0956-7143(92)90120-J.

[73]   Shanmugam DK, Nguyen T, Wang J. A study of delamination on
graphite/epoxy composites in abrasive waterjet machining. Compos Part A
Appl Sci Manuf 2008;39:923–9.
https://doi.org/10.1016/j.compositesa.2008.04.001.

[74]   Walter E, Ashbee KHG. Osmosis in composite materials. Composites
1982;13:365–8. https://doi.org/https://doi.org/10.1016/0010-
4361(82)90144-6.

[75]   Lau WS, Wang M, Lee WB. Electrical discharge machining of carbon fibre
composite materials. Int J Mach Tools Manuf 1990;30:297–308.
https://doi.org/10.1016/0890-6955(90)90138-9.

[76]   Habib S, Okada A, Ichii S. Effect of cutting direction on machining of carbon
fibre reinforced plastic by electrical discharge machining process. Int J Mach
Mach Mater 2013;13:414–27. https://doi.org/10.1504/IJMMM.2013.054272.

[77]   Black, J.T., Kosher RA. Materials and Processes in Manufacturing. 11th ed.
John Wiley & Sons; 2012.

[78]   Cenna AA, Mathew P. Evaluation of cut quality of fibre-reinforced plastics—A
review. Int J Mach Tools Manuf 1997;37:723–36.
https://doi.org/10.1016/S0890-6955(96)00085-5.

[79]   Pan CT, Hocheng H. The anisotropic heat-affected zone in the laser grooving
of fiber-reinforced composite material. J Mater Process Technol 1996;62:54–
60. https://doi.org/10.1016/0924-0136(95)02192-2.

[80]   Voisey KT, Fouquet S, Roy D, Clyne TW. Fibre swelling during laser drilling of
carbon fibre composites. Opt Lasers Eng 2006;44:1185–97.
https://doi.org/10.1016/j.optlaseng.2005.10.008.

[81]   Tagliaferri V, Di Ilio A, Visconti C. Laser cutting of fibre-reinforced polyesters.
Composites 1985;16:317–25. https://doi.org/10.1016/0010-4361(85)90284-
8.

[82]   Mathew J, Goswami GL, Ramakrishnan N, Naik NK. Parametric studies on
pulsed Nd:YAG laser cutting of carbon fibre reinforced plastic composites. J
Mater Process Technol 1999;89–90:198–203. https://doi.org/10.1016/S0924-
0136(99)00011-4.

[83]   Caprino G, Tagliaferri V. Maximum cutting speed in laser cutting of fiber
reinforced plastics. Int J Mach Tools Manuf 1988;28:389–98.
https://doi.org/10.1016/0890-6955(88)90052-1.

[84]   Fenoughty KA, Jawaid A, Pashby IR. Machining of advanced engineering
materials using traditional and laser techniques. J Mater Process Technol
1994;42:391–400. https://doi.org/10.1016/0924-0136(94)90145-7.

[85]   Negarestani R, Li L. Laser machining of fibre-reinforced polymeric composite materials. Mach. Technol. Compos. Mater., Elsevier; 2012, p. 288–308. https://doi.org/10.1533/9780857095145.2.288.

[86]   Dell'Erba M, Galantucci LM, Miglietta S. An experimental study on laser drilling and cutting of composite materials for the aerospace industry using excimer and CO2 sources. Compos Manuf 1992;3:14–9. https://doi.org/10.1016/0956-7143(92)90178-W.

[87]   Garrison BJ, Srinivasan R. Laser ablation of organic polymers: Microscopic models for photochemical and thermal processes. J Appl Phys 1985;57:2909–14. https://doi.org/10.1063/1.335230.

[88]   Takahashi K, Tsukamoto M, Masuno S, Sato Y. Heat conduction analysis of laser CFRP processing with IR and UV laser light. Compos Part A Appl Sci Manuf 2016;84:114–22. https://doi.org/10.1016/j.compositesa.2015.12.009.

[89]   Xu H, Hu J, Yu Z. Absorption behavior analysis of Carbon Fiber Reinforced Polymer in laser processing. Opt Mater Express 2015;5:2330. https://doi.org/10.1364/ome.5.002330.

[90]   Oh S, Lee I, Park Y Bin, Ki H. Investigation of cut quality in fiber laser cutting of CFRP. Opt Laser Technol 2019;113:129–40. https://doi.org/10.1016/j.optlastec.2018.12.018.

[91]   Schneider F, Wolf N, Petring D. High power laser cutting of fiber reinforced thermoplastic polymers with cw- and pulsed lasers. Phys Procedia 2013;41:415–20. https://doi.org/10.1016/j.phpro.2013.03.096.

[92]   Weber R, Hafner M, Michalowski A, Graf T. Minimum Damage in CFRP Laser Processing Single 2011;12:302–7. https://doi.org/10.1016/j.phpro.2011.03.137.

[93]   Herzog D, Jaeschke P, Meier O, Haferkamp H. Investigations on the thermal effect caused by laser cutting with respect to static strength of CFRP. Int J Mach Tools Manuf 2008;48:1464–73. https://doi.org/10.1016/j.ijmachtools.2008.04.007.

[94]   Freitag C, Onuseit V, Weber R, Graf T. High-speed Observation of the Heat Flow in CFRP during Laser Processing. Phys Procedia 2012;39:171–8. https://doi.org/10.1016/j.phpro.2012.10.027.

[95]   Leone C, Genna S, Tagliaferri V. Fibre laser cutting of CFRP thin sheets by multi-passes scan technique. Opt Lasers Eng 2014;53:43–50. https://doi.org/10.1016/j.optlaseng.2013.07.027.

[96]   Leone C, Genna S. Heat affected zone extension in pulsed Nd:YAG laser cutting of CFRP. Compos Part B Eng 2018;140:174–82. https://doi.org/10.1016/j.compositesb.2017.12.028.

[97]   Niino H. Laser cutting of carbon fiber reinforced plastics (CFRP and CFRTP) by

IR fiber laser irradiation. J Laser Micro/Nanoengineering 2016;11:104–10. https://doi.org/10.2961/jlmn.2016.01.0020.

[98] Jung K-W, Kawahito Y, Katayama S. Ultra high speed laser cutting of CFRP using a scanner head. Trans JWRI 2013;42:9–14.

[99] Rao S, Sethi A, Das AK, Mandal N, Kiran P, Ghosh R, et al. Fiber laser cutting of CFRP composites and process optimization through response surface methodology. Mater Manuf Process 2017;32:1612–21. https://doi.org/10.1080/10426914.2017.1279296.

[100] Riveiro A, Quintero F, Lusquiños F, del Val J, Comesaña R, Boutinguiza M, et al. Laser cutting of Carbon Fiber Composite materials. Procedia Manuf 2017;13:388–95. https://doi.org/10.1016/j.promfg.2017.09.026.

[101] Li M, Li S, Yang X, Zhang Y, Liang Z. Fiber laser cutting of CFRP laminates with single- and multi-pass strategy: A feasibility study. Opt Laser Technol 2018;107:443–53. https://doi.org/10.1016/j.optlastec.2018.06.025.

[102] Hempstead B, Thayer B, Williams S. Composite Automatic Wing Drilling Equipment (CAWDE), 2006. https://doi.org/10.4271/2006-01-3162.

[103] Marsh G. Composites and metals - A marriage of convenience? Reinf Plast 2014;58:38–42. https://doi.org/10.1016/S0034-3617(14)70108-0.

[104] Kim KS, Yoo JS, Yi YM, Kim CG. Failure mode and strength of uni-directional composite single lap bonded joints with different bonding methods. Compos Struct 2006;72:477–85. https://doi.org/10.1016/j.compstruct.2005.01.023.

[105] Haga O, Koyama H, Kawada K. Mechanical properties of a new type super hybrid material. Adv Compos Mater 1996;5:139–49. https://doi.org/10.1163/156855196X00059.

[106] Hart-Smith LJ. A peel-type durability test coupon to assess interfaces in bonded, co-bonded, and co-cured composite structures. Int J Adhes Adhes 1999;19:181–91. https://doi.org/https://doi.org/10.1016/S0143-7496(98)00033-5.

[107] Kanerva M, Saarela O. The peel ply surface treatment for adhesive bonding of composites: A review. Int J Adhes Adhes 2013;43:60–9. https://doi.org/10.1016/j.ijadhadh.2013.01.014.

[108] Encinas N, Oakley BR, Belcher MA, Blohowiak KY, Dillingham RG, Abenojar J, et al. Surface modification of aircraft used composites for adhesive bonding. Int J Adhes Adhes 2014;50:157–63. https://doi.org/10.1016/j.ijadhadh.2014.01.004.

[109] Palmieri F, Watson K, Morales G, Williams T, Hopkins J, Wohl C, et al. Laser Ablative Surface Treatment for Enhanced Bonding of Ti-6Al-4V Alloy. ACS Appl Mater Interfaces 2013;5. https://doi.org/10.1021/am302293m.

[110] Palmieri FL, Belcher MA, Wohl CJ, Blohowiak KY, Connell JW. Laser ablation surface preparation for adhesive bonding of carbon fiber reinforced epoxy composites. Int J Adhes Adhes 2016;68:95–101. https://doi.org/10.1016/j.ijadhadh.2016.02.007.

[111] Hartwig A, Vitr G, Schlett V. Treatment of an epoxy-resin by eximer laser radiation. Int J Adhes Adhes 1997;17:373–7. https://doi.org/10.1016/S0143-7496(97)00057-2.

[112] Bénard Q, Fois M, Grisel M, Laurens P. Surface treatment of carbon/epoxy and glass/epoxy composites with an excimer laser beam. Int J Adhes Adhes 2006;26:543–9. https://doi.org/10.1016/j.ijadhadh.2005.07.008.

[113] Wolynski A, Herrmann T, Mucha P, Haloui H, L'huillier J. Laser ablation of CFRP using picosecond laser pulses at different wavelengths from UV to IR. Phys Procedia 2011;12:292–301. https://doi.org/10.1016/j.phpro.2011.03.136.

[114] Nattapat M, Marimuthu S, Kamara AM, Esfahani MRN. Laser Surface Modification of Carbon Fiber Reinforced Composites. Mater Manuf Process 2015;30:1450–6. https://doi.org/10.1080/10426914.2015.1019097.

[115] Fischer F, Kreling S, Dilger K. Surface Structuring of CFRP by using Modern Excimer Laser Sources. Phys Procedia 2012;39:154–60. https://doi.org/10.1016/j.phpro.2012.10.025.

[116] Kreling S, Fischer F, Delmdahl R, Gäbler F, Dilger K. Analytical Characterization of CFRP Laser Treated by Excimer Laser Radiation. Phys Procedia 2013;41:282–90. https://doi.org/10.1016/j.phpro.2013.03.080.

[117] Leone C, Papa I, Tagliaferri F, Lopresto V. Investigation of CFRP laser milling using a 30 W Q-switched Yb:YAG fiber laser: Effect of process parameters on removal mechanisms and HAZ formation. Compos Part A Appl Sci Manuf 2013;55:129–42. https://doi.org/10.1016/j.compositesa.2013.08.004.

[118] Pagano N, Ascari A, Liverani E, Donati L, Campana G, Fortunato A. Laser interaction with Carbon Fibre Reinforced Polymers. Procedia CIRP 2015;33:423–7. https://doi.org/10.1016/j.procir.2015.06.097.

[119] Semak V, Matsunawa A. The role of recoil pressure in energy balance during laser materials processing. J Phys D Appl Phys 1997;30:2541–52. https://doi.org/10.1088/0022-3727/30/18/008.

[120] Fischer F, Kreling S, Jäschke P, Frauenhofer M, Kracht D, Dilger K. Laser Surface Pre-Treatment of CFRP for Adhesive Bonding in Consideration of the Absorption Behaviour. J Adhes 2012;88:350–63. https://doi.org/10.1080/00218464.2012.660042.

[121] Völkermeyer F, Fischer F, Stute U, Kracht D. Laser-based approach for bonded repair of carbon fiber reinforced plastics 2011;12:537–42.

https://doi.org/10.1016/j.phpro.2011.03.066.

[122] Rotel M. Pre-bonding technology based on excimer laser surface treatment 2000:4–10.

[123] Almuhammadi K, Selvakumaran L, Alfano M, Yang Y, Bera TK, Lubineau G. Laser-based surface preparation of composite laminates leads to improved electrodes for electrical measurements. Appl Surf Sci 2015;359:388. https://doi.org/10.1016/j.apsusc.2015.10.086.

[124] Palmieri FL, Belcher MA, Wohl CJ, Blohowiak KY, Connell JW. International Journal of Adhesion & Adhesives Laser ablation surface preparation for adhesive bonding of carbon fi ber reinforced epoxy composites. Int J Adhes Adhes 2016;68:95–101. https://doi.org/10.1016/j.ijadhadh.2016.02.007.

[125] Li L, Sobih M, Crouse PL. Striation-free Laser Cutting of Mild Steel Sheets. CIRP Ann 2007;56:193–6. https://doi.org/10.1016/j.cirp.2007.05.047.

[126] Bhaskar V, Kumar D, Singh K. Laser processing of glass fiber reinforced composite material: a review. Aust J Mech Eng 2017;17:1–14. https://doi.org/10.1080/14484846.2017.1363989.

[127] Ahmad J. Machining of Polymer Composites. Boston, MA: Springer US; 2009. https://doi.org/10.1007/978-0-387-68619-6.

[128] Tam SC, Lim LEN, Quek KY. Application of Taguchi methods in the optimization of the laser-cutting process. J Mater Process Technol 1992;29:63–74. https://doi.org/10.1016/0924-0136(92)90425-R.

[129] El-Taweel TA, Abdel-Maaboud AM, Azzam BS, Mohammad AE. Parametric studies on the CO2 laser cutting of Kevlar-49 composite. Int J Adv Manuf Technol 2009;40:907–17. https://doi.org/10.1007/s00170-008-1412-x.

[130] Yassaei S, Soleimanian A, Nik ZE. Effects of Diode Laser Debonding of Ceramic Brackets on Enamel Surface and Pulpal Temperature. J Contemp Dent Pract 2015;16:270–4. https://doi.org/10.5005/jp-journals-10024-1674.

[131] Cremers DA, Radziemski LJ. History and fundamentals of LIBS. In: Miziolek AW, Schechter I, Palleschi V, editors. Laser Induc. Break. Spectrosc., Cambridge: Cambridge University Press; 2006, p. 1–39. https://doi.org/DOI: 10.1017/CBO9780511541261.002.

[132] Herzog D, Schmidt-Lehr M, Oberlander M, Canisius M, Radek M, Emmelmann C. Laser cutting of carbon fibre reinforced plastics of high thickness. Mater Des 2016;92:742–9. https://doi.org/10.1016/j.matdes.2015.12.056.

[133] Goeke A, Emmelmann C. Influence of laser cutting parameters on CFRP part quality. Phys Procedia 2010;5:253–8. https://doi.org/10.1016/j.phpro.2010.08.051.

Appendix A.
Laser Cutting Parameters and Results

This section defines the definitions of the observed affected areas on the CFRP after laser cutting as shown in Table 16. This section also provides the laser cutting parameters in Table 17, Table 18 and Table 19 and the results in Table 20 and Table 21.

Parameter	Description	Measurements		Comments
Bottom delamination	Measured on the beam exit side	Minimum length of detaching layer	0.6 mm	-
		Minimum area percentage	45%	Affected area against unaffected area at the specified length
Top delaminaton	Measured on the irradiated side	Minimum length of detaching layer	0.6 mm	-
		Minimum area percentage	45%	Affected area against unaffected area at the specified length
Epoxy removal	Measured on the irradiated side	Minimum length of removed epoxy	0.5 mm	-
		Minimum area percentage	65%	Affected area against unaffected area at the specified length
Fibre damage extent	Measured on the irradiated side. Fibres that are just loose are not counted as broken	Minimum number of items observed	20 fibres	-
		Minimum area percentage	35%	Affected area against unaffected area at the specified length
Surface profile	Local surface depth measured against a plane defined by at least the three highest peaks of the surounding area, within the reference flange diameter of the tool.	Minimum number of locations measured on a cut edge	5 fibres	The measurements are performed with the Elcometer E123A surface profile tool, featuring a 30 degrees tip.

Table 16: Definition of observed affected areas.

Test	Description	Sample	Power	Stand-off Z	Nozzle gap	Linear speed
46b	Replication	18	1500 W	0	1 mm	2.5 m/min
47		18	1500 W	0	1 mm	2.5 m/min
48		18	1500 W	0	1 mm	3 m/min
49		18	1500 W	0	1 mm	3.5 m/min
50		19	1500 W	0	1 mm	2.5 m/min
51	Multi pass	19	1500 W	0	1 mm	5 m/min
52		19	1500 W	0	1 mm	7.5 m/min
53		20	1500 W	0	1 mm	10 m/min
54		20	1500 W	0	1 mm	10 m/min
55	Standoff	20	1500 W	1 mm	1 mm	2.5 m/min
56		21	1500 W	-1 mm	1 mm	2.5 m/min
57		21	1500 W	2 mm	1 mm	2.5 m/min
58		21	1500 W	1.3 mm	1 mm	12 m/min
59	Nozzle diameter	22	1500 W	1.3 mm	1 mm	2.5 m/min
60		22	1500 W	1.3 mm	1 mm	5 m/min
61		22	1500 W	1.3 mm	1 mm	7.5 m/min
62		23	1500 W	1.3 mm	1 mm	10 m/min
63		23	1500 W	1.3 mm	1 mm	12 m/min
64	Trenching (TR)	23	1500 W	1.3 mm	1 mm	15 m/min
65		24	1500 W	1.3 mm	1 mm	7.5 m/min
66		24	1500 W	1.3 mm	1 mm	7.5 m/min
67		24	1500 W	1.3 mm	1 mm	7.5 m/min
68	TR + DA	25	1500 W	1.3 mm	1 mm	7.5 m/min
69	Double aperture	25	1500 W	1.3 mm	1 mm	10 m/min
70		25	1500 W	1.3 mm	1 mm	10 m/min
71		26	1500 W	1.3 mm	1 mm	2.5 m/min
72		26	1500 W	1.3 mm	1 mm	2.5 m/min
73	Verification	26	1500 W	1.3 mm	1 mm	10 m/min
74		27	1500 W	0	1 mm	7.5 m/min
75		27	1500 W	1.3 mm	1 mm	7.5 m/min

Table 17: Laser cutting process parameters.

Test	Cutting speed	Nozzle diameter	Gas pressure (bar)	Gas flow (lt/min)	Passes
46b	2.5 m/min	1.0 mm	16	126	1
47	2.5 m/min	1.0 mm	16	126	1
48	3 m/min	1.0 mm	16	126	1
49	3.5 m/min	1.0 mm	16	126	1
50	2.5 m/min	1.0 mm	8	83	1
51	2.5 m/min	1.0 mm	16	126	2
52	2.5 m/min	1.0 mm	16	126	3
53	3.33 m/min	1.0 mm	16	126	3
54	5 m/min	1.0 mm	16	126	2
55	3.5 m/min	1.0 mm	16	126	1
56	2.5 m/min	1.0 mm	16	126	1
57	2.5 m/min	1.0 mm	16	126	1
58	4 m/min	1.0 mm	16	126	3
59	2.5 m/min	2.0 mm	16	126	1
60	2.5 m/min	2.0 mm	16	126	2
61	3.75 m/min	2.0 mm	16	126	2
62	3.33 m/min	2.0 mm	16	126	3
63	4 m/min	2.0 mm	16	126	3
64	15 m/min	1.0 mm	16	126	1
65	7.5 m/min	1.0 mm	16	126	1
66	7.5 m/min	1.0 mm	16	126	1
67	7.5 m/min	2.0 mm	16	126	1
68	7.5 m/min	2.0;1.5 mm	16	126	1
69	3.33 m/min	2.0;1.5 mm	16	126	3
70	3.33 m/min	2.0;1.5 mm	16	126	3
71	2.5 m/min	2.0;1.5 mm	16	126	1
72	2.5 m/min	2.0;1.5mm	16	126	1
73	3.33 m/min	1.0 mm	16	126	3
74	2.5 m/min	1.0 m	16	126	3
75	2.5 m/min	1.0 mm	16	126	3

Table 18: Laser cutting process parameters.

Test	Modulation (Hz)	Modulation duty (%)	Trench gap (µm)
46b	0	100	N/A
47	0	100	N/A
48	0	100	N/A
49	0	100	N/A
50	0	100	N/A
51	0	100	N/A
52	0	100	N/A
53	0	100	N/A
54	0	100	N/A
55	0	100	N/A
56	0	100	N/A
57	0	100	N/A
58	0	100	N/A
59	0	100	N/A
60	0	100	N/A
61	0	100	N/A
62	0	100	N/A
63	0	100	N/A
64	0	100	50
65	0	100	50
66	0	100	100
67	0	100	100
68	0	100	100
69	0	100	N/A
70	0	100	N/A
71	0	100	N/A
72	0	100	N/A
73	0	100	N/A
74	0	100	100
75	0	100	100

Table 19: Laser cutting process parameters.

Test	Fibre damage extent (μm)	Epoxy removal (μm)	Top delamination (μm)	Bottom delamination (μm)	Surface profile (μm)
46b	95	230	95	40	242.2
47	45	420	70	30	N/A
48	20	600	120	30	N/A
49	55	350	180	0	N/A
50	160	380	230	310	N/A
51	180	520	190	0	230.2
52	60	670	100	0	236
53	35	230	80	60	214
54	80	180	140	0	N/A
55	35	410	80	0	N/A
56	42	230	220	130	318.4
57	70	310	150	60	223.2
58	45	300	30	20	263.5
59	220	560	260	140	163
60	110	260	130	90	227.2
61	70	295	100	75	216.2
62	55	190	80	60	134.4
63	40	110	100	75	210.2
64	35	140	70	20	N/A
65	20	55	200	170	161.2
66	10	120	90	40	134.4
67	60	470	180	180	N/A
68	35	110	140	120	193.4
69	50	130	110	60	262.8
70	50	145	110	40	218.6
71	80	190	130	50	N/A
72	80	210	120	230	156.4
73	60	740	70	0	263
74	80	540	70	20	N/A
75	65	140	130	70	160

Table 20:Laser cutting results.

Test	Comments
46b	Some top fraying
47	Significant top fraying
48	Significant top fraying
49	Significant top fraying
50	Some top fraying
51	Some top fraying
52	Almost no frying, mainly burned top delamination
53	Significant top fraying
54	Significant top fraying
55	Some top fraying
56	Almost no frying, mainly burned top delamination
57	Little fraying, mainly burned top delamination
58	Little fraying
59	Fraying
60	Little fraying
61	Some fraying
62	Almost no frying, mainly burned top delamination
63	Almost no frying, mainly burned top delamination
64	Little fraying
65	Some top fraying
66	Almost no frying, mainly burned top delamination
67	Some fraying, burned top delamination
68	Little fraying, burned top delamination
69	Little fraying
70	Almost no fraying, limited burned delamination
71	Some top fraying
72	Fraying
73	Almost no fraying, limited burned delamination
74	Almost no fraying, limited burned delamination
75	Almost no fraying, limited burned delamination

Table 21: Laser cutting results.

Appendix B.

Regression Analysis

Response surface methodology (RSM) is a widely used statistical technique for finding out the optimum operating conditions for enhancing the process efficiency. This technique is frequently used where several input parameters are affecting the output or performance characteristics of the process. With the RSM technique, a suitable mathematical relationship is developed between different independent variables that show their complex interactions that influence the desired output parameters called response. RSM includes statistical experimental design, regression model and optimisation.

Let x_1, x_2......x_k be input variables that can be varied and measured in the experiment, with minimal error. Then the output function or response "y" is:

$$y = f(x_1, x_2, \ldots \ldots \ldots, x_n) + \varepsilon \qquad (17)$$

Where "f" is real response function. The term "ε" is variability of different source that is independent to f. Generally, the "ε" represents the effects such as background noise, observational error upon the response and the impact of different variables. Generally, RSM makes use of polynomial with second order.

$$y = \beta_0 + \sum_{i=1}^{k} \beta_i x_i + \sum_{i=1}^{k} \beta_{ii} x^2 + \sum_{i=1}^{k-1} \sum_{j=2}^{k} \beta_{ij} X_i X_j + \epsilon \qquad (18)$$

Where parameters β_i, β_{ii} and β_{ij} are regression coefficients and they can be produced with the help of experiment data fitting.

There are three types of linear regression models simple linear regression, multiple linear regression, and polynomial regression. Simple linear regression defined as a relationship between a single independent variable (input) and a corresponding dependent variable (output). Multiple linear regression defined as a relationship between two or more independent variable and a corresponding dependent variable.

In polynomial regression, the relationship between independent and dependent variable is modelled to n^{th} degree polynomial. The regression model for fibre damage between 20 – 55 μm and 55 – 95 μm polynomial regression equations. Regression model for 95 – 220 μm and trenching are multiple linear regression models and regression model for double aperture is simple linear regression model.

The design was divided into five models. Three models are to determine the fibre damage between 20 – 55 μm, 55 – 95 μm and 95 – 220 μm. The remaining two models take account of double aperture and trenching methods.

The input process parameters considered in this experiment are the stand-off (SZ), cutting speed (CS), number of passes (NP) and nozzle diameter (ND). A range of trial experiments were conducted to find out the working ranges of different input process parameters for the fibre damage (FD) between 20 – 220 μm.

Experiments were conducted and the responses were measured for fibres damages 20 – 55 μm, 55 – 95 μm and 95 – 220 μm as shown in Table 22, Table 23 and Table 24 respectively. Statistical analyses for fibre damage of the laser cut CFRP was carried out using a Minitab software.

x_{SZ}	x_{CS}	x_{ND}	x_{NP}	y_{FD}	Equation	Error
0	3.00	1.0	1	20	20.17	0.83
0	3.33	1.0	3	35	34.87	0.38
1.3	2.50	1.0	1	35	35.11	0.30
1.3	4.00	2.0	3	40	40.05	0.12
-1	2.50	1.0	1	42	42.23	0.54
0	2.50	1.0	1	45	45.17	0.37
1.3	4.00	1.0	3	45	45.05	0.10
0	3.50	1.0	1	55	55.17	0.30
1.3	3.33	2.0	3	55	55.41	0.74
Average error						**0.41**

Table 22: Design table for fibre damage (20 – 55 μm)

x$_{SZ}$	x$_{CS}$	x$_{ND}$	x$_{NP}$	y$_{FD}$	Equation	Error
0	3.50	1.0	1	55	54.94	0.11
1.3	3.33	2.0	3	55	54.96	0.07
0	2.50	1.0	3	60	59.96	0.06
1.3	3.33	1.0	3	60	59.96	0.06
2	2.50	1.0	1	70	69.88	0.17
1.3	3.75	2.0	2	70	69.88	0.17
0	5.00	1.0	2	80	79.92	0.11
0	2.50	1.0	1	95	94.96	0.04
Average error						**0.10**

Table 23: Design table for fibre damage (55 – 95 µm)

x$_{SZ}$	x$_{CS}$	x$_{ND}$	x$_{NP}$	y$_{FD}$	Equation	Error
0	2.50	1.0	1	95	95	0.00
1.3	2.50	2.0	2	110	110.06	0.05
0	2.50	1.0	2	180	180	0.00
1.3	2.50	2.0	1	220	220.6	0.03
Average error						**0.02**

Table 24: Design table for fibre damage (95 – 220 µm)

The equation for the fibre damage between 20 to 55 µm, y$_{20-55}$ is shown in (19) and its coefficients in Table 25. This equation is polynomial regression and assumes stand – off between -1 to 1.3 mm, cutting speed between 2.5 to 4 m/min, nozzle diameter between 1 to 2 mm, number of passes between 1 and 3 and the remaining assumptions are in Appendix A.

$$y_{20-55}\ (\mu m) = \ \varepsilon_1 + \ \beta_1 x_{SZ} + \ \beta_2 x_{CZ} + \ \beta_3 x_{ND} + \ \beta_4 x_{NP} + \ \beta_5 x_{SZ}^2 + \ \beta_6 x_{CS}^2 + \ \beta_7 x_{SZ} x_{CS} + \ \beta_8 x_{SZ} x_{NP} \qquad (19)$$

Coefficient	ϵ_1	β_1	β_2	β_3	β_4	β_5	β_6	β_7	β_8
Value	1076	289.4	-710	-5	-0.8333	-6.5	120	-148.1	77.29

Table 25: Coefficients for fibre damage between 20 – 55 µm

The important process parameters affecting the fibre damage between 20 to 55 μm are stand-off distance, cutting speed, nozzle diameter and number of passes. Figure 77 show contour plots of the behaviour of the fibre damage according to equation 19.
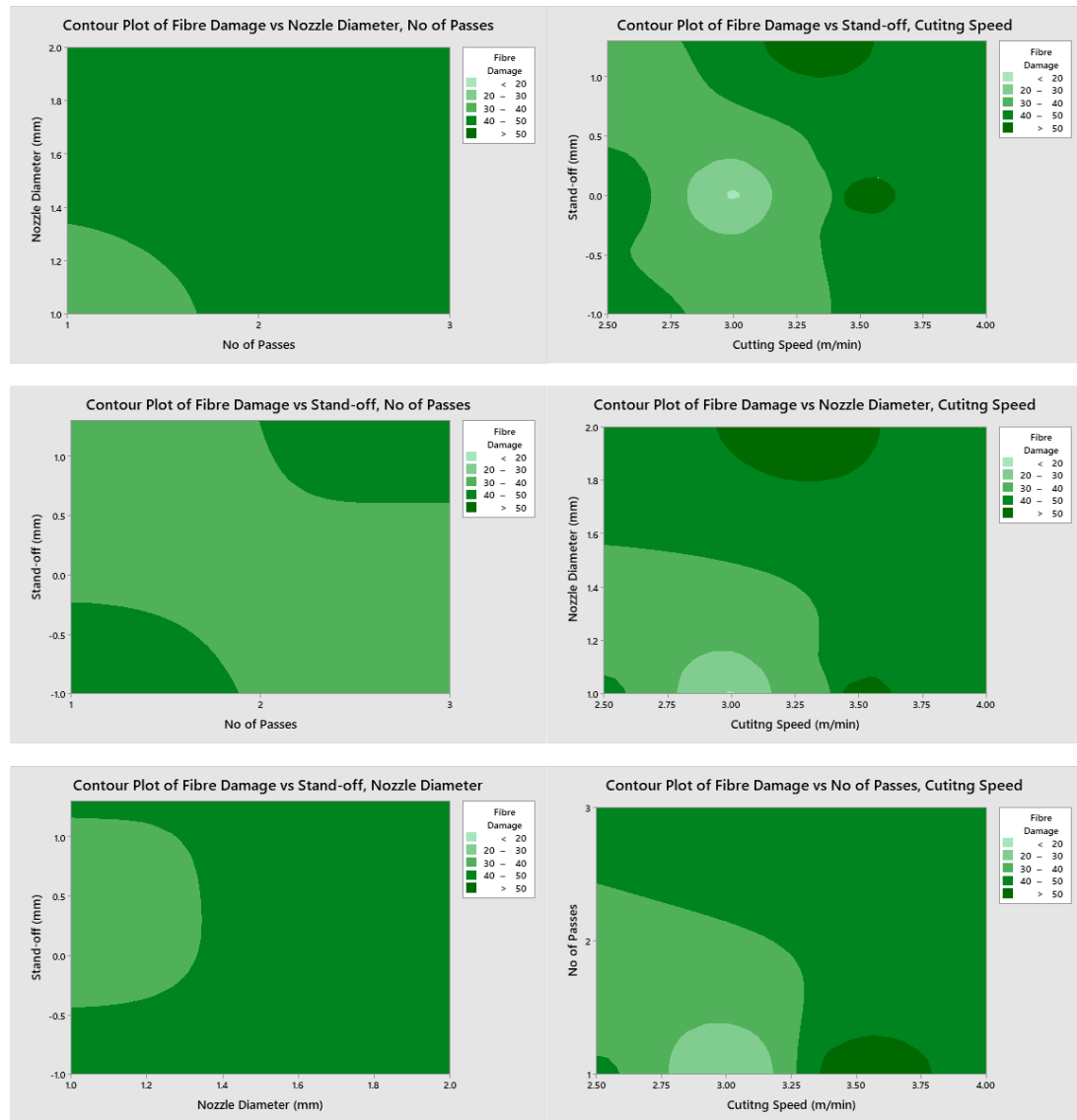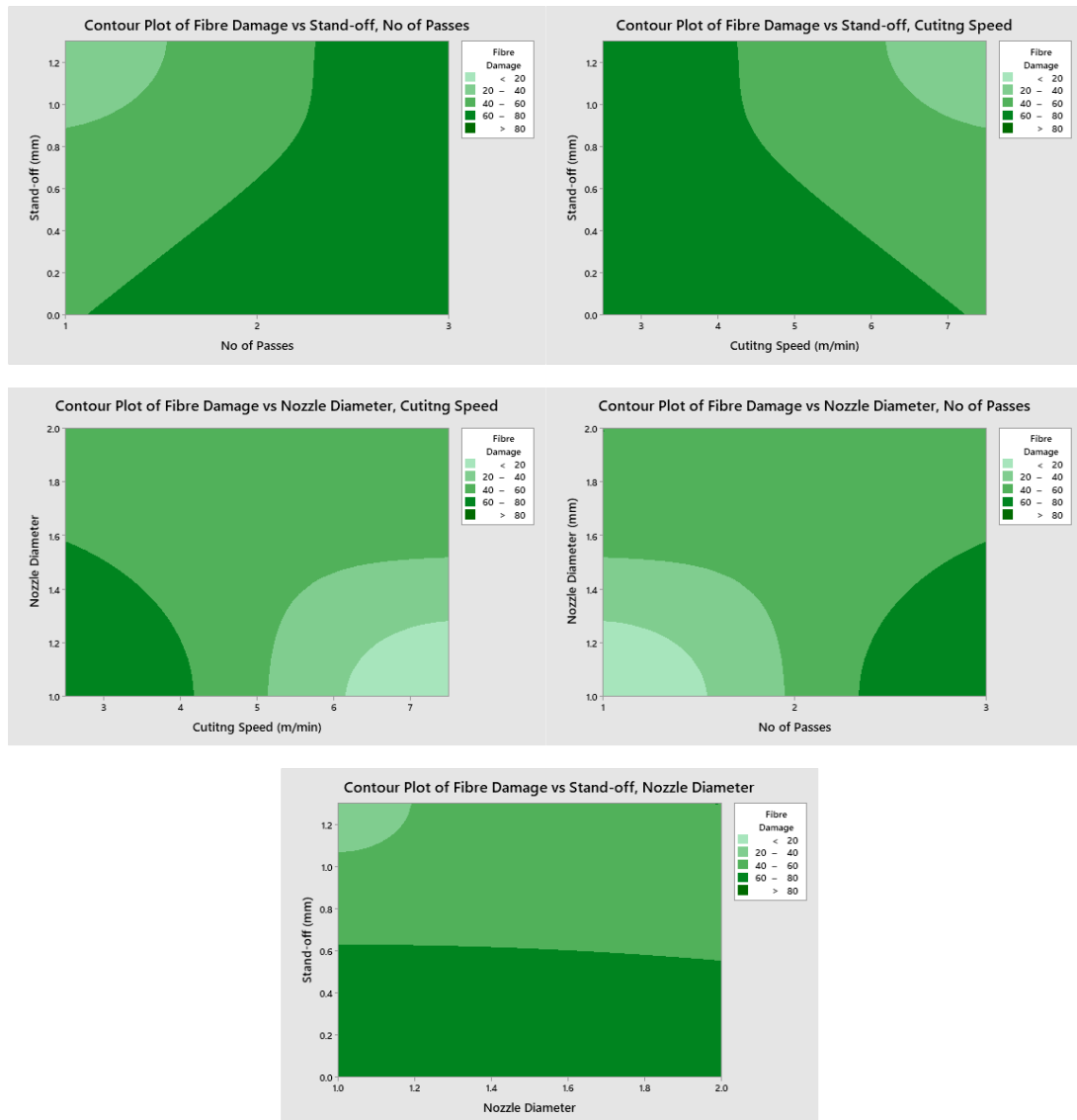

Figure 77: Contour plots of fibre damage between 20 and 55 μm with respect to various unput parameters, based on equation 19.

The equation for the fibre damage between 55 to 95 μm, y_{55-95}, is presented in equation 20 and its coefficients in Table 26. This equation is also a polynomial regression and assumes stand-off between 0 to 2 mm, cutting speed between 2.5 to 5 m/min, nozzle diameter between 1 and 2 mm, number of passes between 1 and 3. The remaining assumptions are in Appendix A.

$$y_{55-95}\ (\mu m) = \ \varepsilon_2 + \ \beta_9 x_{SZ} + \ \beta_{10} x_{CZ} + \ \beta_{11} x_{ND} + \ \beta_{12} x_{NP} + \ \beta_{13} x_{SZ}^2 + \ \beta_{14} x_{CS}^2 +$$
$$\beta_{15} x_{NP}^2 \hspace{6cm} (20)$$

Coefficient	ϵ_2	β_9	β_{10}	β_{11}	β_{12}	β_{13}	β_{14}	β_{15}
Value	445.6	104.6	-220.7	-5	-9.184	-58.57	26.78	-2.079

Table 26: Coefficients for fibre damage between 55 – 95 μm.

Standoff, cutting speed, nozzle diameter and number of passes are the process parameters affecting fibre damage. Figure 78 shows contour plots of the behaviour of fibre damage according to equation 20.
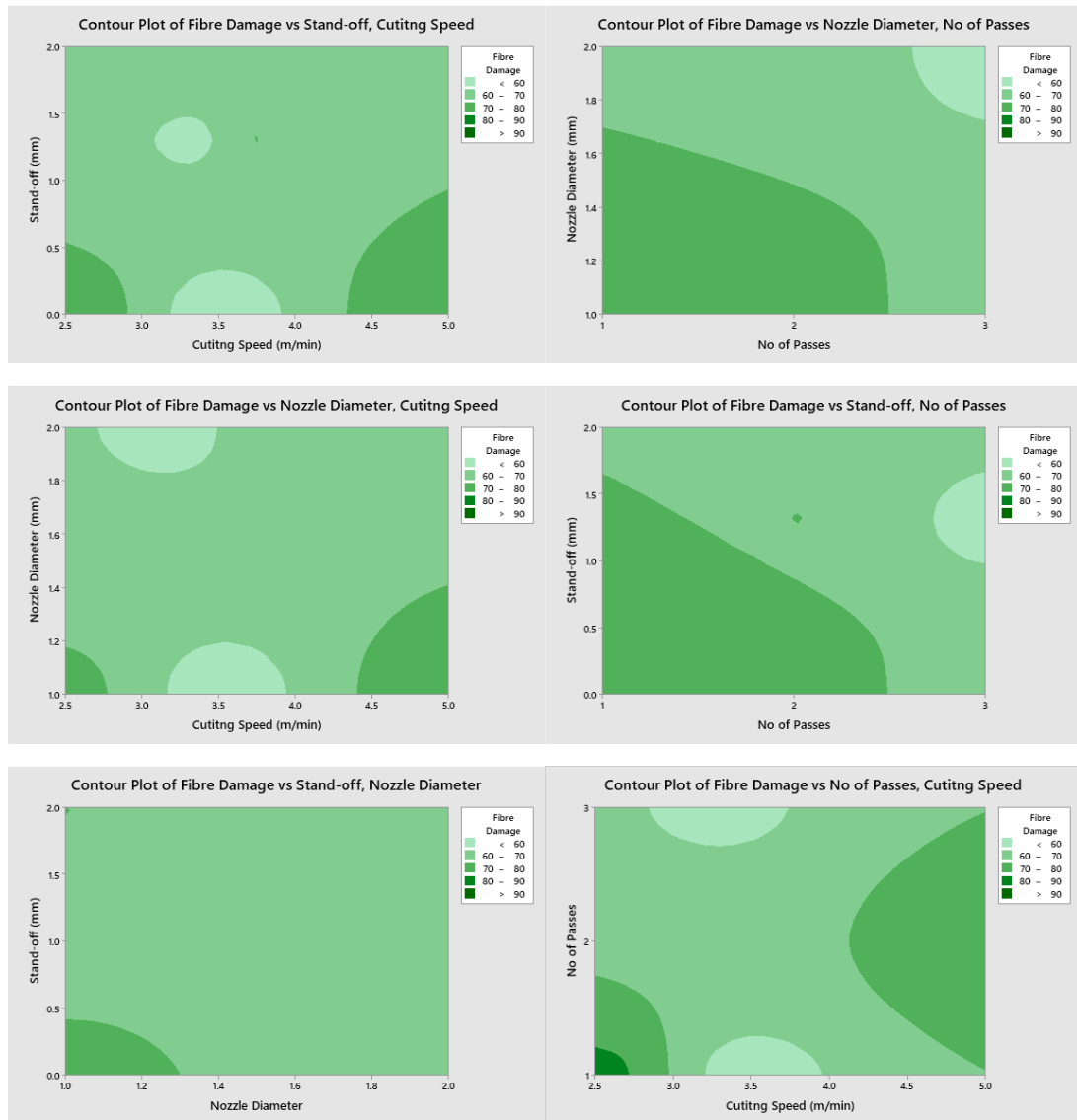
Figure 78: Contour plots of fibre damage between 55 and 95 μm with respect to various input parameters based on equation 20.

131

The equation for the fibre damage between 95 to 220 µm, y_{95-220}, is presented in equation 21 and its coefficient in **Table *27*: Coefficients for fibre damage between 95 – 220 µm.**Table 27. This equation is multiple linear regression and assumes stand-ff between 0 to 1.3 mm, nozzle diameter between 1 and 2 mm, number of passes between 1 and 2. The remaining assumptions are Appendix A.

$$y_{95-220} \, (\mu m) = \; \varepsilon_3 + \; \beta_{16} x_{SZ} + \; \beta_{17} x_{NP} + \; \beta_{18} x_{SZ} x_{NP} \tag{21}$$

Coefficient	ϵ_3	β_{16}	β_{17}	β_{18}
Value	10	246.2	85	-150

Table 27: Coefficients for fibre damage between 95 – 220 µm.

The important process parameters affecting fibre damage between 95 and 220 µm are stand-off and number of passes. Figure 79 shows contour plots of the behaviour of the fibre damage according to equation 21.
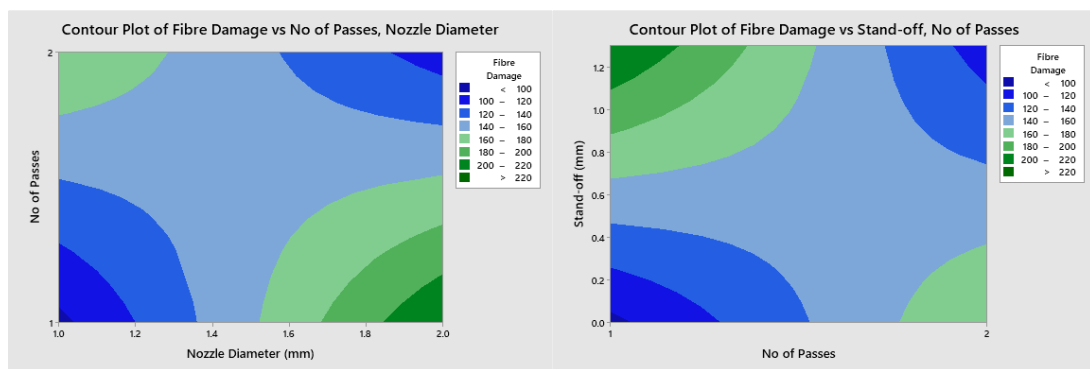
Figure 79: Contour plot of fibre damage between 95 – 220 µm with respect to various input parameters based on equation 21.

Further experiments were conducted, and responses measured to analyse the effects of double aperture and trenching on the fibre damages as shown in Table 28 and Table 29, respectively. Statistical analyses for the fibre damage of the laser cut CFRP was carried out using Minitab.

x_{CS}	x_{SZ}	x_{NP}	y_{FD}	Equation	Error
3.3	1.3	3	50	51.2	2.4
3.3	1.3	3	50	51.2	2.4
2.5	1.3	1	80	80	0
2.5	1.3	1	80	80	0
Average error					1.2

Table 28: Effect of double aperture on the fibre damage.

x_{SZ}	x_{CS}	x_{ND}	x_{NP}	y_{FD}	Equation	Error
1.3	7.5	1	1	10	9.998	0.020
1.3	7.5	2	1	60	59.998	0.003
0	2.5	1	3	80	80	0.000
1.3	2.5	1	3	65	64.998	0.003
Average error						0.007

Table 29: Effect of trenching on the fibre damage.

The equations of the fibre damage for double aperture, y_{DA}, and trenching, y_T, are presented in equations 22 and 23 respectively and the coefficient in Table 30. The equation for the fibre damage for double aperture is a linear regression model assumes the cutting speed between 2.5 and 3.3 m/min, number of passes between 1 and 3. The equation of the fibre damage based on trenching is a multiple regression models and assumes stand-off between 0 and 1.3 mm, cutting speed between 2.5 and 7.5 m/min, nozzle diameter between 1 and 2 mm, number of passes between 1 and 3, the remaining assumptions for both double aperture and trenching are in Appendix A.

$$y_{DA} \ (\mu m) = \ \varepsilon_4 + \ \beta_{19} x_{CS} \qquad (22)$$

$$y_T \ (\mu m) = \ \varepsilon_5 + \ \beta_{20} x_{SZ} + \ \beta_{21} x_{CS} + \ \beta_{22} x_{ND} \qquad (23)$$

Coefficient	ε_4	ε_5	β_{19}	β_{20}	β_{21}	β_{22}
Value	170	57.5	-36	-11.54	-11	50

Table 30: Coefficients for fibre damage based on double aperture and trenching.

The important process parameters affecting fibre damage based on trenching tests are stand-off, cutting speed, nozzle diameter and number of passes. Figure 80 shows contour plots of the behaviour of the fibre damage according to equation 23.

Figure 80: Contour plots of fibre damage based on trenching with respect to various input parameters based on equation 23.

Appendix C.

Images of Laser Cut CFRP Samples.

This section shows images of laser cut areas on the surface of the CFRP material.
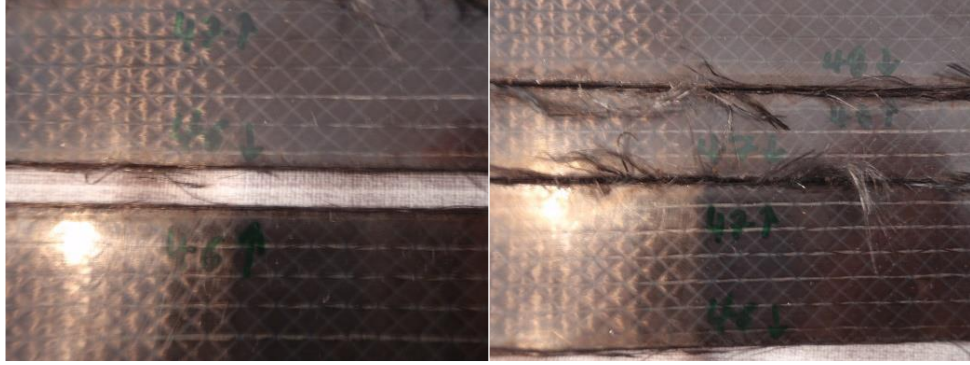
Figure 81: Images of top side laser cut surface of tests 46b (left) and 47 (right).

Figure 82: images of top side laser cut surface of tests 48 (left) and 49 (right).

Figure 83: Images of top side laser cut surface of tests 50 (left) and 51 (right).
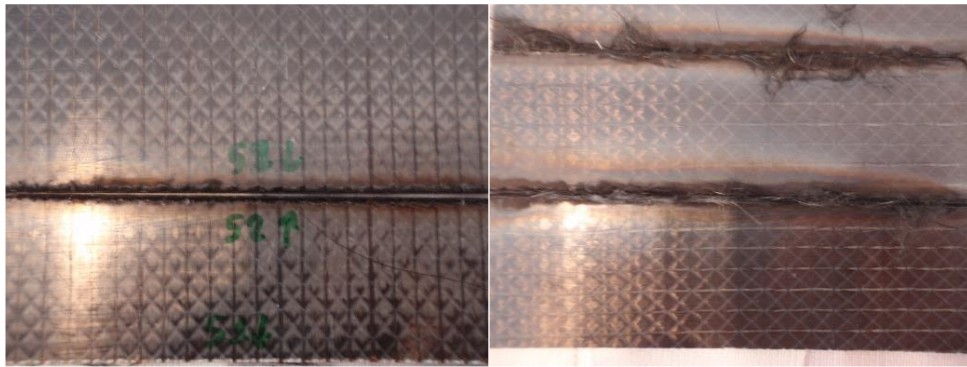
Figure 84: Images of top side laser cut surfaces of tests 52 (left) and 53 (right).
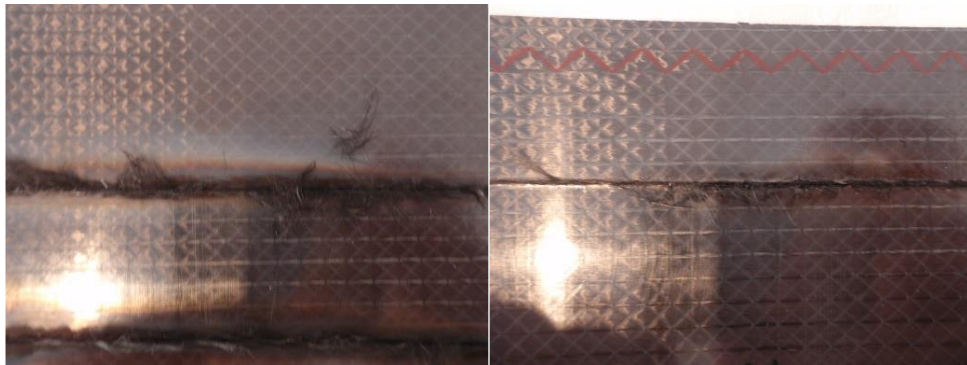
Figure 85: Images of top side laser cut surfaces of tests 55 (left) and 55 (right).
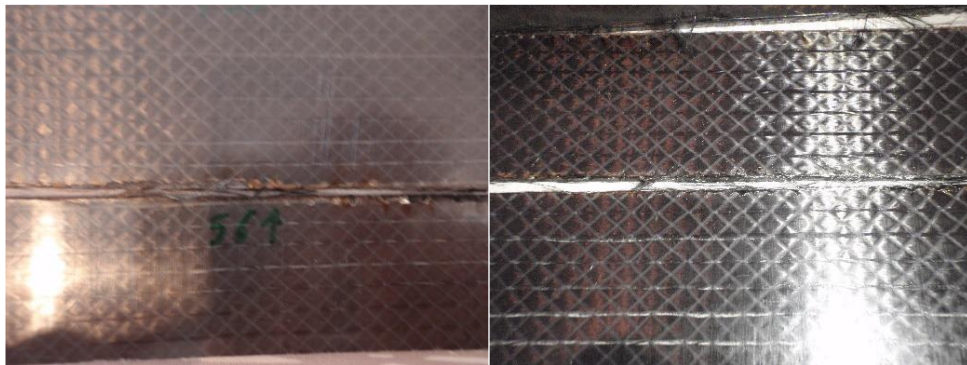
Figure 86: Images of top side laser cut surfaces of tests 56 (left) and 57 (right).

Figure 87: Images of top side laser cut surfaces of tests 58 (left) and 59 (right).

Figure 88: Images of top side laser cut surfaces of tests 60 (left) and 61 (right).

Figure 89: Images of top side laser cut surfaces of tests 62 (left) and 63 (right).

Figure 90: Images of top side laser cut surfaces of tests 64 (left) and 65 (right).
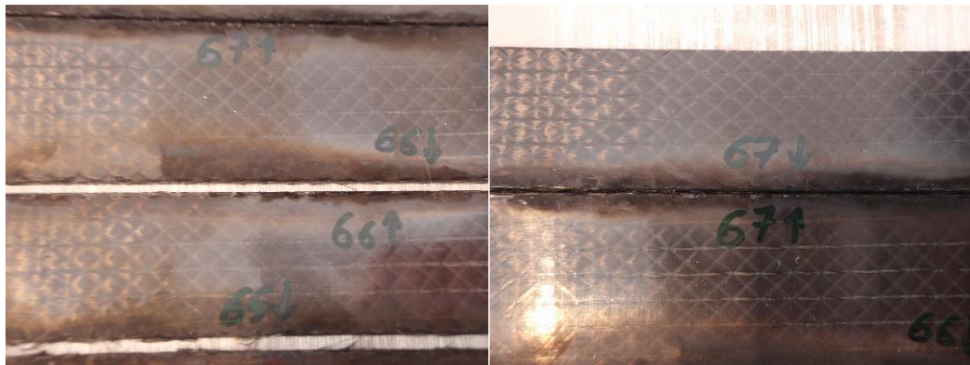
Figure 91: Images of top side laser cut surfaces of tests 66 (left) and 67 (right).
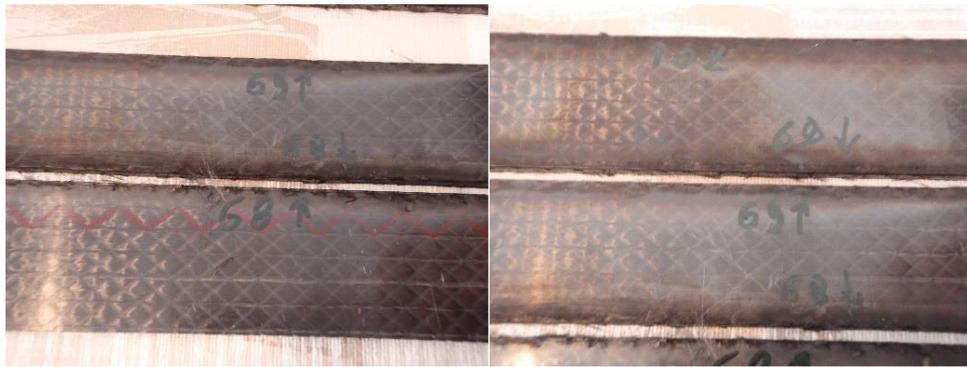
Figure 92: Images of top side laser cut surfaces of tests 68 (left) and 69 (right).

Figure 93: Images of top side laser cut surfaces of tests 70 (left) and 71 (right).
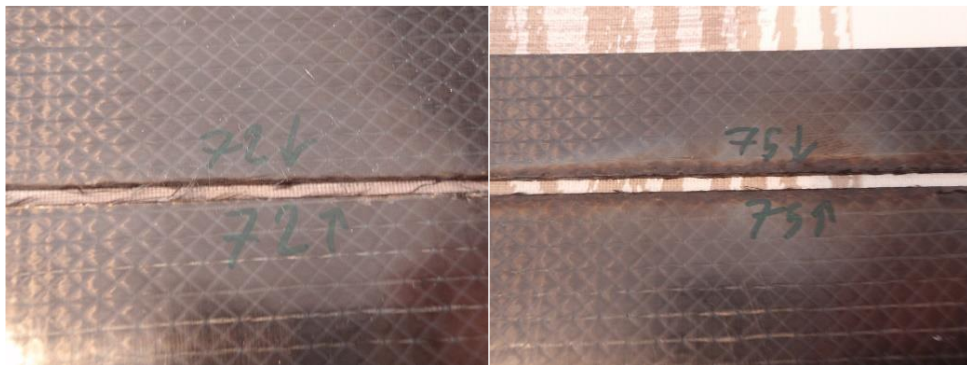
Figure 94: Images of top side laser cut surfaces of tests 72 (left) and 73 (right).

Figure 95: Images of top side laser cut surfaces of tests 74 (left) and 75 (right).

Appendix D.

Microscope Images of Laser Cut CFRP Samples

This section shows the microscope images of laser cut surfaces of CFRP material.

Figure 96: Microscope images of edge side (left) and top side (right) of laser cutting test 46b.
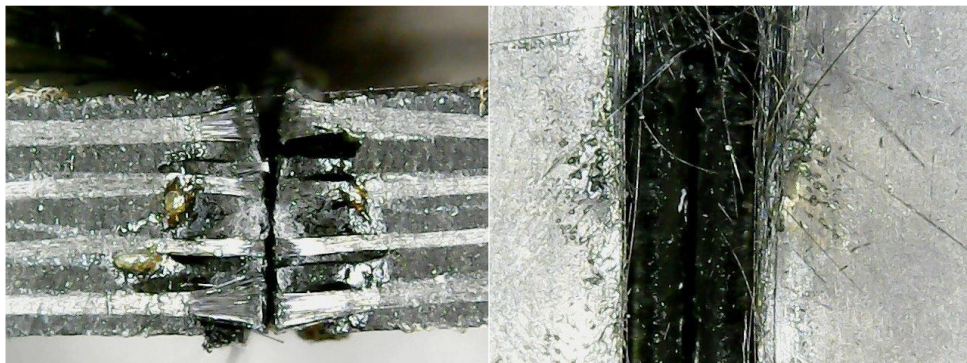
Figure 97: Microscope images of edge side (left) and top side (right) of laser cutting test 47.
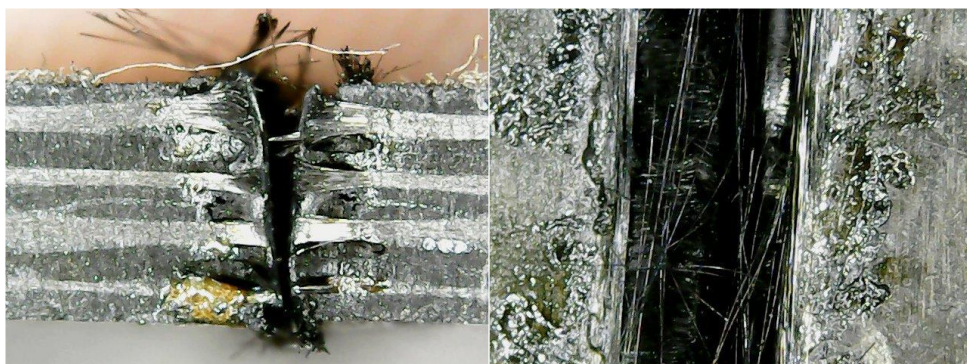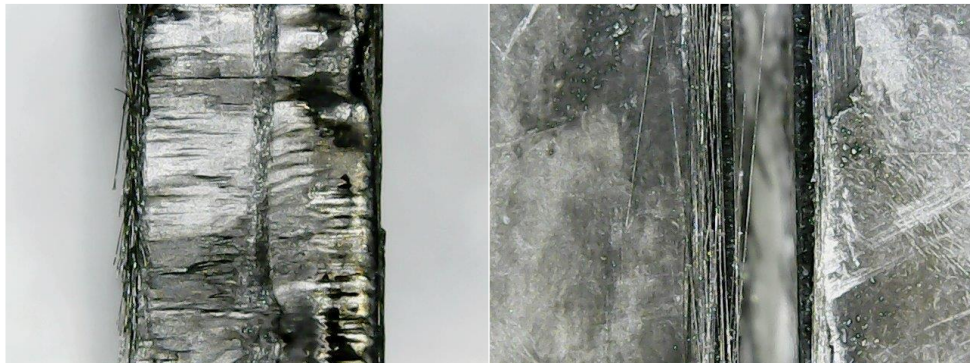

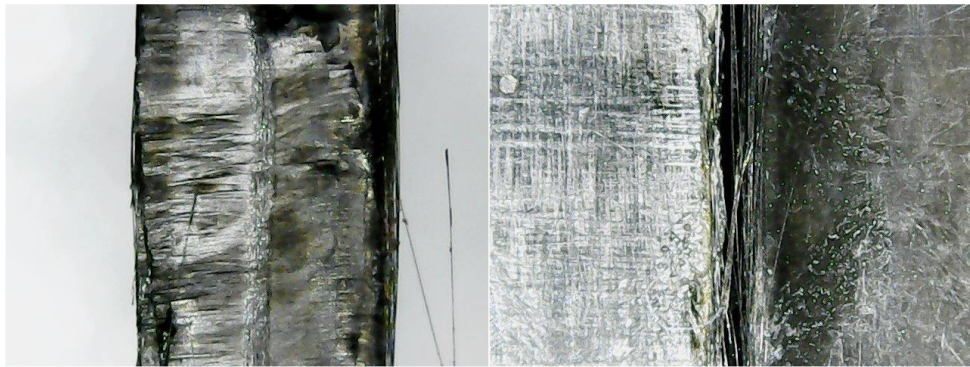**Figure 98: Microscope images of edge side (left) and top side (right) of laser cutting test 48.**
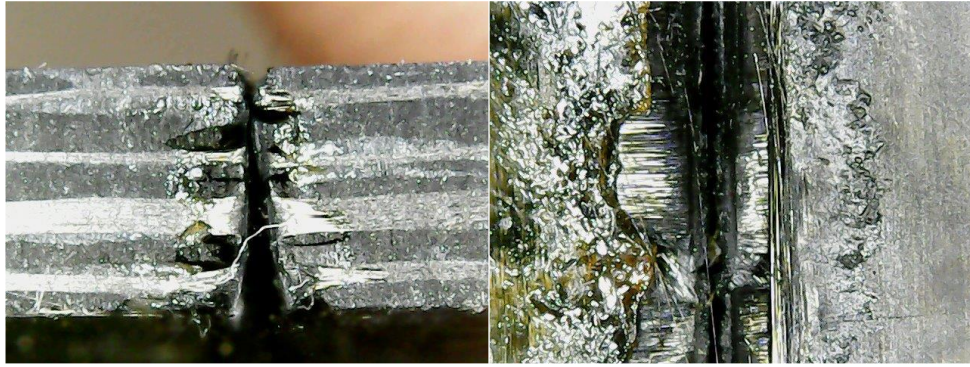
Figure 99: Microscope images of edge side (left) and top side (right) of laser cutting test 49.
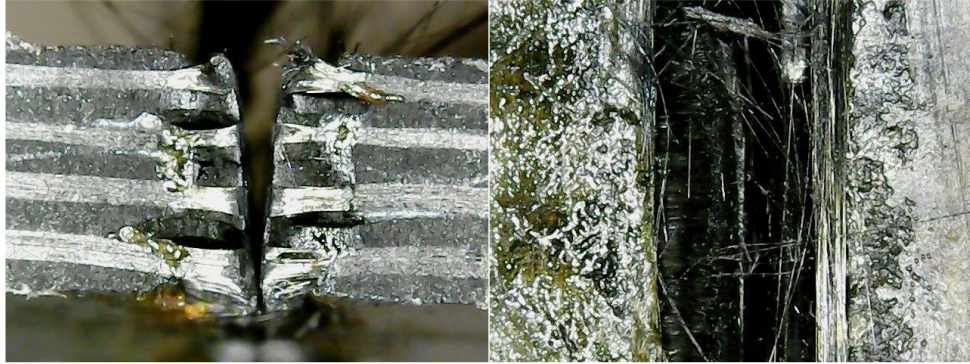
Figure 100: Microscope images of edge side (left) and top side (right) of laser cutting test 50.

Figure 101: Microscope images of edge side (left) and top side (right) of laser cutting test 51.
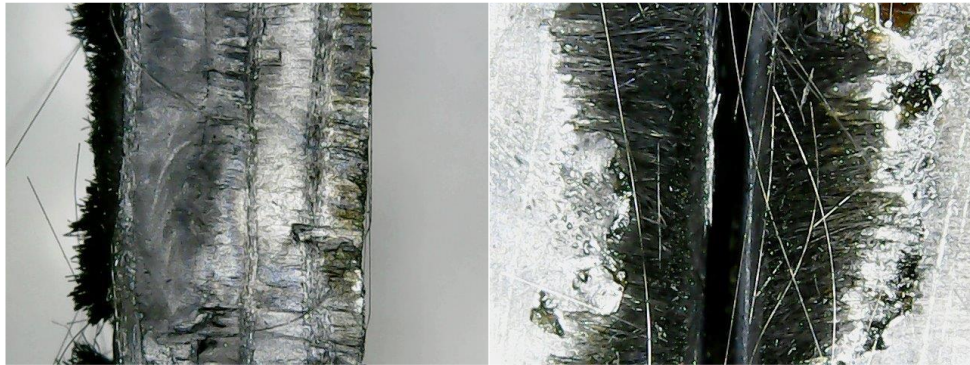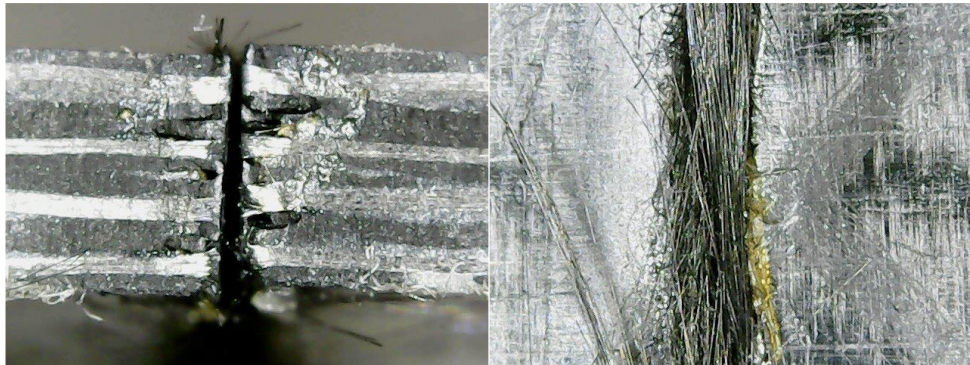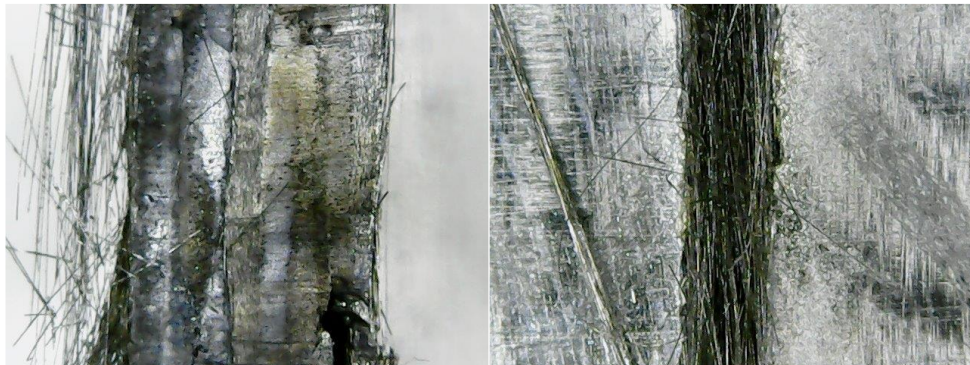

Figure 102: Microscope images of edge side (left) and top side (right) of laser cutting test 52.
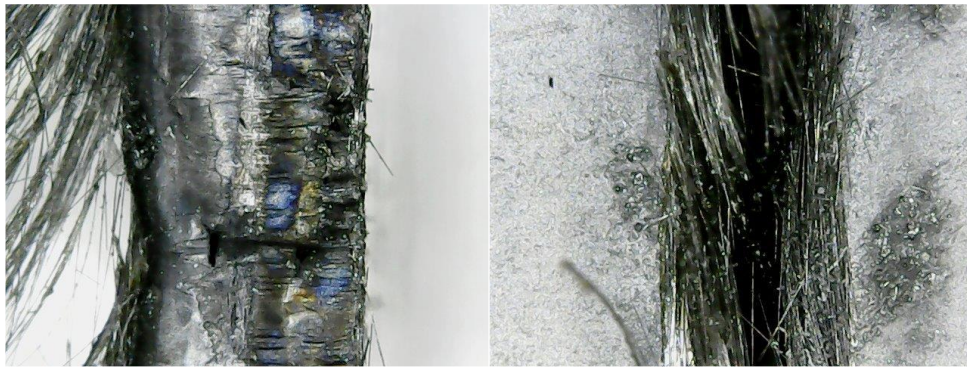
Figure 103: Microscope images of edge side (left) and top side (right) of laser cutting test 53.
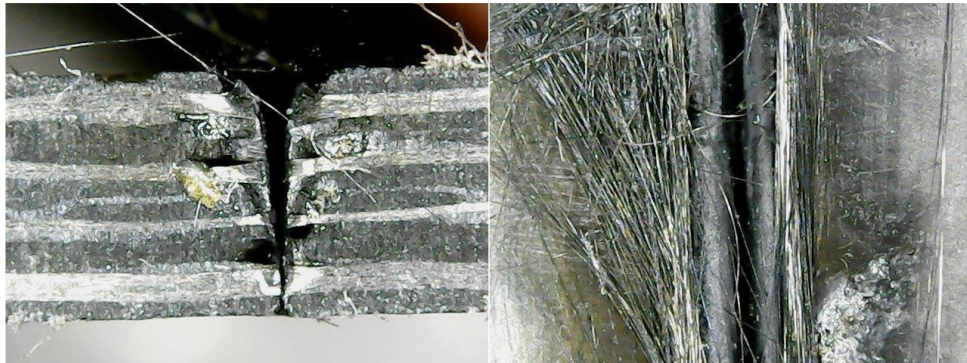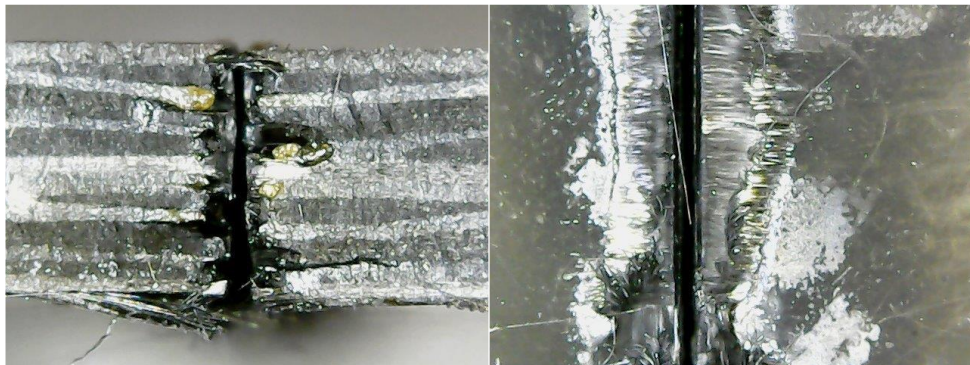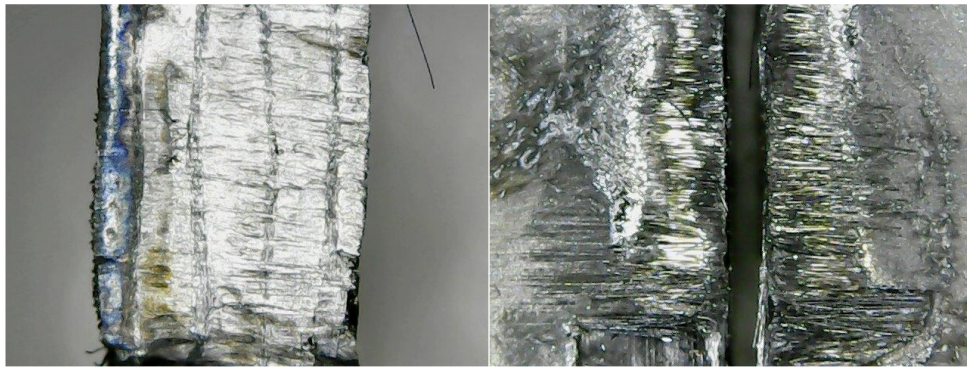

Figure 104: Microscope images of edge side (left) and top side (right) of laser cutting test 54.
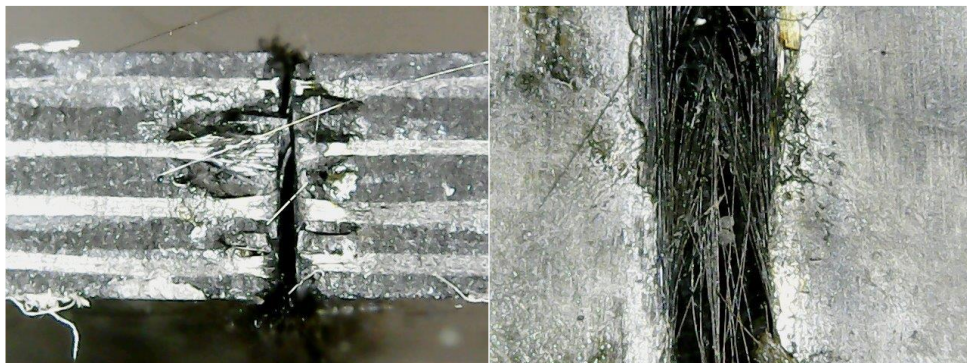
Figure 105: Microscope images of edge side (left) and top side (right) of laser cutting test 55.
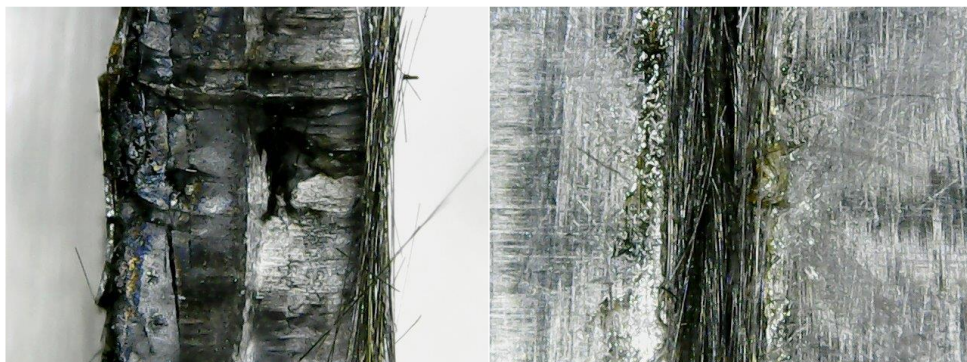
Figure 106: Microscope images of edge side (left) and top side (right) of laser cutting test 56.
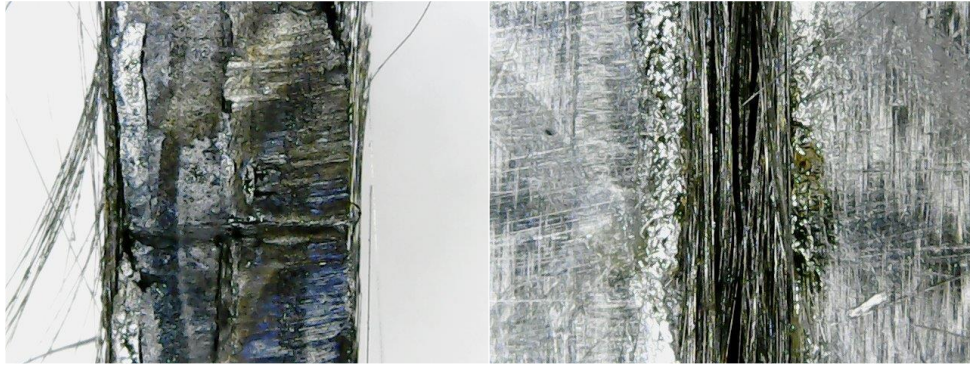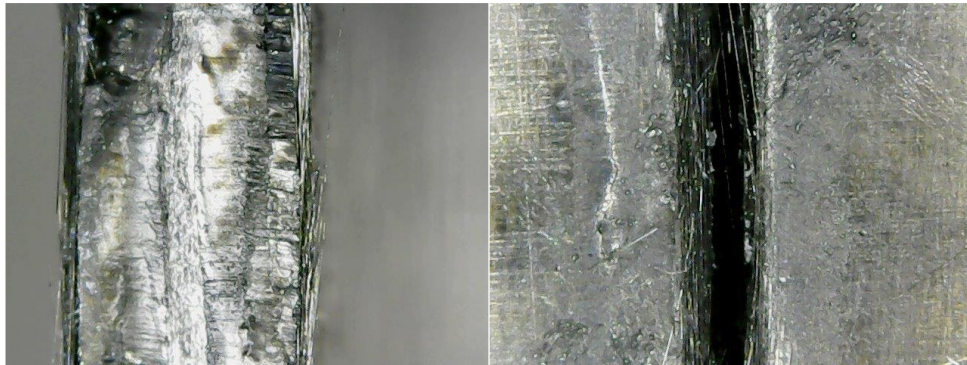
Figure 107: Microscope images of edge side (left) and top side (right) of laser cutting test 57.
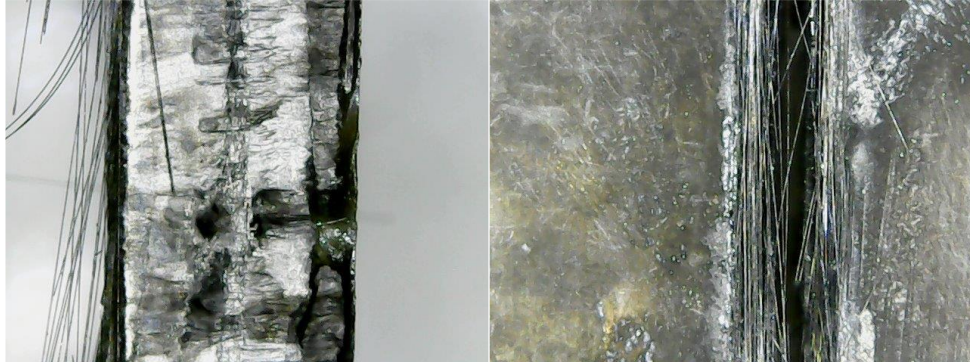
Figure 108: Microscope images of edge side (left) and top side (right) of laser cutting test 58.
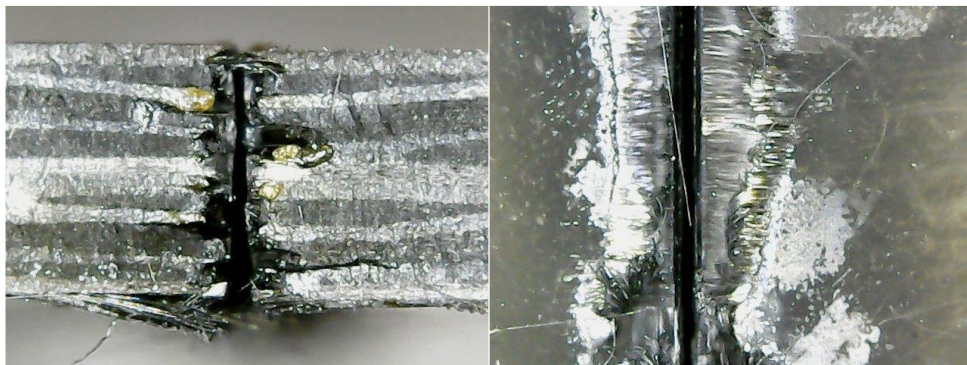

Figure 109: Microscope images of edge side (left) and top side (right) of laser cutting test 59.
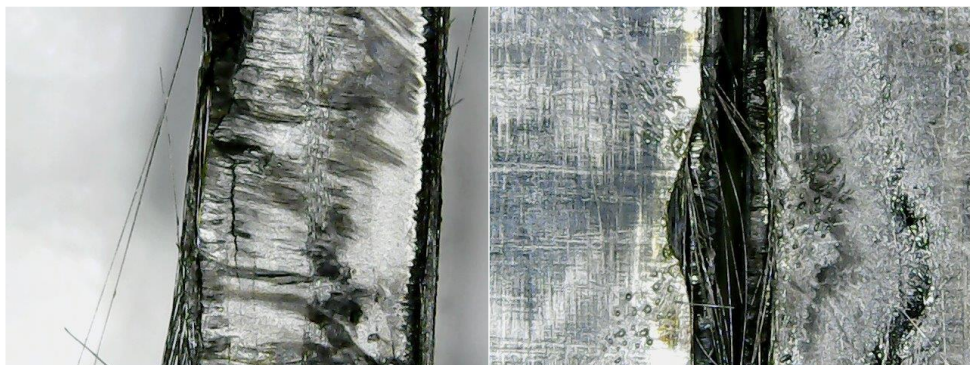
Figure 110: Microscope images of edge side (left) and top side (right) of laser cutting test 60.
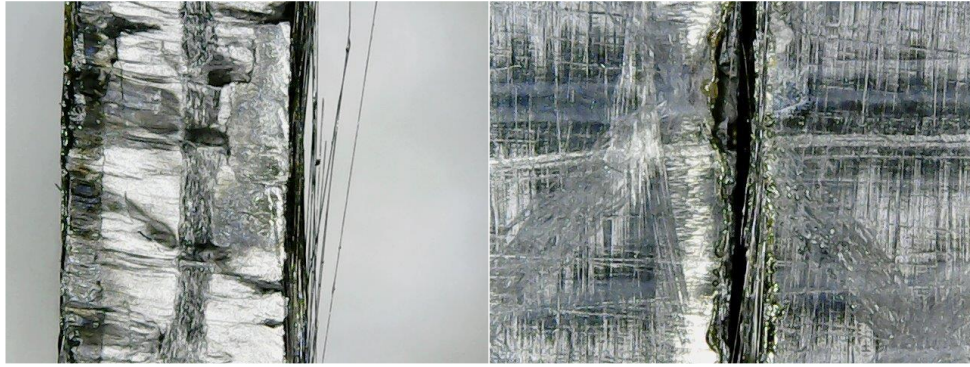
Figure 111: Microscope images of edge side (left) and top side (right) of laser cutting test 61.
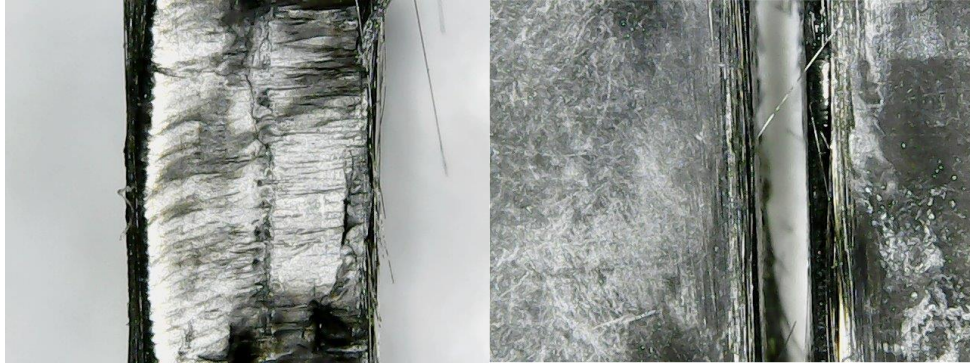
Figure 112: Microscope images of edge side (left) and top side (right) of laser cutting test 62.

Figure 113: Microscope images of edge side (left) and top side (right) of laser cutting test 63.
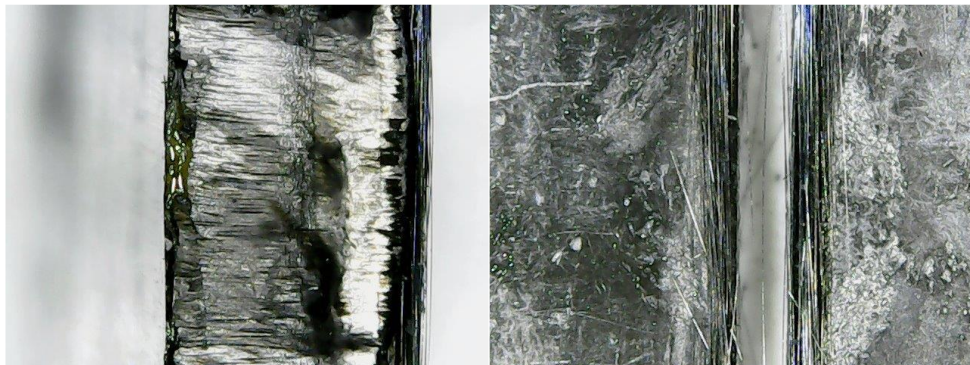
Figure 114: Microscope images of edge side (left) and top side (right) of laser cutting test 64.

Figure 115: Microscope images of edge side (left) and top side (right) of laser cutting test 65.
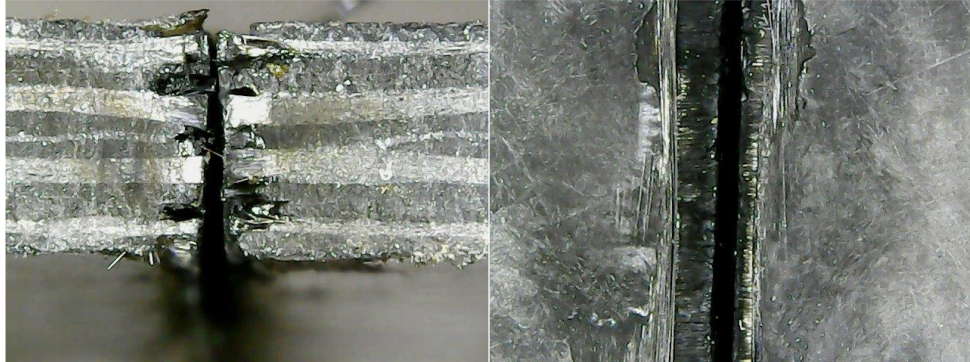
Figure 116: Microscope images of edge side (left) and top side (right) of laser cutting test 66.

Figure 117: Microscope images of edge side (left) and top side (right) of laser cutting test 67.

Figure 118: Microscope images of edge side (left) and top side (right) of laser cutting test 68.

Figure 119: Microscope images of edge side (left) and top side (right) of laser cutting test 69.

Figure 120: Microscope images of edge side (left) and top side (right) of laser cutting test 70.

Figure 121: Microscope images of edge side (left) and top side (right) of laser cutting test 71.

Figure 122: Microscope images of edge side (left) and top side (right) of laser cutting test 72.

Figure 123: Microscope images of edge side (left) and top side (right) of laser cutting test 73.

Figure 124: Microscope images of edge side (left) and top side (right) of laser cutting test 74.

Figure 125: Microscope images of edge side (left) and top side (right) of laser cutting test 75.

Appendix E.

Scanning Electron Microscope of Laser Cut CFRP Samples

This section shows the Scanning Electron Microscope (SEM) micrographs of the laser cut CFRP samples. The SEM images were taken using the Hitachi SU − 6600 Field Emission Scanning Electron Microscope (FE − SEM).

Figure 126: Hitachi SU − 6600 FE − SEM of Advanced Material Research Laboratory (University of Strathclyde)
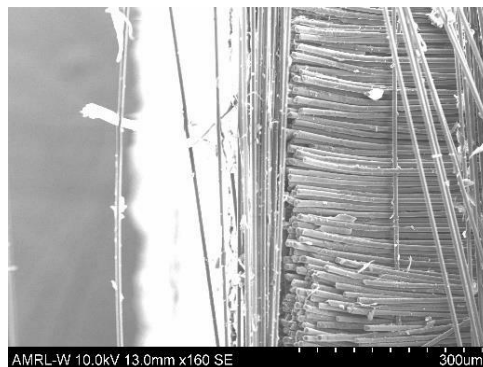
Figure 127: SEM image of laser cut surface of test 46b.
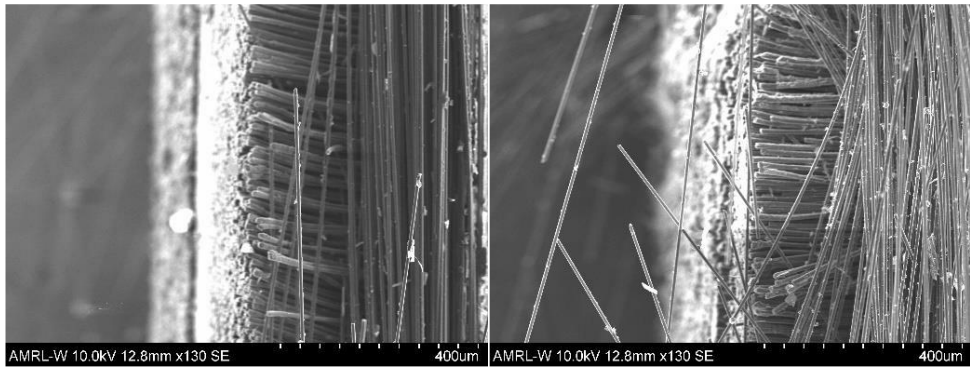
Figure 128: SEM image of laser cut surface of test 47.
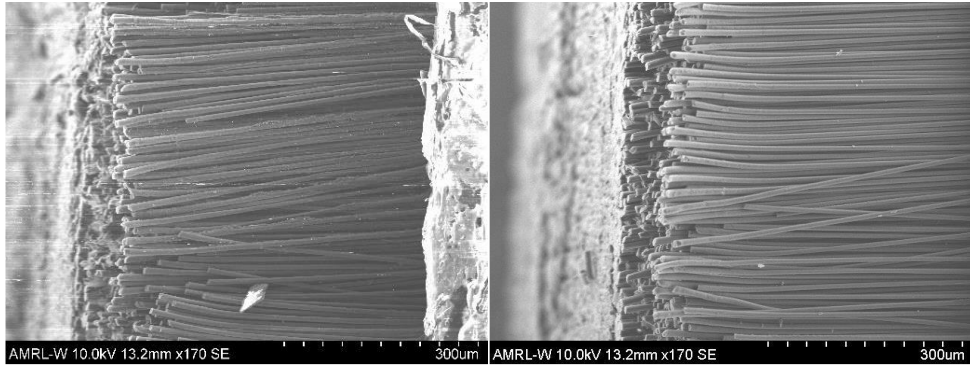
Figure 129: SEM laser cut surface of test 48.
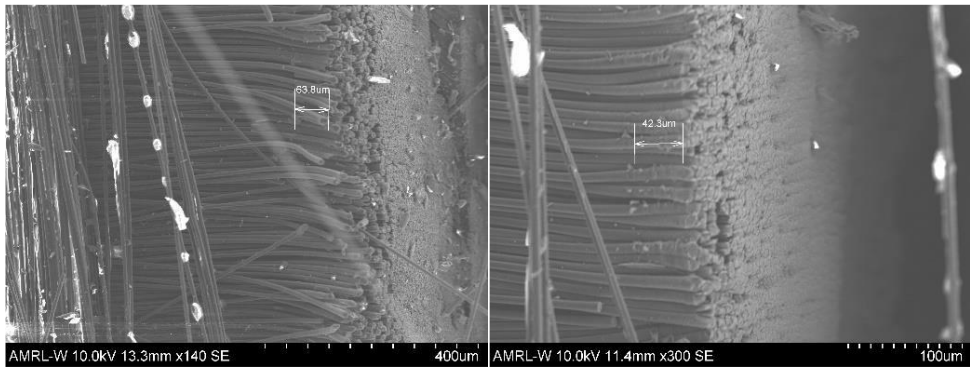
Figure 130: SEM laser cut surface of test 53.
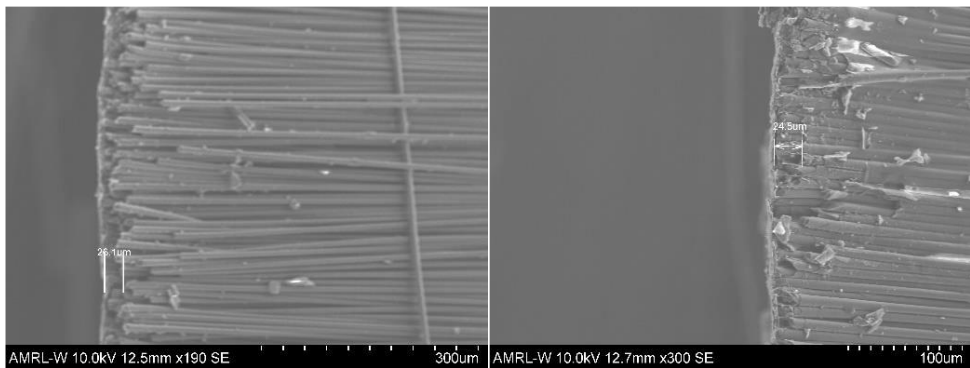
Figure 131: SEM image of laser cut surface of test 56.
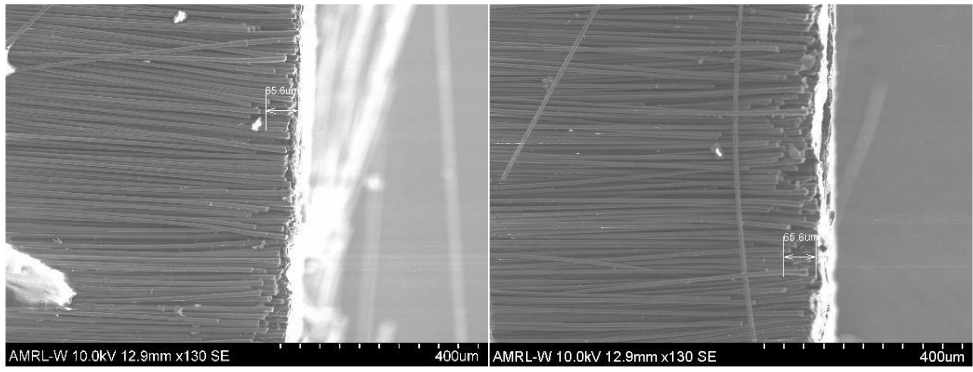
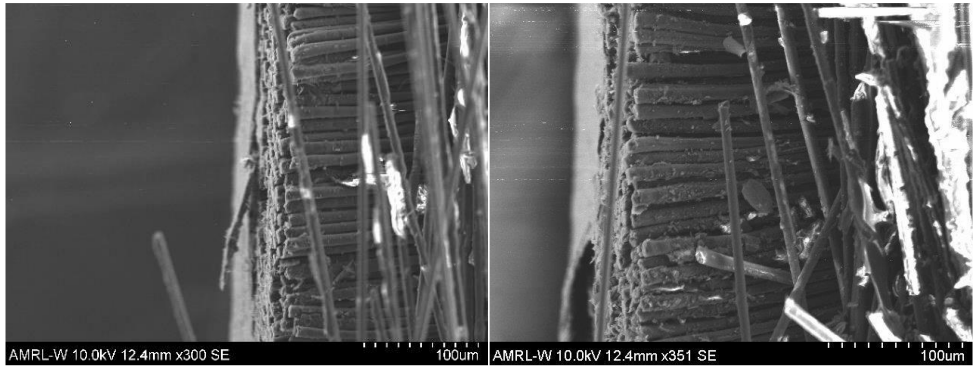**Figure 132: SEM image of laser cut surface of test 58.**

Figure 133: SEM image of laser cut surface of test 65.

Appendix F.

Laser Cleaning Parameters and Results

This section defines the definitions of the observed affected areas on the CFRP after laser cleaning as shown in Table 31. This section also provides the laser cleaning of EP and PU parameters as shown in Table 32 and Table 33, respectively and the results in Table 34 and Table 35, respectively.

Measurement definitions	
Damaged fibres	This is the count of damaged fibres per 0.25 mm^2 of exposed fibre area only, averaged measurements from 5 different areas of the processed site if adequate exposed area exists.
Adhesive debonded	Percentage of site area that has debonded from the sealant surface. The adhesive layer is still present. It appears with a lighter "desert sand" colour, than the sealant debonded area. This is because internal reflection happens above the sealant and thus light does not transmit far enough to be absorbed by the darker carbon fibre bulk material.
Sealant debonded	Percentage of site area which has debonded at the boundary of the sealant and the fibres. The adhesive layer and sealant are still present and possibly still adhered to each other and behaving as one layer. The area appears somewhat darker with an "ash grey" or "pastel grey colour" as the continuity of material with similar optical properties in the visible range permits the transition of some light towards the dark carbon fibres and their binder that absorb more of this light. Due to the nature of the semi-transparent fibre mesh layers on the surface and their embodiment inside the semi-transparent material resembling in optical characteristics to the sealant or epoxy, the boundary considered here is below the mesh layer and reaches the level of the carbon fibre and its dark binder.
Adhesive detached	Percentage of site area that has detached from the bulk material at the adhesive to sealant interface. The sealant or sub-layers are exposed.
Sealant detached	Percentage of site area that has detached from the bulk material at the sealant to carbon fibre and dark binder boundary (similar to the "sealant debonded" definition). The carbon fibres or dark binder material are exposed.

Table 31: Measurement definitions of the laser cleaning carried out on EP and PU adhesives.

Test	Defocus (cm)	Energy setting (J)	Pulse repetition rate	Passes	Diagonal offset (mm)
EP 5.2	61	0.411	5	2	0.5
EP 5.1	61	0.952	5	2	0.5
EP 9.2	61	0.952	5	2	0.5
EP 12.5	61	1.492	5	2	0.5
EP 8.2	61	0.952	5	2	0.5
EP 3.2	61	0.952	5	2	0.5
EP 10.2	61	0.952	5	2	0.5
EP 11.2	61	0.952	5	2	0.5

Table 32: Process parameters for laser cleaning of EP adhesive.

Test	Defocus (cm)	Energy setting (J)	Pulse repetition rate	Passes	Diagonal offset (mm)	Speed (mm/s)
PU 8.2	50	1.492	5	2	0.5	6
PU 5.2	50	1.492	5	2	0.5	4
PU 3.2	50	1.492	5	2	0.5	5
PU 11.1	50	1.492	5	2	0.5	5

Table 33: Process parameters for laser cleaning of PU adhesive.

Test	Adhesive debonded	Sealant debonded	Adhesive detached	Sealant detached	Damaged fibres
EP 5.2	11.63	38.56	11.48	34.77	26
EP 5.1	41.57	38.15	6.67	8.71	53
EP 9.2	16.86	32.72	19.37	3.88	39
EP 12.5	12.41	22.99	22.46	44.99	84
EP 8.2	7.07	16.57	29.02	43.41	36
EP 3.2	3.81	5.68	25.26	62.19	59
EP 10.2	2.91	9.66	15.46	60.88	67
EP 11.2	8.28	3.96	10.75	70.15	46

Table 34: Process results for laser cleaning of EP adhesive.

Test	Adhesive detached	Sealant detached	Damaged fibres
PU 8.2	55.06	51.56	56
PU 5.2	32.75	30.60	123
PU 3.2	57.58	55.83	85
PU 11.1	70.87	64.59	78

Table 35: Process results for laser cleaning of PU adhesive.

Appendix G.

Laser Cleaned CFRP Samples

This section shows images of laser cleaned areas on the surface of the CFRP material. The adhesives that were removed with a laser were PU adhesive shown in Figure 134 and Figure 135 and EP adhesive as shown in Figure 136 and Figure 137.

Figure 134: CFRP samples 3.2 (top) and 5.2 (bottom) after laser cleaning of PU adhesive.

Figure 135: CFRP samples 8.2 (top) and 11.1 (bottom) after laser cleaning of PU adhesive.

Figure 136: CFRP samples 3.2 (top) and 10.2 (bottom) after laser cleaning of EP adhesive.

Figure 137: CFRP sample 11.1 (top and bottom) after laser cleaning of EP adhesive.

Appendix H.

SEM Images of Laser Cleaned Areas of PU adhesives on the CFRP Samples.

This section shows the SEM images of the laser cleaned areas of PU adhesive from the CFRP samples. The SEM images were taken using the Hitachi SU − 6600 FE − SEM.
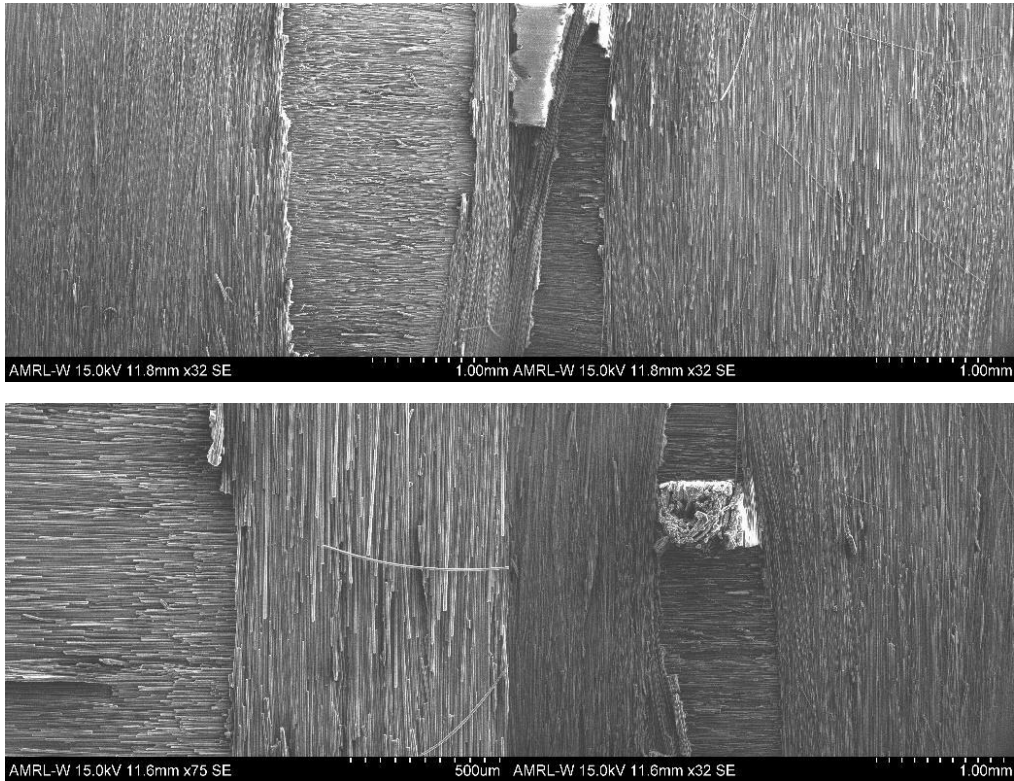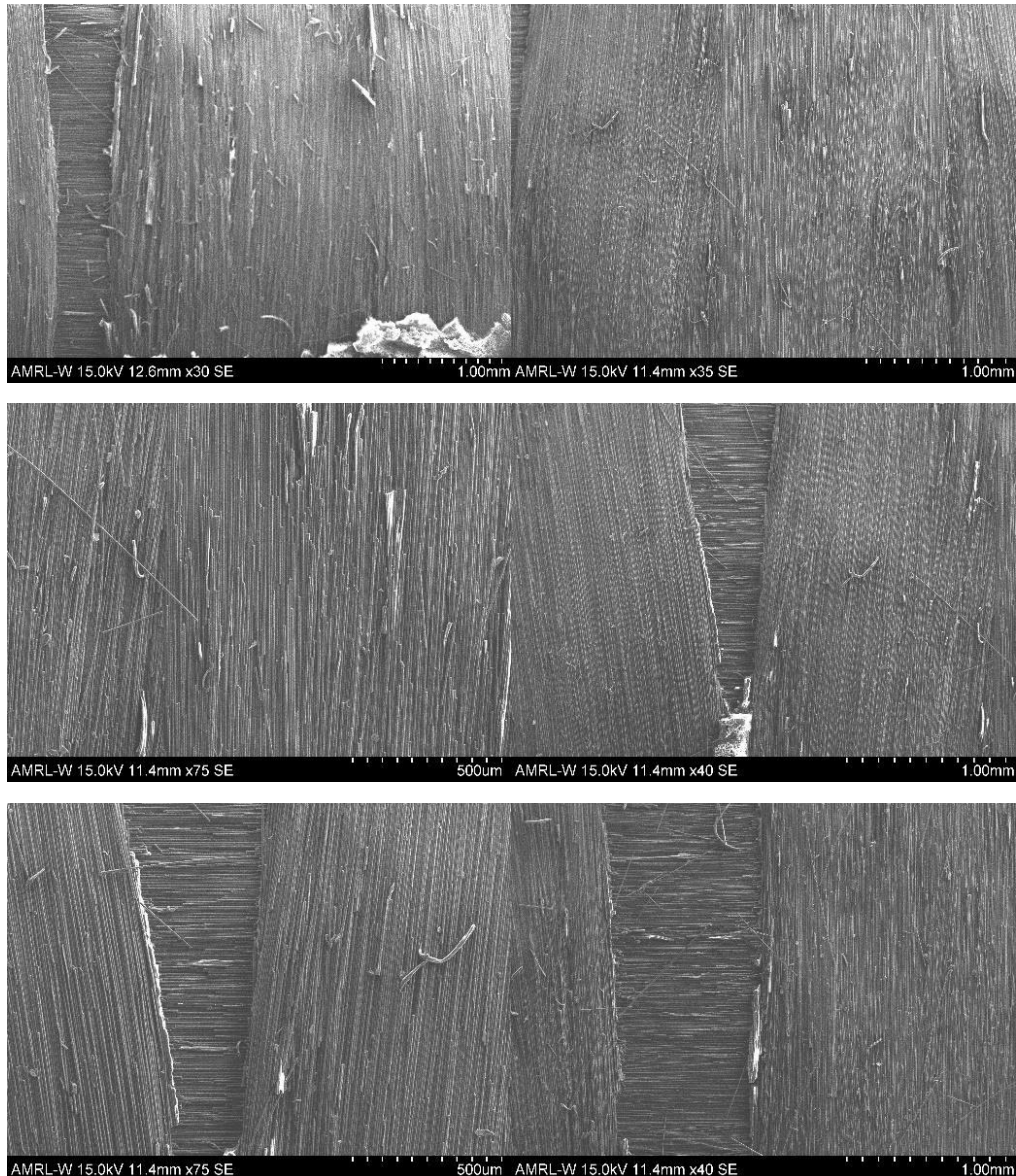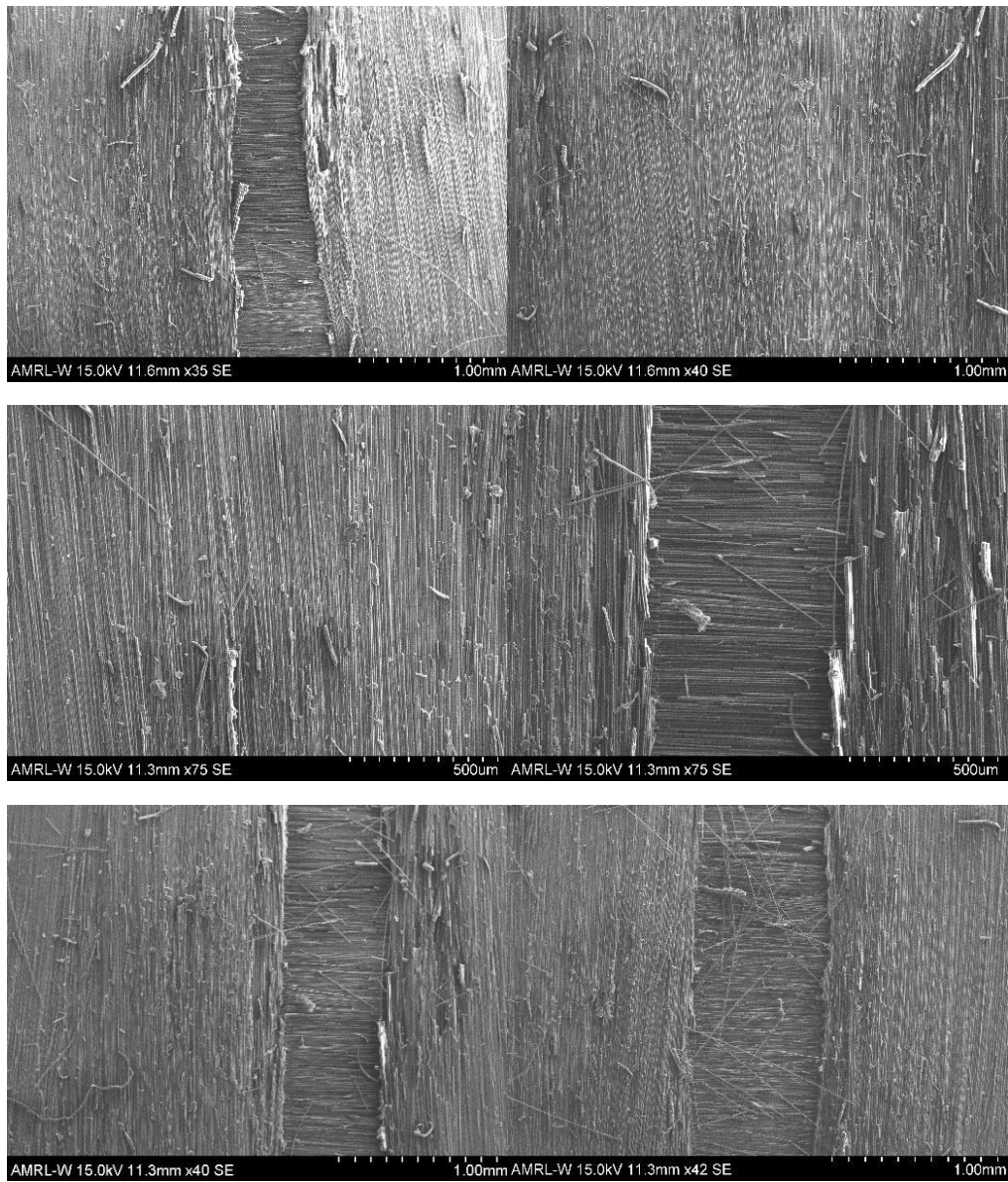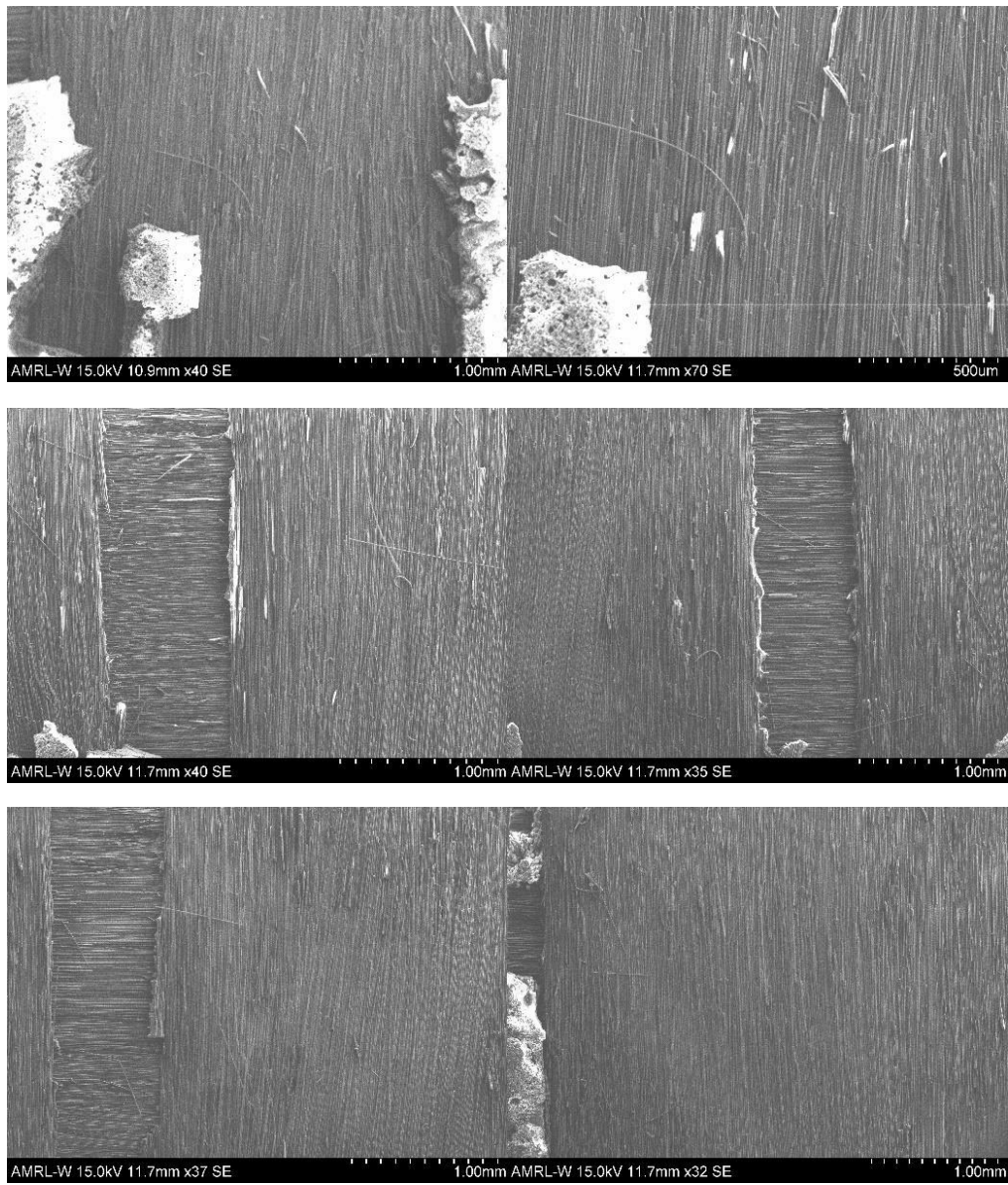

Figure 138: SEM image of laser cleaned areas of PU adhesive on sample 3.2.
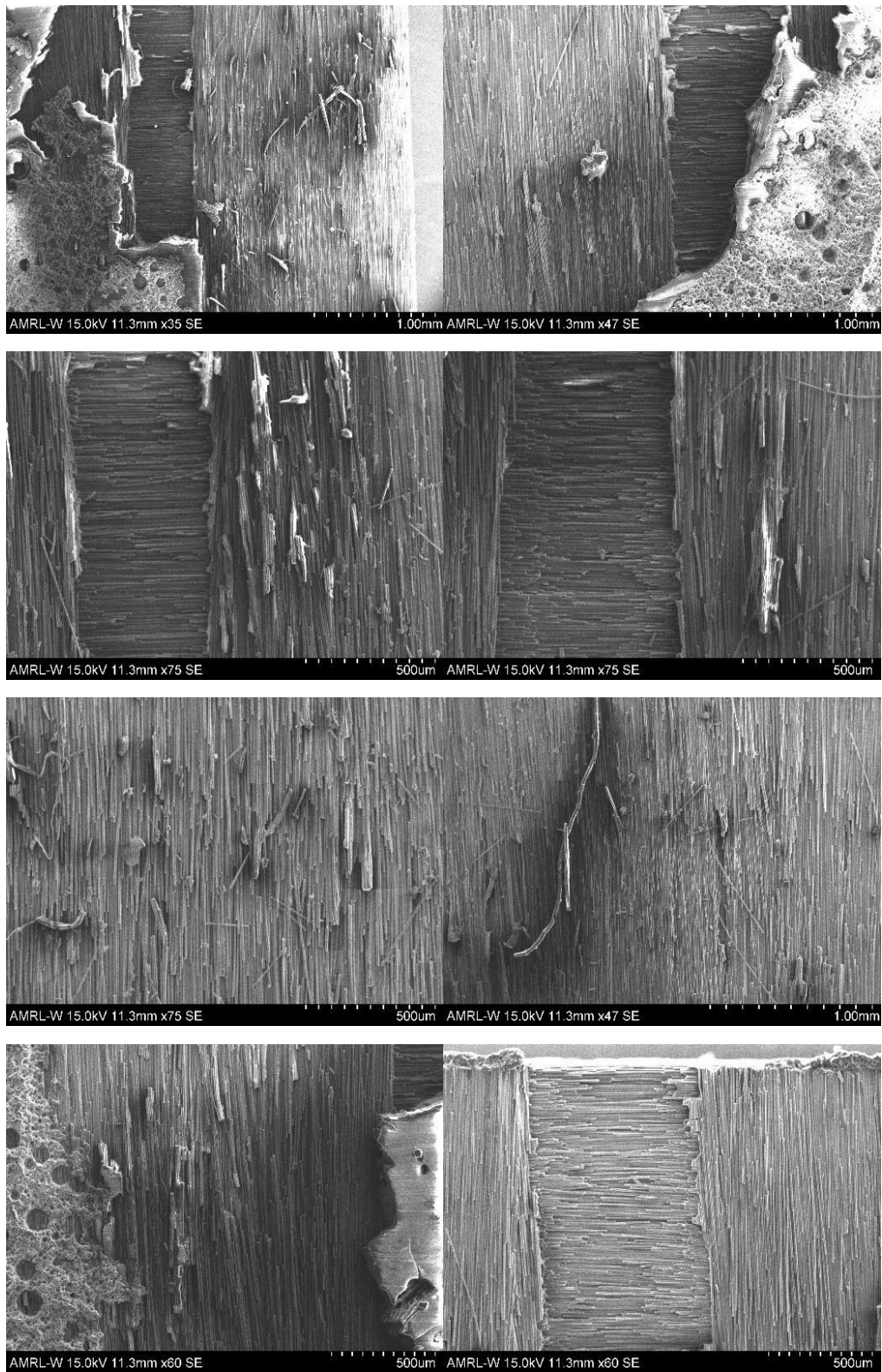
Figure 139: SEM images of laser cleaned areas of PU adhesive on sample 5.2.
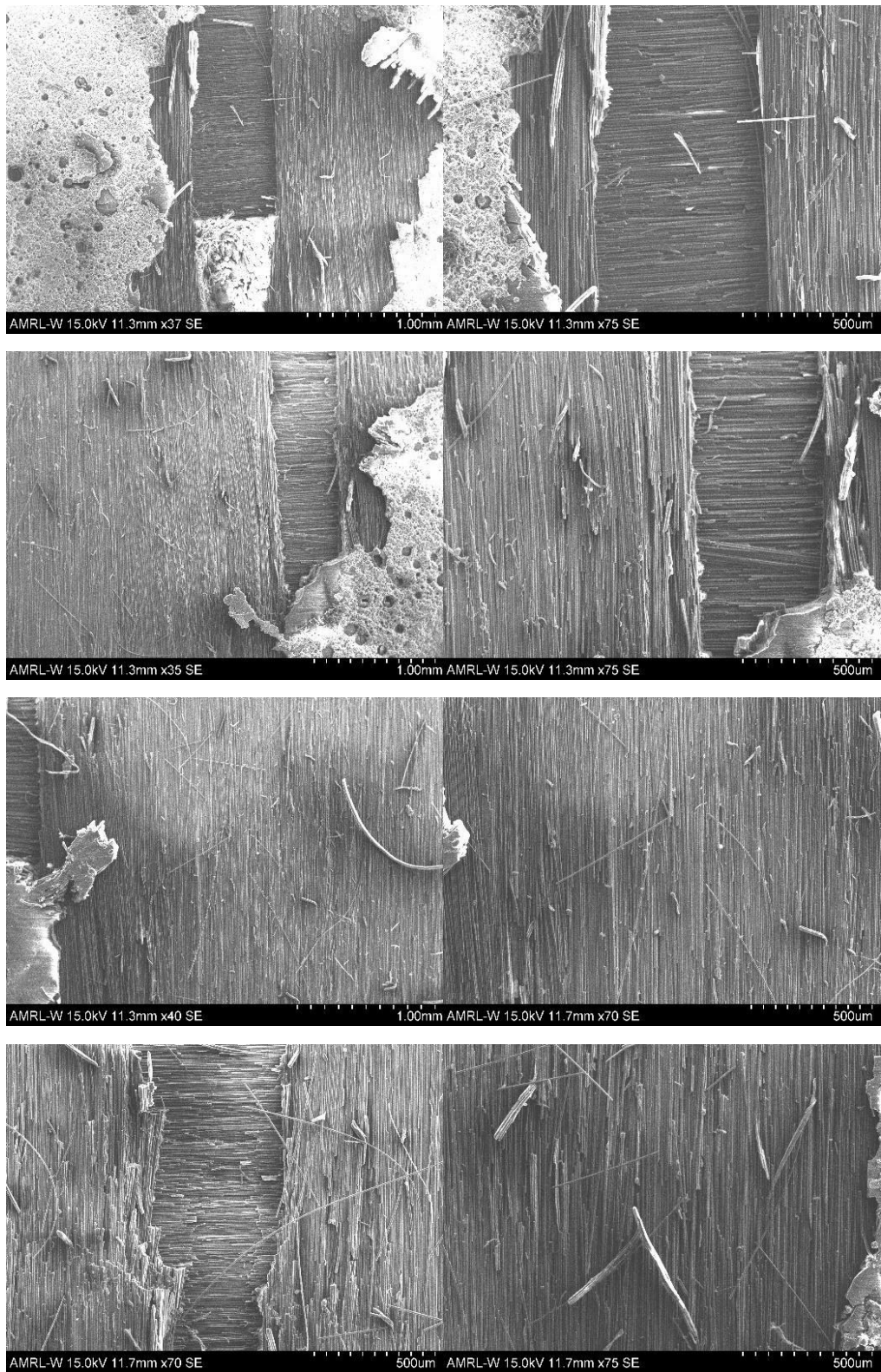
Figure 140: SEM images of laser cleaned areas of PU adhesive on sample 8.2.
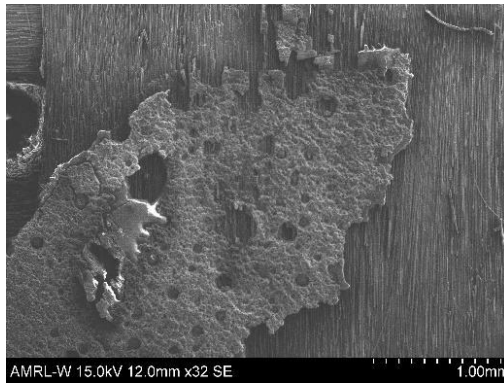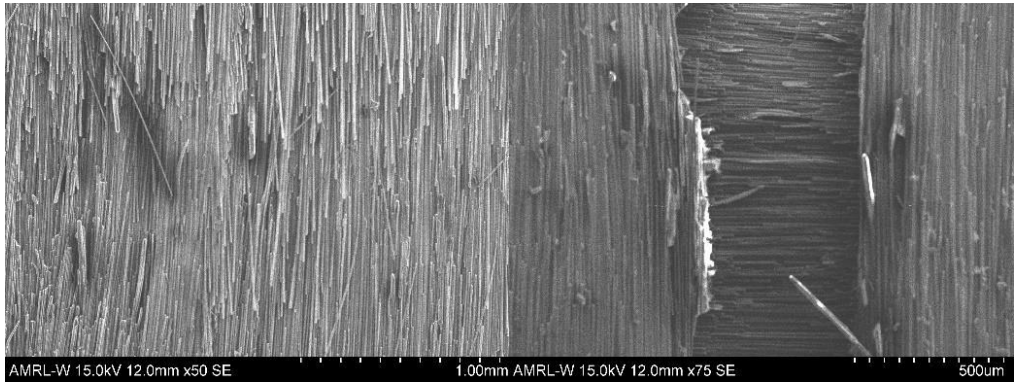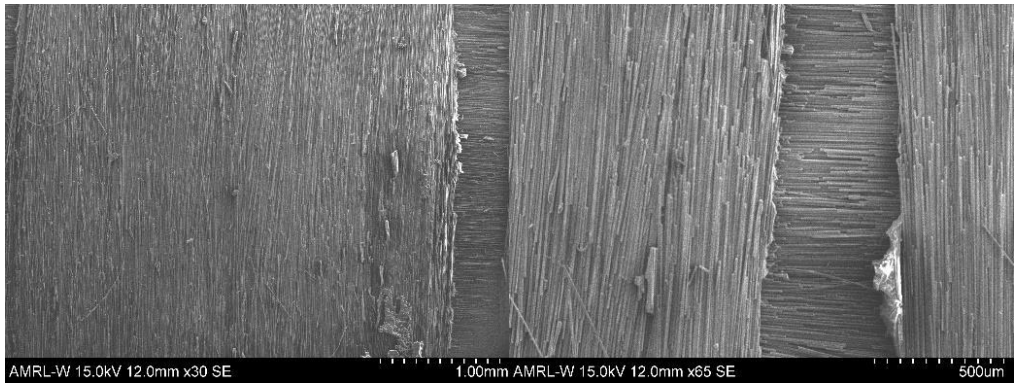
Figure 141: SEM images of laser cleaned areas of PU adhesive on sample 11.1.

Appendix I.

SEM Images of Laser Cleaned Areas of EP adhesive on the CFRP Samples.

This section shows the SEM images of the laser cleaned areas of EP adhesive from the CFRP samples. The SEM images were taken using the Hitachi SU – 6600 FE – SEM.

Figure 142: SEM images of laser cleaned area of EP adhesive for sample 3.2.

Figure 143: SEM images of laser cleaned area of EP adhesive for sample 10.2.

Figure 144: SEM images of laser cleaned area of EP adhesive for sample 11.2.

Appendix J.

Rebonding and Tensile Shear Test of Laser Cleaned Samples

Geometry of the Samples

The test samples for the investigation had the geometry of tensile shear samples according to DIN EN 1465. The samples consist of two CFRP – parts which are joined by and adhesive (Figure 145).
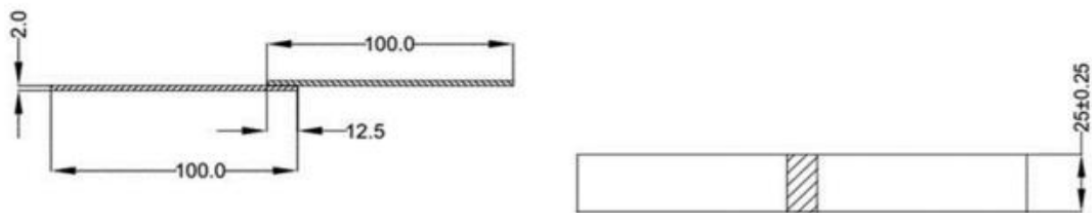

Figure 145: Geometry of tensile shear samples.

Adhesive Bonding

The original samples were bonded using and EP based adhesive and a PU based adhesive (Figure 146). The joining parts were then separated non-destructively and cleaned using lasers. Once cleaned the samples were cleaned, a virgin sample was glued together with each cleaned sample.

Figure 146: CFRP-CFRP sample bonded using PU adhesive.

Testing the Samples

After re-bonding, the samples were tested regarding the test of the bond. First the samples were measured with regards to the area of the joint. A universal testing machine was then used for destructive test, which enables tests in the load range up to 20 kN (tension and pressure). The sample was clamped vertically for straight load

path, the sample was drawn until connection failed (Figure 44). Important test parameters before and during the test:

- Storage before the test in air-conditioned test room for min 16 hours according to DIN EN ISO 291 (class II).
- Test climate 23.1 ^{0}C to 23.4 ^{0}C and 49.0 % to 52.4 % humidity.
- Preload: 10 N.
- Test speed: 0.95 mm/min.

Table 36 shows the numerical results of the reference samples.

	EP adhesive	PU adhesive
Number of samples	5	6
F_{max} (average)	5770.9 N	1360.6 N
Standard deviation (average)	99.8 N	225.0 N

Table 36: Numerical results of the reference samples.

A mixed failure was occurred for the samples bonded with EP adhesive. There was mostly adhesive failure for the samples glued using PU adhesive. The failure of both samples lies on the side of the laser cleaned joining samples. This was expected, since there was still adhesive residue compared to the virgin samples. The types of failure are shown in figures below.

- Part EP 10.2 rebonded using EP adhesive.
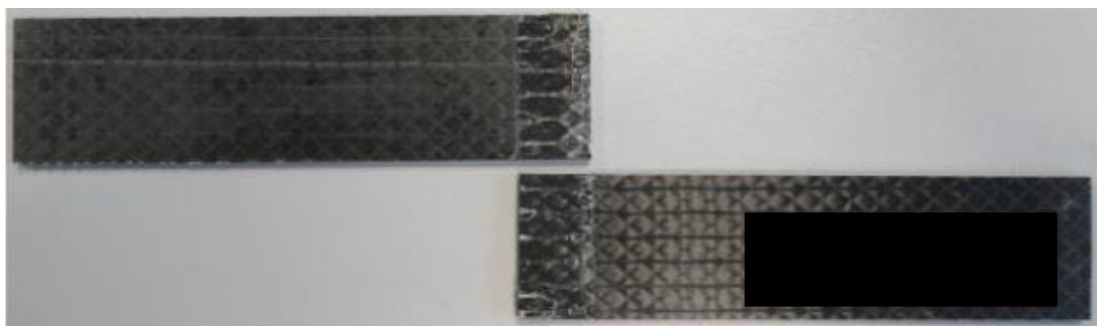
Figure 147: Failure mode of rebonded test sample EP 10.2.

Figure 148: Virgin part EP 10.2.   **Figure 149: Laser cleaned part EP 10.2.**
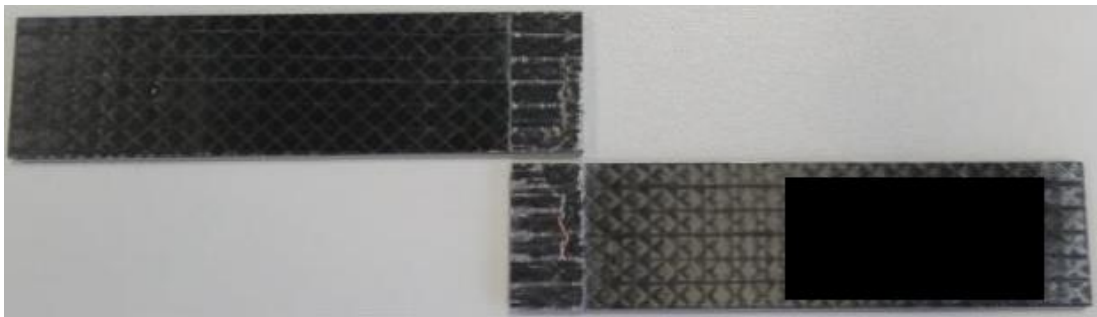
- Part EP 11.2 rebonded using EP adhesive.

Figure 150: Failure mode of rebonded test sample EP 11.2.
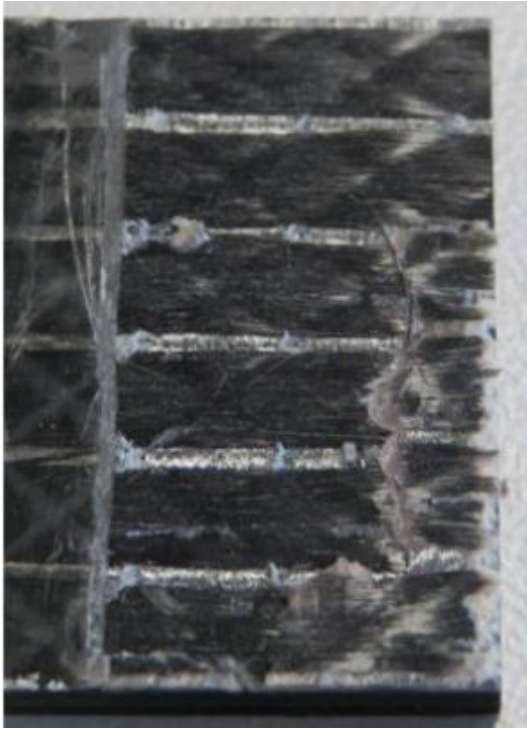
Figure 151: Original virgin part EP 11.2.   **Figure 152: Laser cleaned part EP 11.2.**
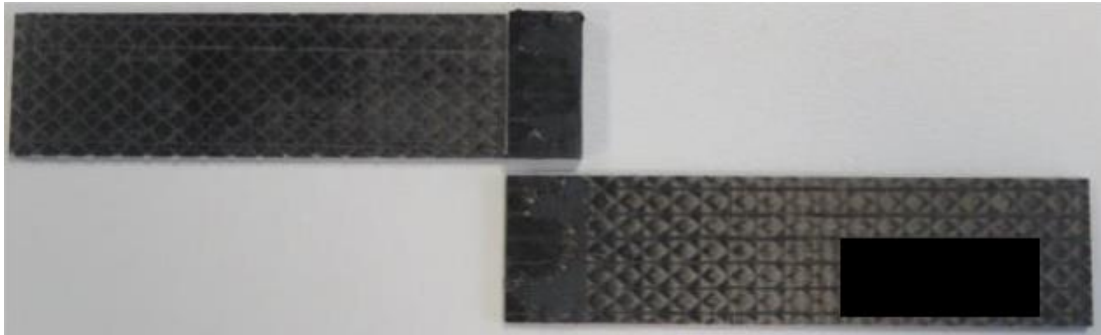
- Part PU 3.2 rebonded using PU adhesive.

Figure 153: Failure mode of rebonded teat sample PU 3.2.

Figure 154: Original virgin part PU 3.2.   **Figure 155: Laser cleaned part PU 3.2.**

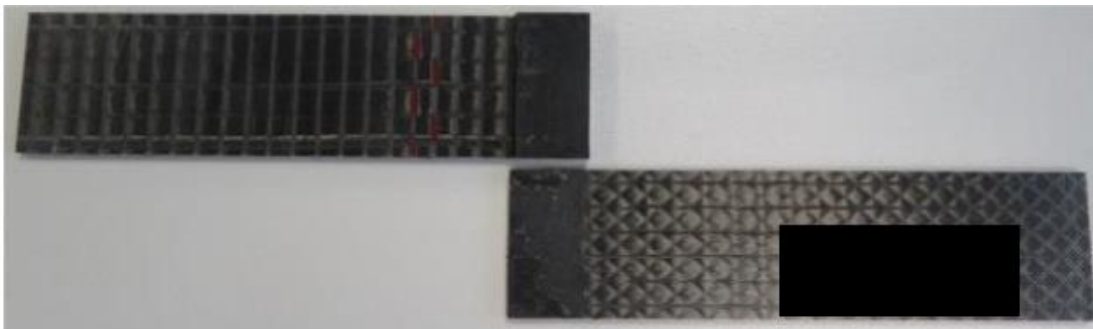- Part PU 5.2 rebonded using PU adhesive.

Figure 156: Failure mode of rebonded test samples PU 5.2.

Figure 157: Original virgin part PU 5.2.

Figure 158: Laser cleaned part PU 5.2.

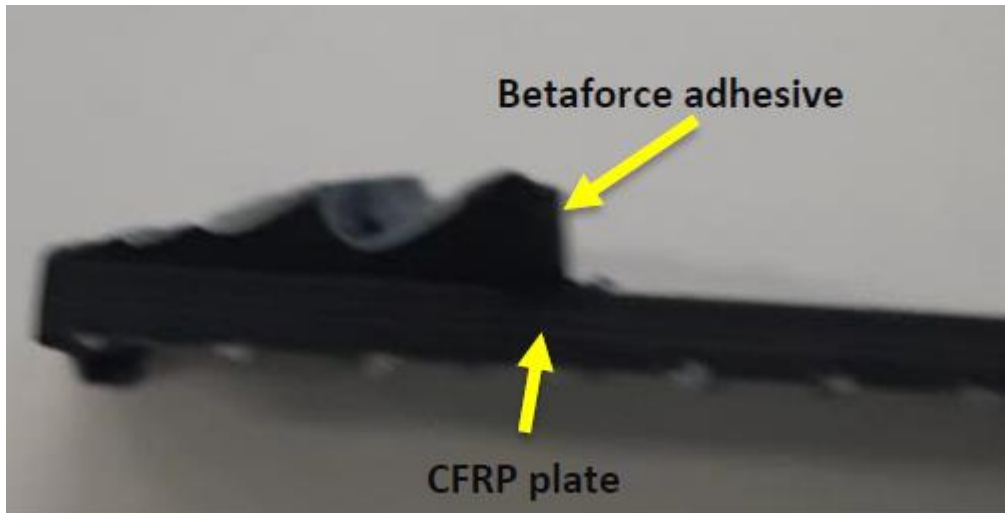# Appendix K.

XCT Scans of samples with PU and EP Adhesive

Figure 159: Image of PU adhesive on CFRP sample

Figure 160: Slice of 3D XCT scan of PU adhesive glue on CFRP sample.

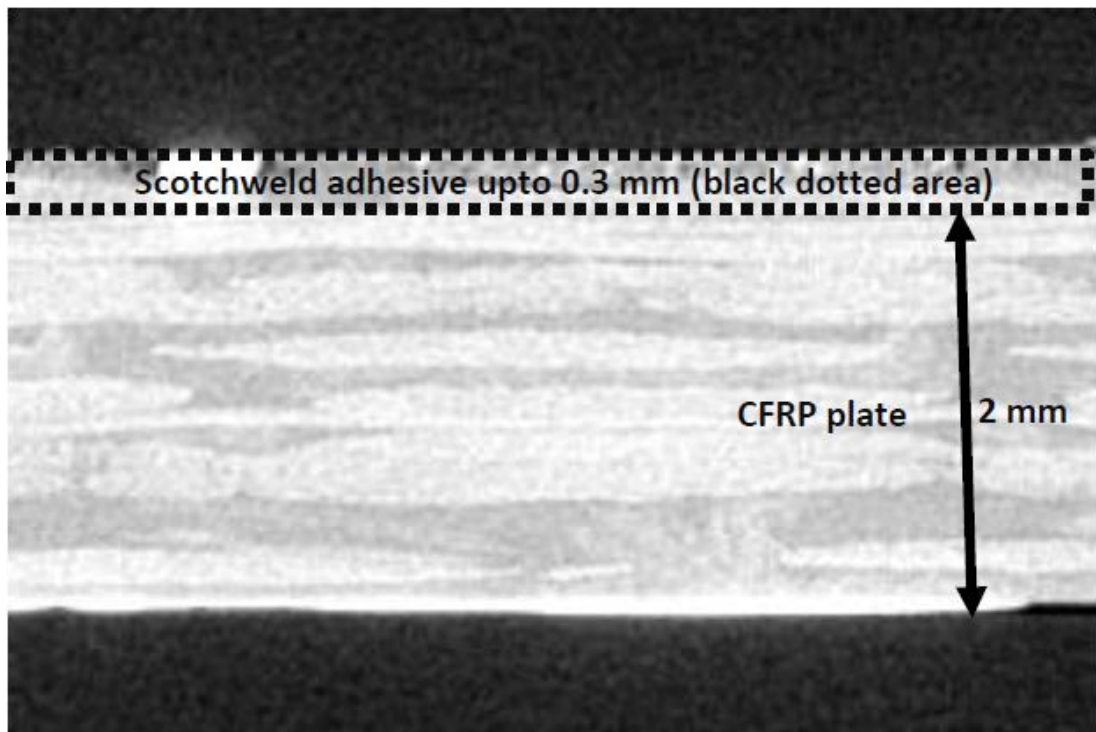**Figure 161: Image of EP adhesive on CFRP sample.**

Figure 162: Slice of 3D XCT scan of EP adhesive on CFRP sample.